Dissertation

submitted to the

Combined Faculties for the Natural Sciences and for Mathematics

of the Ruperto-Carola University of Heidelberg, Germany

for the degree of

Doctor of Natural Sciences

presented by

M. Sc. (Biotechnology) Katharina Deborah Aichelin

born in Heidelberg

Oral-examination:

Development of a CD22-specific chimeric antigen receptor (CAR) for the adoptive T cell therapy of leukemia and lymphoma

Referees:

Prof. Dr. Peter Angel

Prof. Dr. Jürgen Krauss

Abstract

Ex vivo engineering of patient T cells for the specific redirection toward cancer cells is a promising immunotherapeutic strategy to treat hematological malignancies. In this doctoral thesis, a novel CD22 specific chimeric antigen receptor (CAR) was generated for the adoptive T cell therapy of CD22 positive leukemia and lymphoma. The humanized anti-CD22 (hCD22) single chain variable fragment (scFv) was used as antigen binding domain of a third generation CAR, comprising the signal transduction domains CD3ζ, CD28 and 4-1BB. Due to its high affinity and biophysical stability, the hCD22 scFv was compared to the murine anti-CD22 antibody fragment (mCD22) in terms of scFv and CAR stability. Furthermore, to enhance clinical CAR efficacy and CAR safety, the hCD22 CAR was optimized by mutagenesis.

Stability experiments revealed that the mCD22 scFv has a high stability in human serum, comparable to its derived hCD22 scFv. CD22 specific activation of T cells expressing the corresponding hCD22 or mCD22 CAR proved biophysical stability of both scFv derived CARs.

By mutating the hCD22 CAR human Fc spacer domain (ΔFc), binding to human Fc receptor expressing cells was blocked, thus reducing on-target, off-tumor CAR related toxicity. The blocking of interleukin-2 (IL-2) secretion caused by the LCK mutation introduced in the hCD22 CAR CD28 signaling domain (ΔCD28) needs to be further investigated as absence of IL-2 release was observed for both the parental and the mutated hCD22 CAR variants. Specific CAR T cell activation was observed for the parental, the ΔFc, the ΔCD28 and the double mutated ΔFc-ΔCD28 hCD22 CAR confirming that both introduced mutations did not affect CAR efficacy *in vitro*. However, the ΔFc-ΔCD28 hCD22 CAR exhibited a slightly lower anti-tumor efficacy in comparison to the ΔFc, the ΔCD28 and the parental hCD22 CAR. By additionally engineering the hCD22 scFv to further improve the stability of the derived ΔFc-ΔCD28 CAR, CAR T cell activation was not enhanced.

This doctoral thesis provides the basis for the clinical development of a novel CD22 CAR T cell therapy for the treatment of CD22 positive leukemia and lymphoma.

Zusammenfassung

Die Modifikation von Patienten-T-Zellen *ex vivo* zu deren spezifischen Ausrichtung gegen Krebszellen ist eine vielversprechende immuntherapeutische Strategie zur Behandlung von hämatologischen Neoplasien. In dieser Doktorarbeit wurde ein neuartiger CD22-spezifischer chimärer Antigenrezeptor (CAR) zur adoptiven T-Zell-Therapie von CD22-positiven Leukämien und Lymphomen generiert. Das humanisierte anti-CD22 (hCD22) scFv-Fragment (*single chain variable fragment*) wurde als Antigenbindungsdomäne eines CARs der dritten Generation, der die CD3ζ-, CD28- und 4-1BB-Signaltransduktionsdomäne enthält, integriert. Aufgrund dessen hohen biophysikalischen Stabilität wurde das hCD22-scFv mit dem murinen anti-CD22-Antikörperfragment (mCD22) hinsichtlich der scFv- und CAR-Stabilität verglichen. Darüber hinaus wurde der hCD22-CAR durch Mutagenese optimiert, um die CAR-Wirksamkeit und -sicherheit zu optimieren.

Stabilitätsexperimente zeigten, dass das mCD22-scFv eine hohe Stabilität in humanem Serum aufweist, die mit dem abgeleiteten hCD22-scFv vergleichbar ist. Der Nachweis der biophysikalischen scFv- und CAR-Stabilität erfolgte durch die CD22-spezifische Aktivierung der hCD22- bzw. mCD22-CAR tragenden T-Zellen.

Durch Mutation der humanen Fc-Spacer-Domäne (ΔFc) des hCD22-CAR wurde die Bindung an Fc-Rezeptor-exprimierenden Zellen geblockt und so die unspezifische CAR-Toxizität reduziert. Das durch die LCK-Mutation in der CD28-Signaldomäne (ΔCD28) verursachte Blockieren der Interleukin 2 (IL-2)-Sekretion muss weiterhin analysiert werden, da sowohl bei den T-Zellen mit den mutierten als auch den parentalen hCD22-CARs keine IL-2-Freisetzung beobachtet wurde. Die spezifische CAR-T-Zell-Aktivierung mittels parentalem, ΔFc, ΔCD28 und doppelt-mutiertem ΔFc-ΔCD28 hCD22-CAR bestätigte, dass die beiden eingefügten Mutationen die CAR-Wirksamkeit nicht beeinflussen. T-Zellen mit dem ΔFc-ΔCD28 hCD22-CAR zeigten eine minimal geringere antitumorale Wirksamkeit im Vergleich zu denjenigen, die den ΔFc, ΔCD28 und parentalen hCD22-CAR trugen. Durch die zusätzliche Modifikation des hCD22-scFv zur Erhöhung der Stabilität des ΔFc-ΔCD28 CAR wurde die T-Zell-Aktivierung nicht verbessert. Diese Doktorarbeit liefert die Grundlage zur klinischen Entwicklung einer neuartigen CD22-CAR-T-Zell-Therapie zur Behandlung CD22-positiver Leukämien und Lymphome.

Table of content

Abbreviations

°C	degree Celsius
µg	microgram (10^{-6} gram)
µl	microliter (10^{-6} liter)
µM	micromolar (10^{-6} mol/L)
µm	micrometer (10^{-6} meter)
A	adenine
Abs	absorbance
ACT	adoptive cell therapy
ADCC	antibody-dependent cellular cytotoxicity
AICD	activation induced cell death
ALL	acute lymphoblastic leukemia
AML	acute myeloid leukemia
APC	allophycocyanin
AS	anti-sense
ATCC	American Type Culture Collection
BiTE	bispecific T-cell engager
bp	base pair
BSA	bovine serum albumin
BsAb	bispecific antibody
C	cytosine
CAIX	carbonic anhydrase IX
CAR	chimeric antigen receptor
CD	cluster of differentiation
CDC	complement-dependent cytotoxicity
CDR	complementary determining region
CEA	carcinoembryonic antigen
C_H	heavy chain constant domain
CIP	calf-intestinal alkaline phosphatase
C_L	light chain constant domain
CLL	chronic lymphoblastic leukemia
CML	chronic myeloid leukemia
CMV	cytomegalovirus

CNS	central nervous system
CO_2	carbon dioxide
ColE1	Colicin E1
cPPT	central polypurine tract
Cy	cyanine
Db	diabody
DMEM	Dulbecco's modified Eagle's medium
DMSO	dimethyl sulfoxide
DNA	deoxyribonucleic acid
dNTP	deoxynucleoside triphosphate
dsFv	disulfide-bond stabilized Fv
DTT	dithiothreitol
E. coli	*Escherichia coli*
EDTA	ethylenediaminetetraacetic acid
ELISA	enzyme-linked immunosorbent assay
Env	envelope
Fab	fragment antigen binding
FACS	fluorescence-activated cell sorting
FBS	fetal bovine serum
Fc	fragment crystallizable
FcγR	Fcγ receptor
FITC	fluorescein isothiocyanate
FPLC	fast protein liquid chromatography
FR	framework region
Fv	fragment variable
g	gram or centrifugal force
G	guanine
h	hour (s)
HAMA	human anti-mouse antibody
hCD22	humanized CD22
HEK	human embryonic kidney
hFc	human Fc
HLA	human leucocyte antigen

HRP	horseradish peroxidase enzyme
HSCT	hematopoietic stem cell transplant
HSV	herpes simplex virus
IFNγ	interferon gamma
Ig	immunoglobulin
IL	interleukin
IMAC	immobilized metal ion affinity chromatography
IR	intergenic region
IRES	internal ribosomal entry site
ITAM	immunoreceptor tyrosine-based activation motifs
kb	kilobase
kDa	kilodalton
L	leucine or protein ladder or light
LB	lysogeny broth
LCK	protein tyrosine kinase LCK
LTR	long terminal repeat sequence
mAb	monoclonal antibody
mAU	milli absorption units
mCD22	murine CD22
MFImax	maximum median fluorescence intensity
mg	milligram (10^{-3} gram)
MHC	major histocompatibility complex
min	minute (s)
ml	milliliter (10^{-3} liter)
mM	millimolar (10^{-3} mol/L)
MOI	multiplicity of infection
Myc	myelocytomatosis oncogene
ng	nanogram (10^{-9} gram)
NHL	non-Hodgkin’s lymphoma
NK	natural killer
nm	nanometer (10^{-9} meter)
NOD	non-obese diabetic
NSG	NOD SCID gamma

OD	optical density
ori	origin of replication
pA	polyadenylation signal
PAGE	polyacrylamide gel electrophoresis
PBMC	peripheral blood mononuclear cell
PBS	phosphate buffered saline
PCR	polymerase chain reaction
PE	pseudomonas-Exotoxin
PE	phycoerythrin
PEI	polyethylenimine
PGK	phosphoglycerate kinase
PI	propidium iodide
ROR1	receptor tyrosine kinase-like orphan receptor 1
rpm	rotation per minute
RPMI	Roswell Park Memorial Institute medium
RRE	rev response elements
RT	room temperature
scFv	single chain variable fragment
SCID	severe combined immunodeficiency
SDS	sodium dodecyl sulfate
SEC	size-exclusion chromatography
sec	second (s)
SV40	Simian Virus 40
T	thymine
T reg	regulatory T cell
TAA	tumor-associated antigen
TAE	tris acetate EDTA buffer
TCR	T cell receptor
TIL	tumor infiltrating lymphocyte
Tm	melting temperature
TMB	3,3’,5,5’-Tetramethylbenzidine
TNF	tumor necrosis factor
U	unit (s)

V_H	heavy chain variable domain
V_L	light chain variable domain
w/v	weight per volume
WHO	World Health Organization
WPRE	woodchuck hepatitis virus posttranscriptional regulatory element
Y	tyrosine

1 Introduction

1.1 Antibody based therapy

1.1.1 Monoclonal antibodies and antibody fragments

Nowadays, therapeutic monoclonal antibodies (mAbs) constitute the largest and fastest growing class of biopharmaceuticals. Due to their specific interaction with pathogens and immune cells, their biophysical stability and their long half-life, they are regarded as very powerful (Jefferis, 2012).

More than a century ago, first suggestions to use antibodies for the elimination of tumor cells and pathogens emerged with Paul Ehrlichs “magic bullet” concept (Strebhardt and Ullrich, 2008). However, it is only since the discovery of hybridoma technology in 1975 that mAbs of murine origin, directed against specific antigens, could be generated. As they are produced by a single cell clone and have the same amino acid sequence, monoclonal hybridoma-derived antibodies are characterized by their identical affinity and specificity (Kohler and Milstein, 1975). However, adverse events rapidly occurred after their clinical application in patients. Because of their murine origin, high immunogenicity induced by the development of human anti-murine antibodies (HAMA) could be observed (Kim et al., 2005). To reduce the immunogenicity, murine constant domains of the heavy and light chains were replaced with human counterparts by genetic engineering to form so-called chimeric antibodies (Morrison et al., 1984) (Figure 1). By additionally replacing the murine framework regions of the variable domains with human amino acid sequences, the murine components are even more reduced, leading to humanized antibodies (Krauss et al., 2003a). Methods such as phage display or transgenic mice even permit the generation of fully human antibodies (Ribatti, 2014) (Figure 1).

Immunoglobulins (Ig) are divided into five distinct subclasses (isotypes): IgA, IgD, IgE, IgG and IgM. Nevertheless, only IgG class antibodies are currently used for therapeutic purposes (Redman et al., 2015; Reichert, 2017). An IgG (150 kDa) is composed of two identical light and two identical heavy chains, covalently connected by multiple disulfide bridges. While a light chain comprises one constant domain (C_L) and one variable domain (V_L), a heavy chain consists of three constant domains (C_H1-C_H2-C_H3) and one single variable domain (V_H) (Kim et al., 2005). From

a functional point of view, an IgG is separated into one single crystallizable constant fragment (Fc) connected via a flexible hinge region to two identical antigen-binding fragments (Fabs) (Kim et al., 2005). Each variable domain of a Fab contains three hypervariable complementary-determining regions (CDRs) flanked by four framework regions. While these regions are responsible for specific and high affinity antigen binding, the Fc region mediates the effector functions (Pandey and Mahadevan, 2014) (Figure 1).

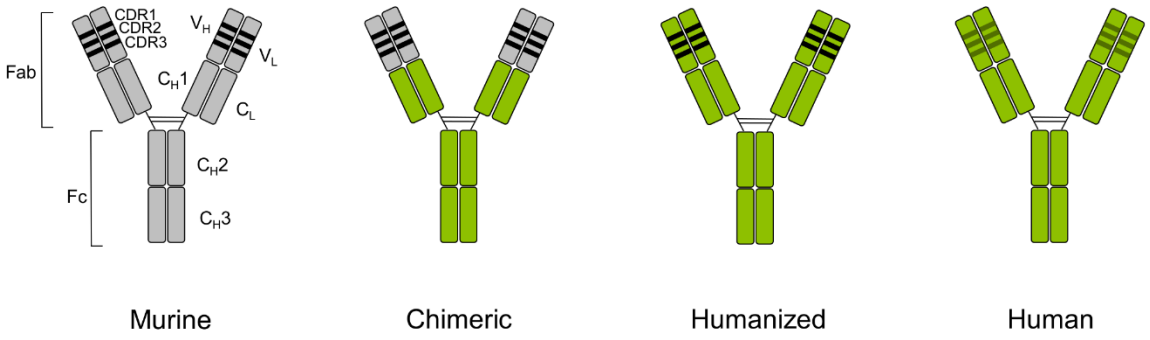

Figure 1: Schematic representation of a murine, chimeric, humanized and human monoclonal IgG antibody. Grey: murine amino acid sequences; light green: human amino acid sequences; black: murine CDRs; dark green: human CDRs. Adapted from Kim *et al.*, 2005.

MAbs feature a long half-life but show poor tumor penetration due to their high molecular weight (Yokota et al., 1992). These undesired properties have been circumvented thanks to the generation of small antibody fragments by enzymatic digestion of IgG. Indeed, digestion with the protease papain allowed to obtain a monovalent Fab fragment (50 kDa) which consists of a V_L and a V_H domain as well as a C_L and a C_H1 domain of the original mAb (Figure 2). The smallest antibody fragment able to preserve the antigen binding ability is the variable fragment (Fv) composed of the V_L and V_H domains (Essig et al., 1993). When these variable parts are connected via a short, engineered peptide linker of 14 to 25 amino acids, a so-called single chain variable fragment (scFv) of about 25 kDa is formed (Bird et al., 1988; Essig et al., 1993). When associated by a disulfide bond, a disulfide-bond stabilized Fv (dsFv) is created. The small-sized scFv and Fab fragment consistently conserve the specific binding affinity of the entire antibody and present an improved tumor penetration and a faster blood clearance (Essig et al., 1993; Yokota et al.,

1992). Besides monovalent fragments, multivalent antibody fragments can also be generated, for example by reducing the size of the flexible linker (Frenzel et al., 2013). The bivalent diabody (Db) is a representative example for this purpose (Figure 2).

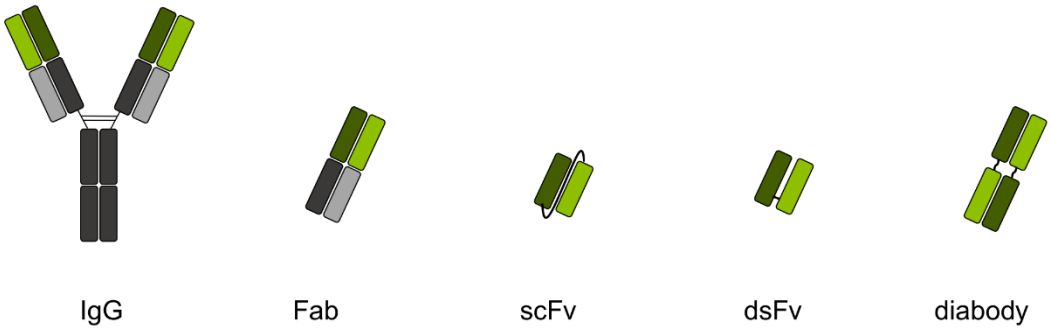

Figure 2: Schematic representation of different recombinant antibody formats. Grey: constant domains; green: variable domains. Adapted from Frenzel *et al*., 2013.

1.1.2 Mechanism of action

Therapeutic antibodies that specifically target tumor associated antigens (TAA) can attack the tumor cells through either direct and/or indirect mechanisms of the immune system. By binding a TAA, an antibody can directly impact the downstream signaling, acting either as an antagonist or an agonist by respectively inhibiting or modulating the induced signal transduction. For example, Rituximab, a chimeric antibody, directly induces apoptosis by binding the cluster of differentiation 20 (CD20) (Johnson and Glennie, 2003).

To specifically lyse tumor cells, mAbs can also activate other components of the immune system through their Fc fragment. By interacting with Fcγ receptor expressing cells, the antibody indirectly triggers antibody-dependent cell-mediated cytotoxicity (ADCC). Complement dependent cytotoxicity (CDC) occurs after interaction between the Fc fragment and the C1q protein which activates the complement (Redman et al., 2015).

Besides these indirect antitumor effector functions, mAbs, but also scFvs, can be conjugated to cytotoxic effector substances, for example enzymes, toxins, radionuclides or cytokines which transmit extended artificial effector functions

(Schrama et al., 2006). Resulting conjugates or fusion proteins are called immunotoxin, immunoRNase, immunocytokine or radioimmunoconjugate, depending on their added effector. This strategy can enhance the therapeutic impact.

Advances in antibody engineering and design led to new approaches using T cells and their effector functions against tumor cells (Satta et al., 2013; Stamova et al., 2012). Bispecific antibodies (BsAbs) and chimeric antigen receptors (CARs) are adaptor molecules combining specific TAA recognition with potent T cell attack mechanisms. In one single molecule, BsAbs possess the specificity of two antibodies. Bispecific T cell engagers (BiTE) contain two scFvs, one targeting a TAA and another targeting CD3 on T cells. In this way, T cell activation is triggered independently of the T cell receptor (TCR) specificity, leading to the release of granzyme B and perforin and consequently to tumor cell lysis (Baeuerle and Reinhardt, 2009; Satta et al., 2013). In CARs, a TAA specific scFv is directly fused with the signaling part of a TCR and expressed on the surface of T cells. This enables the activation of T cell effector functions in a major histocompatibility complex (MHC) independent manner (Satta et al., 2013; Wu et al., 2016).

1.2 Adoptive T cell therapy

Despite major advances in the field of monoclonal antibodies, their therapeutic application in different formats is often limited due to short half-life, insufficient tumor penetration and frequent reactivity with normal tissue. Newly acquired knowledge regarding immunology and oncology permit the development of an increasing number of adoptive immunotherapy strategies to treat cancer. The goal of the adoptive cell therapy (ACT) is to arm T lymphocytes from patients with a specific reactivity against tumor associated antigens (TAA) to trigger an immune response leading to targeted tumor cell lysis. To achieve this, highly active, tumor specific lymphocytes are isolated, genetically modified *ex vivo* and expanded before a subsequent autologous administration into patients (Figure 3). In this way, antibody based approaches have emerged for the development and use of antigen specific T lymphocytes (Dudley and Rosenberg, 2003; Rosenberg et al., 2008).

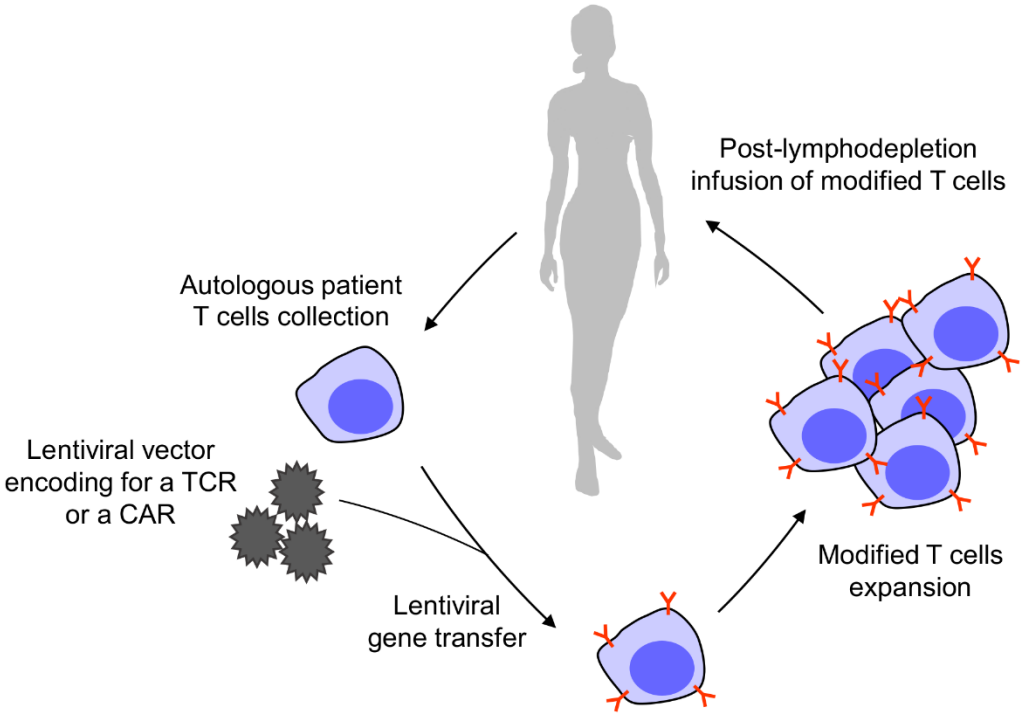

Figure 3: Schematic representation of the adoptive cell therapy. T cells isolated from tumor patient blood are genetically modified *ex vivo* by lentiviral vectors encoding for a TCR or a CAR which confers specificity against cancer cells. Subsequently, the modified T cells are expanded *ex vivo* and re-infused back into the patient after lymphodepletion.

In contrast to mAbs, tumor infiltrating lymphocytes (TILs) isolated from human tumor tissue have the capacity to actively penetrate tissue. Clinical effectiveness of ACT was seen when using autologous TILs to treat patients with metastatic melanoma (Dudley et al., 2002; Muul et al., 1987; Rosenberg et al., 1994). After ACT, the anti-tumor reaction maintained by these TILs led to a repeated immune reaction with cytotoxic activities against tumor cells and consequently to tumor regression. An important improvement of the therapeutic efficacy of ACT was obtained through lymphodepletion prior to CAR T cell infusion (Dudley et al., 2002). Indeed, by depleting regulatory lymphocytes prior to the administration of TILs and interleukin-2 (IL-2) infusion, the anti-tumor T cell expansion in patients was enhanced.

Nevertheless, the complex, time consuming TIL preparation and culture from tumor tissue remain a challenge and the therapeutic application is consequently limited. Protocol optimizations concerning the stimulation and cultivation of tumor specific

TILs were continuously performed (Dudley et al., 2003). Partial or complete remissions were observed for more than 50% of patients with refractory metastatic melanoma after a combinatorial therapy including lymphodepletion followed by TIL ACT. Besides cancer regression, proliferation of TILs with unknown tumor specificity lead to autoimmune reactions in some patients (Dudley et al., 2005). To avoid this unwanted T cell autoreactivity and potential cross-reactivity with antigens on healthy tissue, it would be preferable to use T cells with a defined specificity.

The specificity of a T cell is determined by the T cell receptor (TCR). Advances in genetic engineering of T cells and in gene transfer techniques enabled the transgenic expression of a recombinant TCR on the surface of engineered T lymphocytes (Morgan et al., 2006). By selectively recognizing a defined TAA, the recombinant TCR induces enhanced tumor cell killing. However, the target recognition of an engaged TCR is dependent on the MHC complex, present on targeted cells. As part of the tumor immune escape machinery, dysregulation in MHC antigen processing and presenting mechanisms occur frequently in tumors (Seliger et al., 1997). Therefore, TCR engineered T cells often do not recognize tumor cells, limiting their application (Garcia-Lora et al., 2003). Furthermore, cell surface antigens such as glycolipids or carbohydrates are expressed on many tumor cells without MHC presentation and cannot be recognized by TCRs. To overcome these limitations, the engineering of T cells that express antibody based chimeric antigen receptors appeared to be a promising strategy.

1.3 Chimeric antigen receptor: structure, function, challenges

In the early 1990s, pioneering work demonstrated the redirection of T cell specificity and function by a chimeric antigen receptor (CAR), a recombinant receptor combining a scFv with a T cell signaling domain (Eshhar et al., 1993; Gross et al., 1989). Nowadays, CARs emerged as a novel and powerful therapy for hematological malignancies. A CAR consists of four regions: an extracellular antigen binding domain, a spacer or hinge domain, a transmembrane region and an intracellular signaling domain (Dotti et al., 2014; Sadelain et al., 2013) (Figure 4).

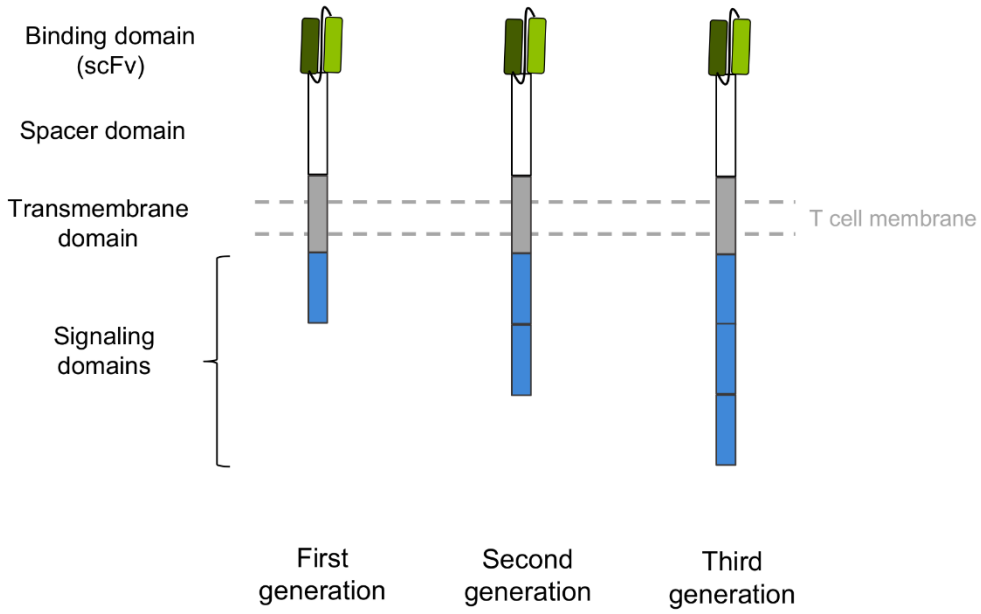

Figure 4: Schematic representation of the chimeric antigen receptor (CAR) structure. CARs target TAAs in a MHC-independent manner and consist of one scFv as targeting moiety, one spacer domain, one transmembrane domain and one or more signaling domains. First generation CARs contain one single cytoplasmic activation domain. Second and third generation CARs have one or two additional co-stimulatory domains.

The extracellular part commonly corresponds to a scFv, derived from the binding region of a monoclonal antibody. A CAR will thus have the affinity and specificity of the chosen antibody fragment. These artificial receptors mainly recognize TAAs but they can also bind non-classical T cell antigens independently of MHC as for example gangliosides and carbohydrates. While a high binding affinity predicts an efficient CAR T cell activation, studies revealed that when a certain affinity threshold is obtained, the CAR T cell activation is not further improved (Chmielewski et al., 2011). Beside affinity, the spatial position of the epitope also impacts CAR function (Hombach et al., 2007). The CAR mediated T cell activation is affected and modulated by the origin, the flexibility and the size of the spacer domain located between the scFv and the transmembrane domain (Maus et al., 2014). Commonly used hinges are IgG1 derived Fc, CD8 and CD28 spacer regions (Gacerez et al., 2016). By optimizing the distance between the tumor and the T cell, the provided flexibility enables, for some CARs, more efficient target binding and a stable expression on the surface of T cells (Guest et al., 2005a). Depending on the number

of domains within this cytoplasmic moiety, CARs are classified into three generations (Gacerez et al., 2016) (Figure 4). However, the optimal intracellular configuration still remains an open issue. The intracellular TCR derived signaling region, composed of one or more domains, triggers T cell activation upon antigen recognition (Figure 5). Following phosphorylation of the immunoreceptor tyrosine-based activation motifs (ITAMs) of the signaling region, a downstream signaling cascade is initiated, resulting in CAR T cell amplification, cytokine secretion and cell killing activity.

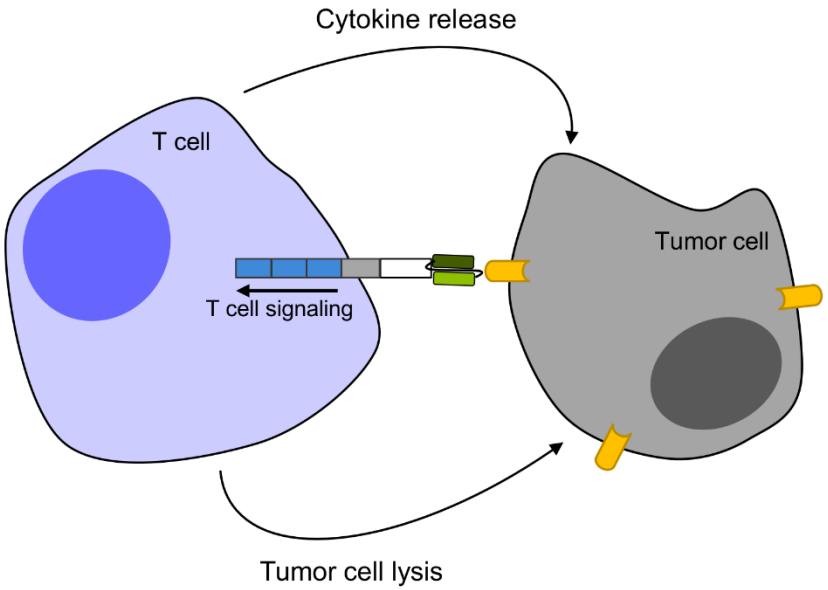

Figure 5: CAR mechanism of action. Upon CAR interaction with the cognate antigen via the extracellular antibody fragment, an intracellular downstream signaling cascade is initiated, resulting in CAR T cell amplification and cytokine release which subsequently trigger a MHC-independent tumor cell lysis.

First generation CARs present a scFv as binding moiety linked to an activation domain by a transmembrane portion, the TCR derived CD3ζ chain (Figure 4). This single cytoplasmic domain initiates signal transduction upon CAR antigen binding. While potent *in vivo*, several clinical studies revealed that the therapeutic efficacy of first generation CARs is limited due to poor persistence of CAR T cells, caused by a transient activation (Kershaw et al., 2006; Till et al., 2008). Significant progress was achieved by adding, besides the activation portion, one or two co-stimulatory domains resulting in a second or third generation CAR, respectively (Figure 4). These moieties are either derived from CD28, the most common and well-studied

co-stimulatory receptor, or from tumor necrosis factor (TNF) receptor family members involved in normal T cell activation, like OX40 (CD134) or 4-1BB (CD137). The addition of these domains enhances the CAR potency, resulting in full T cell activation and in improved tumor attack. Cytokine secretion as well as CAR T cell amplification and persistence are enhanced by the presence of these co-stimuli (Finney et al., 1998; Hombach et al., 2001a).

Each co-stimulatory domain induces distinct T cell effector functions, although a few overlaps exist (Abken, 2014). While they all increase the secretion of interferon γ (IFNγ), interleukin-2 (IL-2) release is only triggered upon CD28 co-stimulation but not upon 4-1BB or OX40. Amplified cell killing activity, enhanced T cell persistence and expansion is observed for CD28 containing CARs compared to other second generation CARs harboring 4-1BB or OX40 (Hombach and Abken, 2011). However, T cell amplification is also triggered more efficiently by 4-1BB than by OX40. Cell survival and activation induced cell death (AICD) is prevented by 4-1BB signaling (Gacerez et al., 2016). OX40 is considered to be a late co-stimulatory molecule which enables the induction of memory T cells that can escape AICD (Hombach and Abken, 2011).

Currently, second generation CARs are the most investigated format and are widely used in clinical trials. Because little advantages were found *in vivo* with third generation CARs, only a few of these CARs are tested in the clinic (Gacerez et al., 2016). The modular CAR architecture, including binding and signaling moieties, allows a large variety of possible combinations. As each region individually contributes to the receptor characteristic, there is no single optimal CAR configuration.

Using CAR modified T cells for cancer immunotherapy provides several advantages. CARs are equipped with antibodies specifically recognizing cognate antigens, mostly TAAs, independently of MHC processing and presentation. This offers the possibility to target a variety of non-classical T cell antigens, including gangliosides and carbohydrates, without excluding MHC presented antigens such as the HLA-A*0201 presented NY-ESO1 peptide (Stewart-Jones et al., 2009). Tumor escape by downregulating the number of extracellular human leucocyte antigen (HLA) molecules or by introducing defects in antigen processing can be overcome by

MHC-independent binding (Curran et al., 2012). A broad range of patients can therefore be treated with CAR T cells, regardless of their HLA type. The modular CAR design enables the fusion of one or more signaling domains. In this way, CAR T cells have, besides improved effector T cell functions, the ability to induce memory T cell phenotypes.

Although the clinical efficacy of CAR T cells has already been proven in hematological malignancies, some major challenges have still to be considered for a broader use in the clinic. CAR toxicity is a major concern and increasing the clinical safety of CAR T cell based therapies remains a priority. On-target, off-tumor activity resulting in the destruction of normal tissues and cytokine storms associated with important immune responses are the two main forms of CAR T cell toxicity. A prominent example of on-target, off-tumor toxicity is B cell aplasia induced by CD19 CAR T cells (Brentjens et al., 2011a; Kochenderfer et al., 2012a). Although this can be managed by intravenous injection of immunoglobulin, such damages might not be prevented in other cases. Therefore, identifying and selecting highly specific tumor targets is essential (Sadelain et al., 2013). For CAR T cells, an ideal antigen is homogenously expressed on tumors but not on healthy tissues. Unlike other side effects, toxicity in form of cytokine release syndrome cannot be controlled by reducing the dosage of CAR T cells, as once administered, they continue to proliferate.

Within this context, new safety mechanisms to control CAR activity and to prevent these toxicities are more and more emerging. Systems including combinatorial CARs, dual CARs or switchable CARs are created to regulate CAR T cell activity in a spatial and temporal way (Gacerez et al., 2016; Maus and Powell, 2015). Furthermore, advances in CAR design allow to reduce toxicity while improving CAR efficacy by introducing the inducible caspase 9 fusion protein (Maus and Powell, 2015) or mutations as for example in the human Fc spacer or in the co-stimulatory CD28 domain.

The IgG1 Fc spacer domain, located between the antibody fragment on the extracellular site and the transmembrane domain of the CAR, seem to be required for the stable and efficient activation of several CD3ζ CAR expressing T cells (Guest et al., 2005b; Moritz and Groner, 1995). However, unintentional spacer binding to IgG1

Fc receptors of innate immune cells causes off-target activation of CAR T cells (Hombach et al., 2010). In this case, CAR T cells are activated independently from their target, resulting in monocyte and natural killer cell lysis as well as in cytokine release. Mutation of the PELLGG and ISR motif corresponding to the Fcγ receptor (FcγR) binding domain and localized in the CH2 region of the spacer domain prevents unspecific CAR T cell activation by FcγR expressing cells (Hombach et al., 2010). Upon antigen binding, CAR T cell mediated immune responses are suppressed by tumor infiltrating regulatory T (T reg) cells, resulting in a less efficient tumor attack (Kofler et al., 2011). The negative impact of T reg cells on the clinical response of adoptive immunotherapy remains a problem (Yao et al., 2012). Lymphodepletion prior to CAR T cell treatment enables the elimination of T reg cells, resulting in a better engraftment and CAR T cell persistence (Dai et al., 2016). However, for the efficiency of CAR therapy, their regulation at a low level might be essential to obtain long-term CAR activity. Mutation of the LCK binding domain localized in the CD28 co-stimulatory region enables to block the IL-2 secretion induced by activated CAR T cells which is responsible for the proliferation and the suppressive activity of T reg cells. This led to an enhanced anti-tumor response even in the presence of T reg cells (Kofler et al., 2011). To elucidate the complexity of CAR downstream signaling, a broader understanding of how each region contributes to the overall CAR activity is necessary. Another challenge is the complex clinical management of CAR T cell therapies. The *ex vivo* manipulation of autologous patient T cells is an expensive process, but allows very personalized therapies.

1.4 Leukemia

1.4.1 Hematological malignancies

Neoplasms of hematopoietic and lymphoid tissues are malignant proliferations which can emanate from each and every B and T cell development stage (Piper, 2012). According to the current WHO classification of 2008, lymphoid neoplasms are classified based on their morphological, immunological, molecular and cytogenetic profile as well as their clinical characteristics (Campo et al., 2011). Depending on their localization (blood, lymph nodes or other lymphatic tissue), hematological

malignancies are referred to as leukemia, lymphoma or extranodal lymphoma (Piper, 2012).

Leukemia originates from the bone-marrow. Depending on the disease progression, it can be characterized as acute or chronic and, according to the myeloid or lymphoid origin, classified into acute lymphoblastic leukemia (ALL), chronic lymphoblastic leukemia (CLL), acute myeloid leukemia (AML) or chronic myeloid leukemia (CML). In 2012, 13 new leukemia cases out of 100 000 individuals were diagnosed in Germany [A]. CLL was diagnosed in more than one third of all leukemia cases. The incidence of leukemia is higher for men in comparison to women. One out of 67 men and one out of 91 women develop leukemia during their life time [B]. Depending on the type of leukemia, the affected age group is different. While CLL mainly affects elderly people, ALL is the most common cancer in children, especially under 5 years of age. However, ALL can occur at any age and the risk continually increases at an age of over 30 years (Piper, 2012) [B].

CLL, the most common type of leukemia, is a very heterogeneous disease. Despite the availability of various potent treatments, CLL cannot be cured with conventional therapies. Even after complete remission, the high risk of relapse results in a poor prognosis for patients with relapsed and refractory CLL (Porter et al., 2015). In 2012, the incidence of pediatric ALL patients in Germany was around five cases out of 100 000 children under five years (Piper, 2012). Combined chemotherapies cured 80-85% of children with ALL but for those who experienced relapsed and refractory disease (15-20%), the prognosis is very poor and the therapy was truly effective for only 30-50% of them (Locatelli et al., 2012). However, while success of chemotherapy is observed for pediatric ALL, this is not the case for adults. Despite a high initial complete remission rate, relapse often occurs and the overall five year survival rate is about 30% (Ai and Advani, 2015). Indeed, at five years after relapse, long term remission remains only at around 7% (Dinner et al., 2014).

1.4.2 Current therapy options

Although significant progress was made in treating CLL, the disease remains incurable. The current standard treatment consists of a chemotherapy using

fludarabine in combination with cyclophosphamide enabling a complete remission of 69% of treated CLL patients (Piper, 2012). Using Rituximab, an anti-CD20 monoclonal antibody, in addition to the previous chemotherapy treatment enhances the outcome (Tam et al., 2008). In many cases the disease progression is inevitable. The bone marrow transplantation remains the only potential curative treatment although the risk of mortality is high (Piper, 2012). While the use of immunochemotherapy increases the overall response rate of CLL patients, there is an urgent need to develop strategies for a long term tumor cell elimination.

The current treatment for ALL consists of a chemotherapy regimen in four steps. Depending on the risk of treatment failure, the therapy intensity varies (Cooper and Brown, 2015; Piper, 2012). The first part is a remission induction therapy which aims to induce complete remission by eliminating the leukemia cells. For patients with induction failure, an allogeneic bone marrow transplant might be an option. The following step is the consolidation phase to remove the residual tumor cells whereas the central nervous system (CNS) prophylaxis is used for ALL eradication from the CNS. The final maintenance regimen lasts over two to three years and reduces the risk of relapse (Cooper and Brown, 2015; Piper, 2012). Allogeneic hematopoietic stem cell transplant (HSCT) is indicated for adults and children with delayed remission (over four weeks) presenting high relapse risk or refractory disease who cannot be rescued with standard chemotherapies. The low cure rates with HSCT range between 10 to 30% (Dinner et al., 2014). As for CLL, there is an obvious need to find new therapies to improve the outcome of ALL in children and adults.

1.4.3 CAR based therapies

In the context of enhancing the overall cure rates for CLL and ALL patients, antibody based therapies represent a promising strategy. Indeed, targeting antigens to activate the immune system either by single agents or in combination with chemotherapy to eliminate leukemia is of growing interest (Dinner et al., 2014; Koehler et al., 2012). The use of immunotherapy offers new mechanisms of action and different side effect profiles. The clinical application of monoclonal antibody based therapies including Rituximab and Epratuzumab, an anti-CD20 and anti-CD22

monoclonal antibody, respectively, improved the overall survival of CLL and ALL patients (Ai and Advani, 2015; Annesley and Brown, 2015; Koehler et al., 2012).

The chimeric antigen receptor based therapy represents another rational and promising approach to overcome the poor prognosis of patients with relapsed and refractory leukemia. CD19 is the most investigated target for CAR T cell therapy. Recent successful Phase I clinical trials with CD19 CAR therapy show promising results in the treatment of leukemia (Oluwole and Davila, 2016). For relapsed and refractory ALL, 67 - 90% of patients achieved a complete remission (Oluwole and Davila, 2016). Complete and long-term remission was also obtained for refractory CLL patients (Kalos et al., 2011). Autologous patient T cells were therefore genetically modified *ex vivo* with a CAR specific for CD19, leading to their redirection toward tumor cells once injected back into the patient. The efficacy of CAR T cell therapy is enhanced by prior lymphodepletion which prepares a favorable environment for the transduced T cells (Gattinoni et al., 2006).

Besides the clinical success of CAR therapy, related treatment toxicity remains challenging and several multicenter Phase II clinical trials are currently investigating clinical CAR efficacy and safety (Oluwole and Davila, 2016). While B cell aplasia, observed in all treated patients, can be managed by lifelong immunoglobulin replacement, further on-target, off-tumor toxicity and cytokine release can lead to adverse effects with severe complications. Furthermore, as CAR T cells target one specific antigen, this selective pressure induces loss of the target as seen after CD19 CAR T cell treatment of ALL (Grupp et al., 2013). Controlling these side effects is a requirement for the establishment of CAR T cell therapy as a powerful treatment regimen to cure hematological malignancies.

Despite the success of CD19 CAR T cell therapy, new antigens need to be found to develop alternative CAR T cell treatments for patients with CD19 negative hematological malignancies. Several ongoing Phase I clinical trials are investigating the efficacy of CAR T cells to treat patients with B-cell malignancies by targeting either the inactive tyrosine-protein kinase transmembrane receptor ROR1, the immunoglobulin kappa chain (Igκ), CD20 or CD22 (Jackson et al., 2016).

The human cell surface CD22 antigen which is essential in B-lineage differentiation, has a B cell-restricted expression, including malignant B cells (Nitschke, 2009;

Tedder et al., 2005; Tu et al., 2011). CD22 is highly expressed in B-ALL ranging from 50-100% expression (Shah et al., 2015). Its restricted expression profile and the clinical success of related therapies like Epratuzumab confirm CD22 as an excellent potential therapeutic target in B cell malignancies. A novel CD22 targeted CAR T cell therapy would therefore be an ideal treatment option. Derived from the clinically established murine IgG1 antibody RFB4 (Campana et al., 1985), the previously generated humanized and highly specific anti-CD22 scFv (Krauss et al., 2003b) is a well-suited antibody for the development of this new therapy.

1.5 Aim of the study

During the treatment of hematological malignancies with antigen specific CAR T cells, surviving target-negative tumor cell subpopulations are often emerging. Consequently, to improve the overall long term survival rate of relapsed and refractory leukemia and lymphoma patients, alternative CAR therapies targeting new antigens are needed. The goal of the present thesis is the generation of a CD22 specific chimeric antigen receptor for the adoptive T cell therapy of CD22 positive leukemia and lymphoma.

For this purpose, a highly stable humanized anti-CD22 scFv is used as antigen binding domain and cloned into a third generation CAR backbone comprising the signal transduction domains of CD3ζ, CD28 and 4-1BB. We first investigate CAR stability by determining if the stability of the scFv is maintained when expressed in a CAR format. The humanized anti-CD22 CAR is expected to be more stable than its murine counterpart which is analyzed in comparison.

Mutations introduced in the human Fc spacer (ΔFc) and in the co-stimulatory CD28 domain (ΔCD28) aim to reduce the on-target, off-tumor toxicity while enhancing tumor specific cell death induction in the presence of regulatory T cells. The novel parental, the ΔFc and ΔCD28 single mutated as well as the double mutated ΔFc-ΔCD28 CD22 CAR variants are characterized *in vitro*. Through lentiviral gene transfer, each CAR variant is transduced into T cells isolated from human blood and its CAR T cell activation is investigated *in vitro.* CD22 CAR T cell dependent target

affinity, cytokine release and lysis of antigen presenting tumor cells are assessed in depth for each variant.

Within this project, a CD22 CAR lead candidate with the best profile regarding effectiveness, stability and safety is selected and will be further developed for a translation into the clinic. For following preclinical studies, the engraftment of leukemia tumor cells is examined in a preliminary *in vivo* study using a suitable mouse model.

2 Materials and methods

2.1 Materials

2.1.1 Laboratory equipment

The laboratory equipment used in this thesis is listed in Table 1.

Table 1: Laboratory equipment

Instruments	Description	Supplier
Balance	2200-2NM	Kern & Sohn GmbH
Centrifuges	Heraeus Megafuge 16R	Thermo Scientific
	Heraeus Megafuge 40R	Thermo Scientific
	J2-MC	Beckman
	Rotina 420R	Hettich
	PCV-2400	Grant-Bio
	Micro 200R	Hettich
CO2 incubator	Nu-5500-E	Nuaire
	Heracell 150	Thermo Scientific
Cryo conservation	CoolCell LX BCS-405	Biocision
Electroblotting system	PowerPac Basic HC	Bio-Rad
	Trans-Blot Semy-Dry Transfer Cell	Bio-Rad
Electrophoresis systems	PowerPac Basic	Bio-Rad
	XCell SureLock Mini-Cell	Bio-Rad
Flow cytometer	FACS Canto	Becton Dickinson
FPLC system	ÄKTA FPLC	GE Healthcare
	ÄKTA Pure	GE Healthcare
Freezer	MDF-U7 4V	Sanyo Electrics
	LGex 3410 Mediline	Liebherr
	Froster-720	Kirsch
Fridge	LKexv 5400 Mediline	Liebherr
	LKexv 1800 Mediline	Liebherr
Gel visualization	Quantum ST4	Vilber Lourmat
Heating block	MRK-13	HLC
Imaging	Photon Imager	Biospace Lab
Microplate reader	Epoch	BioTek
Microscope	CKX31	Olympus
pH-Meter	PB-11	Sartorius
Photometer	NanoDrop ND-1000	Thermo Scientific
	Epoch	BioTek
Pipette controllers	Pipetus	Hirschmann
	PIPETMAN classic	Gilson
	PIPETMANN neo	Gilson

	PIPETGIRL	Integra
Rotating mixer	RM5-30V	Ingenieurbüro CAT
Separator	QuadroMACS Separator	Miltenyi Biotech
Shaker	Innova44	New Brunswick scientific
	Multitron Pro	Infors HT
Sterile benches	Safe 2020	Thermo Scientific
	HERAsafe KSP	Thermo Scientific
Thermal cycler	T3000	Biometra
Vacuum pump	LC16	ATMOS
	N816.3KN.18	KMF Neuberger
Vortex	MS3 digital	IKA
	Vortexgene 2 G560E	Scientific Industries
Water bath	GFL-1003	GFL

2.1.2 Disposables

The disposables used in the present thesis are listed in Table 2.

Table 2: Disposables

Description	**Supplier**
Bottle top vacuum filter	Nalgene
Canula	Becton Dickinson
Cell culture flasks	Greiner Bio-One
Cell culture plates	Greiner Bio-One
Centricon Plus-70	Merk Millipore
Conical tubes (15 ml, 50ml)	Greiner Bio-One
Costar assay plate, 96 well, half area	Corning
Cryogenic storage vials (2ml)	Greiner Bio-One
Dialysis membranes ZelluTrans	Carl Roth
Dispenser tips	Greiner Bio-One; Corning; Biozym
FACS tubes	Becton Dickinson
Gloves (latex-free)	Sempermed
MACS Separation column 25 LS column	Miltenyi Biotech
Micro tubes (1.5 ml, 2ml)	Eppendorf
Nitrocellulose membrane	Neo-Lab
Reagent reservoir	Corning
Serological pipets (5ml, 10ml, 25 ml, 50ml)	Corning
Sterile filter Millex-GS	Merk Millipore
Syringes (1ml, 2ml, 5ml, 10ml, 60ml)	Becton Dickinson
Tissue culture dish with 20 mm grid	Corning

2.1.3 Chromatography columns

Chromatography columns used on the FPLC-system are listed in Table 3.

Table 3: Chromatography columns

Column	Supplier
HisTrap FF (5 mL)	GE Healthcare (17-5255-01)
HiLoad 16/60 Superdex 75 prep grade	GE Healthcare (17-1068-01)
Superdex 200 10/300 GL	GE Healthcare (17-5175-01)

2.1.4 Standard kits

Table 4 gives an overview of the used standard kits.

Table 4: Standard kits

Description	Supplier
Cell proliferation Kit II (XTT)	Roche (11 465 015 001)
EndoFree Plasmid Giga Kit	QIAGEN (12391)
EndoFree Plasmid Mega Kit	QIAGEN (12381)
FITC Annexin V apoptosis Detection Kit	Becton Dickinson (556547)
Human IFNγ ELISA Set	Becton Dickinson (555142)
Human IL-2 ELISA KIT Set	Becton Dickinson (555190)
NucleoBond Xtra Maxi Plus	Macherel-Nagel (740416.50)
Pan T Cell Isolation Kit	Miltenyi Biotech (130-096-535)
QIAprep Spin Miniprep Kit	QIAGEN (27106)
QIAquick Gel Extraction Kit	QIAGEN (28706)
QIAquick PCR Purification Kit	QIAGEN (28106)

2.1.5 Chemicals and reagents

Chemicals and reagents used in this thesis are listed in Table 5.

Table 5: Chemicals and reagents

Product	Supplier
Agar	BD Biosciences (214010)
Agarose	Invitrogen (16500-500)
Carbenicillin	Carl Roth (6344.2)
Coomassie Brilliant Blue R-250 (C.I. 42660)	Carl Roth (3862.1)
Disodium hydrogen phosphate (Na_2HPO_4)	Carl Roth (P030.2)
DMEM	Gibco (31053-028)
DMEM + GlutaMAX	Gibco (61965-026)

DMSO	Serva (20385.01)
DNA gel loading buffer	New England Biolabs (B7021S)
DNA ladder (100 bp and 1000 bp)	New England Biolabs (N3231S and N3232L)
DTT	Carl Roth (6908.3)
Dulbecco´s PBS; no Calcium; no Magnesium	Gibco (14190-094)
EDTA	Sigma (E5134-250G)
Ethanol extra pure	Carl Roth (9065.1)
Ethidium bromide	Carl Roth (2281.1)
FBS	PAN Biotech (P40-47500)
Ficoll Plaque PLUS	GE Healthcare (17-1440-03)
FreeStyle F17, without L-Glutamine	Thermo Scientific (A1383501)
Geneticindisulfate (G418) solution (50mg/ml)	Carl Roth (0239.3)
Glycerol	AppliChem (A3739,0500)
Hydrochloric acid	Carl Roth (4265.1)
IL-2 (PROLEUKIN® S 18 Mio. IE)	Novartis (02238131)
Imidazol	Carl Roth (X998.4)
Isofluran	Baxter
Isopropanol	Carl Roth (9866.2)
Kanamycin	Carl Roth T832.1
Kolliphor P188	Sigma-Aldrich (15759)
L-glutamine 200 mM	Thermo Scientific (25030081)
Luciferin-EF	Promega (E655B)
Methanol	Carl Roth (8388.2)
Milk Powder	Carl Roth (T154.2)
Opti-MEM reduced serum medium	Thermo Scientific (31985062)
Penicillin-Streptomycin (10000 U/ml und 10mg/ml)	Sigma-Aldrich (P0781)
Pierce ECL Western Blotting Substrate	Thermo Scientific (32106)
Polybrene Hexadimethrine bromide	Sigma (107689)
Polyethylenimine	Polysciences (23966)
Potassium chloride	Carl Roth (6781.1)
Potassium dihydrogen phosphate	Carl Roth (P018.1)
Rainbow Fluorescent Particle 3.0 - 3.4 µm	Becton Dickinson (556291)
RPMI-1640 + GlutaMAX	Gibco (61870-010)
Sodium bicarbonate	Carl Roth (A135.1)
Sodium carbonate	Carl Roth (6885.2)
Sodium chloride	Carl Roth (3957.1)
Sodium dihydrogen phosphate	Carl Roth (K300.3)
Sodium dodecyl sulfate	Carl Roth (2326.1)
Spectra multicolor Broad Range Protein Ladder	Thermo Scientific (26634)
Sulfuric acid	In house
TMB Substrate reagent Set	Becton Dickinson (555 214)

TN1, tryptone 1	Organotechnie (19553)
Tris	Carl Roth (4855.2)
Trypsin/EDTA	PAN Biotech (P10-0231 SP)
Tryptan blue	Sigma (T8154)
Trypton/Pepton ex casein	Carl Roth (8952.3)
Tween 20	Gerbu (2001.0500)
X-Vivo 20	Lonza (BE04-448Q)
Yeast Extract	Carl Roth (2363.3)

2.1.6 Buffer and solutions

Buffer and solutions were prepared as shown in Table 6.

If nothing is additionally mentioned, components were diluted in distilled water (dH2O) and pH adjusted with sodium hydroxide or hydrochloric acid.

Table 6: Buffer and solutions

Description	Composition
PBS	PBS, 10x (10%; v/v)
PBS 10X	1,4 M NaCl 27 mM KCl 101 mM Na_2HPO_4 18 mM KH_2PO_4
PBS-T	0,5 ml/l Tween 20 in PBS
MPBS	20 g/l milk powder in PBS
FACS buffer	2 mM EDTA 1% FBS in PBS
IMAC binding buffer (pH 7,4)	20 mM NaH_2PO_4 500 mM NaCl 10 mM Imidazol
IMAC elution buffer (pH 7,4)	20 mM NaH_2PO_4 500 mM NaCl 500 mM Imidazol
Western Blot Transfer buffer	48 mM Tris 39 mM Glycin 1,3 mM SDS 20% (v/v) methanol adjusted to pH 9.0, filter sterilized
Coomassie solution	70 mg/l Coomassie Brilliant Blue G-250

	35 mM HCl
DTT solution (10X)	2,5 M DTT
ELISA Coating Buffer	7,13 g/l NaHCO3 1,59 g/l Na_2CO3 adjusted to pH 9.5
ELISA Assay Diluent	10% FBS in PBS
ELISA Wash Buffer	0,05% Tween-20 in PBS
2N H_2SO_4	13,89 ml H_2SO_4 236,11 ml H_2O
TAE Buffer	242 g/l Tris 100 ml/l EDTA 57,1 ml/l glacial acetic acid
Freezing medium	10% DMSO (v/v) in FBS

2.1.7 Primers

Oligonucleotides used for sequencing (method 2.2.10) or for site-directed mutagenesis (method 2.2.7) are summarized in Table 7.

All primers were purchased from Invitrogen (Life Technologies).

Table 7: Primers for sequencing and mutagenesis

Name	**Sequence (5‘-3´)**
Sequencing primers	
pENTR sense	CATAAACTGCCAGGCATCAAACTAAG
pENTR AS	GATTTTGAGACACGGGCCAGA
PCR2	TTAGCTCACTCATTAGG
Primer for PCR	
RFB4_1	TCGGAAGTGCAGCTGGTGGAG
RFB4_2	TATAGGATCCTTTGATTTCCAGCTT
hCD22_1	GCCACCATGGAAAGGCACTGGATCTTTCTC
hCD22_2	TAGCGGCCGCACGTTTGATTTCCAGTTTGG
Mutagenesis primers	
hIgG1_CH2-Fw	AAGGTCTCCAACAAAGCC
hIgG1_CH2-Rev	TTGTTGGAGACCTTGCAC
CD28_Lck-Fw	CCCACCCGCAAGCATTACCAGGCCTA TGCCGCCGCACGCGACTTCGCAGCCTAT
CD28_Lck-Rev	ATAGGCTGCGAAGTCGCGTGCGGCG GCATAGGCCTGGTAATGCTTGCGGGTGGG

hCD22_LY-Fw	CAATTATTTAAACTGGTACCAACAGAAACCAGGGAAAG
hCD22_LY- Rev	CTTTCCCTGGTTTCTGTTGGTACCAGTTTAAATAATTG

2.1.8 Plasmids

In Table 8, the used vectors are briefly described. The corresponding vector maps are illustrated in the appendix.

Table 8: Plasmids

Vector	Description
pENTR1a	Entry vector for LR reaction of Gateway cloning
pRRL	Lentiviral vector used for transient expression of lentivirus in mammalian cells
Lentiviral helper plasmid #1	Helper plasmid for lentivirus production
Lentiviral helper plasmid #2	Helper plasmid for lentivirus production
pEUC6B	Subcloning vector for scFv cloning
pEE12.4	Used for transient expression of scFv antibodies by mammalian cells

2.1.9 Antibodies

Commercially purchased antibodies and antibodies conjugates are described in Table 9.

Table 9: Antibodies and antibody conjugates

Name	Description
R-Phycoerythrin conjugated AffiniPure F(ab´)$_2$ fragment goat anti-human IgG (Jackson ImmunoResearch, 109-116-098)	Polyclonal F(ab')$_2$ fragment from goat against human IgG (Fc specific), linked to R-Phycoerythrin (PE)
APC Mouse Anti-Human CD3 (Becton Dickinson, 555335)	Monoclonal IgG from mouse against human CD3, linked to Allophycocyanin (APC)
Pacific Blue Mouse Anti-Human CD3 (Becton Dickinson, 558117)	Monoclonal IgG from mouse against human CD3, linked to Pacific Blue
PE-Cy 7 Mouse Anti-Human CD19 (Becton Dickinson, 557835)	Monoclonal IgG from mouse against human CD19, linked to a dye combining Phycoerythrin and cyanine (PE-Cy 7)
PE-Cy 7 Mouse Anti-Human CD14 (Becton Dickinson, 557742)	Monoclonal IgG from mouse against human CD14, linked to PE-Cy 7
OKT-3	Monoclonal IgG from mouse against

(in house)	human CD3
Streptavidin Alexa Fluor 488 (Thermo Scientific, S11223)	Streptavidin covalently bound to Alexa Fluor 488 dye
HRP Mouse Anti-His (Santa Cruz, S8036)	Monoclonal IgG from mouse against histidine tag
Mouse anti c-myc antibody (Roche, 11667149001)	Monoclonal IgG from mouse against c-myc tag (clone 9E10)
FITC Goat Anti-Mouse IgG (Jackson ImmunoResearch, 115-095-008)	Polyclonal IgG from goat against murine IgG (Fc-specific), linked to Fluorescein (FITC)

2.1.10 Enzymes and proteins

Enzymes and proteins used in this thesis are listed in Table 10.

Table 10: Enzymes and proteins

Enzymes / Proteins	Supplier
Alkaline Phosphatase from calf intestine	New England Biolabs
Pfu Plus DNA Polymerase	Thermo Scientific
T4 DNA Ligase	Thermo Scientific
Gateway LR Clonase ™ II	Invitrogen (11791-100)
Restriction enzymes	New England Biolabs
Human Fc (hFc) protein	In house
Recombinant human CD22-hFc (hCD22-hFc)	Prof. Nitschke, Erlangen University
Biotin-Protein L	Genscript

2.1.11 Bacteria strain

Amplification of DNA was performed with the bacterial strain *Escherichia coli* (*E. coli*) XL1-Blue (Table 11).

Table 11: Bacteria strain

Bacteria strain	Supplier
Escherichia coli XL1-Blue Genotype: recA1 endA1 gyrA96 thi-1 hsdR17 supE44 relA1 lac [F´pro AB lac1^{q}ZΔM15 Tn10 (Tet^{r})]	Agilent; #200249

2.1.12 Bacteria culture media and supplements

Bacterial culture media were prepared as shown in Table 12.

Table 12: Bacterial culture media

Description	Composition
LB high salt	10 g/l trypton, 5 g/l yeast extract, 10 g/l NaCl, in dH_2O autoclaved
LB agar	15 g agar in 1l LB
Ampicillin stock solution	100 mg/ml ampicillin sodium salt, in dH_2O, filter sterilized. For the selection of ampicillin resistant bacterial strain, the used concentration was 100 µg/ml.
Kanamycin stock solution	100 mg/ml ampicillin sodium salt, in dH_2O, filter sterilized. For the selection of ampicillin resistant bacterial strain, the used concentration was 100 µg/ml.

2.1.13 Eukaryotic cell line and primary cells

An overview of used cell lines is represented in Table 13. The cell line THP-1 was kindly provided by Prof. Dr. med Hinrich Abken, Universität Köln. The cell line HEK-293-E was licensed from the National Research Council, Biotechnological Research Institute, Montreal, Canada.

Table 13: Human cell lines and primary cells

Cell line	Description; Supplier	Culture medium
HEK-293-E	Human embryonic kidney 293 adapted for suspension culture and optimized for high protein expression *National Research Council*	FreeStyle F17
HEK-293T	Human embryonic kidney 293 cell line stably expressing the SV40 large T antigen *ATCC, CRL 3216*	DMEM
Raji	Burkitt´s lymphoma *ATCC, CCL-86*	RPMI-1640
Nalm-6	Acute lymphoblastic leukemia *DSMZ, ACC-128*	RPMI-1640
Luciferase transfected Nalm-6	Acute lymphoblastic leukemia *in house*	RPMI-1640
Jurkat	Acute T cell leukemia *ATCC, TIB-152*	RPMI-1640

MCF-7	Adenocarcinoma *ATCC, HTB-22*	DMEM
THP-1	Acute monocytic leukemia *Prof. Dr. med H. Abken* *Universität Köln*	RPMI-1640
Human peripheral blood mononuclear cells (PBMC)	Isolated from fresh blood or buffy coats (platelet and leucocyte fraction from blood donations) from healthy donors. Buffy coats were obtained from *DRK Blutspendedienst Mannheim*	X-Vivo 20

2.1.14 Cell culture media

Cell culture media were prepared as described in Table 14.

Table 14: Cell culture media

Description	Composition
DMEM	DMEM + Glutamax + FBS (10%, v/v) + Penicillin (100 U/ml) + Streptomycin (100 µg/ml)
DMEM w/o FBS	DMEM + Penicillin (100 U/ml) + Streptomycin (100 µg/ml)
RPMI-1640	RPMI-1640 + Glutamax + FBS (10%, v/v) + Penicillin (100 U/ml) + Streptomycin (100 µg/ml)
FreeStyle F17	FreeStyle F17 + Kolliphor P188 (10 ml/l) + L-glutamine (20 ml/l) + G418 (0,5 ml)
X-Vivo 20	X-Vivo 20

2.1.15 Mice

The mouse strain used for the preliminary *in vivo* assay is listed in Table 15.

Table 15: Mice

Mouse strain and description	Supplier
NOD.CB17-Prkdc^scid/NCrHsd six to eight weeks of age, female	Envigo (17004F)

2.1.16 Data treating software

Overview of used software and their applications are listed in Table 16.

Table 16: Software

Software	Description	Supplier
FACSDiva	Acquisition and analysis of flow cytometer data	Becton Dickinson
FACSSuite	Acquisition and analysis of flow cytometer data	Becton Dickinson
Gen 5.2	Data processing of used plate reader	BioTek
Genious R6.1.6	Sequence evaluation and vector visualization	Biomatters
GraphPad Prism 5.0	Figure preparation; Statistical analysis	GraphPad software
Mendeley	Reference manager	Elsevier
MS Office 2010	Data evaluation, text processing	Microsoft
ND-1000 V3.8	Protein concentration measurement	Tecan
Photoshop Elements 10	Image processing	Adobe Systems
Photovision +	Image acquisition	Biospace Lab
Quantum ST4	Gel documentation	Vilber Lourmat
SilverFast 8	Image acquisition	LaserSoft Imaging
Unicorn 5.10	Flow cytometry analysis and evaluation	GE Healthcare
Unicorn 6.3	Flow cytometry analysis and evaluation	GE Healthcare

2.2 Molecular based methods

2.2.1 Restriction enzyme digestion

Digestion of DNA with restriction enzymes was performed according to the manufacturer's instructions (New England Biolabs). In a final volume of 20 µl, 2 – 4 units of restriction enzyme per 1 µg of DNA as well as 1x buffer was used to carry out the digestion at 37 °C for 1 h.

For a plasmid digestion, in order to prevent religation, 5 units of alkaline phosphatase calf-intestinal (CIP) was added to dephosphorylate the vector.

2.2.2 Gel electrophoresis and gel extraction

To verify their size (method 2.2.1), digested DNA fragments were analyzed by agarose gel electrophoresis. A 0.8 - 2% agarose gel was prepared by first boiling the desired amount of agarose in 1x TAE buffer and then mixing this solution with 0.5 µg/ml of ethidium bromide, a DNA intercalating agent. Samples blended with 5x gel loading dye were electrophoretically separated together with a size standard in 1x TAE buffer at 75 volts.

DNA band with the correct size was extracted from the agarose gel with a scalpel and purified using the Qiaquick Gel Extraction Kit according to the manufacturer's instructions (QIAGEN).

2.2.3 DNA purification

Purification of specific DNA fragments having the correct size was performed using the Qiaquick PCR purification Kit according the manufacturer's instructions (QIAGEN).

2.2.4 Ligation

In a final volume of 20 µl, 50 ng digested plasmid was mixed together with a 3x molar excess of digested DNA insert, 1 unit of T4 DNA ligase and 2 µl of 10x ligase buffer. Ligation reaction occurred for one hour at room temperature and 2 µl of the preparation was further transformed in *E.coli* XL1-Blue bacteria (method 2.3.1).

2.2.5 Preparation of plasmid DNA

Small and high amount of plasmid DNA were respectively prepared with the QIAprep Spin Miniprep Kit (QIAGEN) and NucleoBond Xtra Maxi Plus (Macherey-Nagel).

Plasmid DNA for lentivirus production (method 2.5.1) was obtained with either the EndoFree Plasmid Mega Kit or EndoFree Plasmid Giga Kit (QIAGEN).

All the preparations were performed according to the manufacturer's instruction.

2.2.6 Polymerase Chain Reaction

The polymerase chain reaction (PCR) was applied to amplify DNA and to introduce new gene sequences as well as restriction sites. For this purpose, the KAPAHifi PCR Kit was used according the manufacturer's instructions. Mixture of a typical PCR reaction is shown in Table 17.

Table 17: PCR reaction

Component	Volume (µl)	Final amount/concentration
DNA	1-5	5-20 ng
5x KAPAHifi buffer	5	1x
dNTP mix (10 mM)	0.75	300 µM each
5' primer (25 µM)	0.5	500 nM
3' primer (25 µM)	0.5	500 nM
KAPAHifi Polymerase (1 U/µl)	0.5	0.02 U/µl
H_2O	*ad* 25	-

Reaction was performed in the thermal cycler T3000 (Biometra) according to the condition presented in Table 18. The appropriate melting temperature of each primer was estimated with the following formula:

$$Tm = [4x(C+G) + 2x(A+T)] - 4\ °C$$

Table 18: PCR conditions

Step	Temperature (°C)	Time	Cycles
Initial denaturation	98	5 min	1X
Denaturation	98	30 sec	
Annealing	Tm	30 sec	18-35X
Elongation	72	30 sec	
Finale elongation	72	7 min	1X
Cooling	4	∞	1X

2.2.7 Site directed mutagenesis

Site directed mutagenesis is a method to introduce specific mutations in a double strand plasmid DNA. The mixture of a typically site directed mutagenesis performed with the Pfu DNA polymerase is presented in Table 19.

Table 19: Site directed mutagenesis preparation

Component	Volume (µl)	Final amount/concentration
Plasmid DNA	1	100 ng
10x Pfu buffer	5	1x
dNTP mix (10 mM)	1.25	0.2 mM each
Mutagenic primer 1 (100 ng/µl)	1.25	125 ng
Mutagenic primer 2 (100 ng/µl)	1.25	125 ng
Pfu Plus Polymerase (5 U/µl)	0.5	2.5 U
H_2O	*ad* 50	-

Reaction was performed in the thermal cycler T3000 (Biometra) according to the following conditions (Table 20):

Table 20: Site directed mutagenesis conditions

Step	Temperature (°C)	Time	Cycles
Initial denaturation	95	5 min	1X
Denaturation	95	1 min	
Annealing	68	30 sec	18X
Elongation	68	1 min/1 Kb	
Finale elongation	68	7 min	1X
Cooling	15	∞	1X

To finalize the site directed mutagenesis, the preparation was digested with DpnI for 2 h at 37 °C in order to cut the methylated non mutated strand. Transformation in competent *E.coli* XL1-Blue bacteria was performed with 10 µl of the DNA mixture.

2.2.8 Gateway cloning

For the gateway reaction, 200 ng DNA of the entry clone containing the CAR gene of interest flanked by attL1 and attL2 sequences was mixed with 200 ng DNA of the destination vector (Figure 6). After adding 1 µl LR clonase enzyme mix to the preparation an incubation of 1 h at room temperature allows the enzyme to first excise the CAR gene from the entry clone and then to integrate it into the destination vector, resulting in the new formed expression clone containing the CAR gene. To stop the reaction, 0.5 µl proteinase K (2 mg/ml) was added and the preparation incubated for 10 min at 37 °C. Transformation in competent *E.coli* XL1-Blue bacteria and selection of carbenicillin resistant expression clones was performed with 2 µl of the DNA mixture. When using the BP clonase, the reaction can be performed in the opposite way.

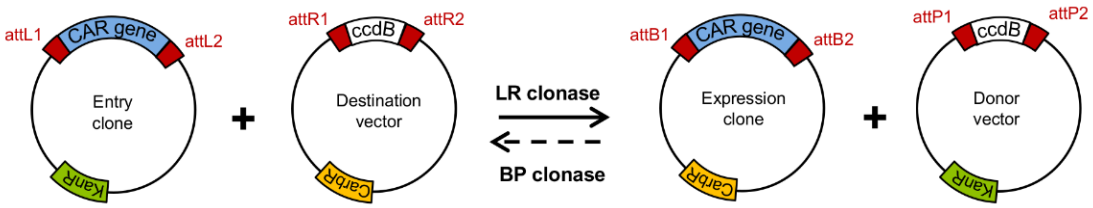

Figure 6: Schematic representation of the gateway cloning

2.2.9 Concentration measurement of DNA

Concentration of H_2O diluted double strand DNA was determined on a spectrophotometer. The absorbance (Abs) of the samples was measured at a wavelength of 260 nm and 280 nm and purity of the preparation was given by the ratio Abs 260 nm / Abs 280 nm.

2.2.10 Sequencing

Sequencing of plasmid DNA was carried out by the company GATC using the customized sequencing primers pENTR sense, pENTR AS and PCR2. Their sequences are shown in Table 7 and their binding positions are represented on the vector maps in appendix.

2.3 Bacteria and cell based methods

2.3.1 Transformation of bacteria

Chemically-competent XL1-Blue bacteria were slowly thawed on ice and 100 µl was added to the transforming DNA (10 µl of ligation or 2 µl of gateway reaction) carrying carbenicillin or kanamycin resistance already present in a cold Eppendorf tube. The bacteria/DNA suspension was first incubated on ice for 30 min, then at 42 °C for 90 sec and finally again on ice for 5 min. After adding 1 ml of LB medium, the mixture was shaken at 200 rpm and 37 ºC for 30 - 60 min. Bacteria were spread on LB agar plates containing carbenicillin (100 µg/ml) or kanamycin (50 µg/ml). The plates were incubated over night at 37 ºC and a single colony was picked from the plate the next day.

2.3.2 Cultivation of cells

The suspension cell line HEK-293-E was cultivated in a humidified shaker under constant conditions (120 rpm, 37 °C, 5% CO_2) in FreeStyle F17 medium with 0.1%

Kolliphor P188, 4 mM Glutamin and 25 µg/ml G418. Cells were splitted two to three times per week never allowing the maintained cells to exceed $2x10^6$ cells/ml.

Adherent cell lines HEK-293T and MCF-7 were cultivated in DMEM with GlutaMAX supplemented with 10% fetal bovine serum (FBS), 100 U/ml penicillin and 100 mg/ml streptomycin in a humidified incubator with 5% CO_2 at 37 °C. Suspension cell lines Nalm-6, Raji, Jurkat and THP-1 were cultivated under the same conditions in RPMI-1640 with GlutaMAX supplemented with 10% FBS, 100 U/ml penicillin and 100 mg/ml streptomycin whereas luciferase transfected Nalm-6 cells were cultivated in the same medium with additionally G418 (0.2 mg/ml). All these cell lines were maintained in 20 ml adapted culture medium, in T75 culture flasks and splitted two times per week (final cell density of $2x10^5$ cells/ml). Adherent cell lines were washed with 10 ml PBS and detached from a T75 flask by first adding 2 ml of a trypsin-EDTA solution and then incubating the suspension for 5 - 10 min at 37 °C. Cells were finally resuspended with 8 ml fresh medium. Suspension cells were directly diluted from the culture flask.

2.3.3 Freezing and thawing cells

For freezing, cell lines were centrifuge at 200 g for 10 min (adherent cells being previously detached from the bottom of a T75 flask as described in the method 2.3.2). After one washing step with adapted cell culture medium, the obtained cell pellet was resuspended in FBS with 10% (v/v) DMSO. This cell suspension, with a concentration of 0.5 - $1x10^7$ cells/ml was transferred in a cryovial and frozen to -80 °C at 1 °C/min in a cryo freezing container. Storage takes place in liquid nitrogen.

Cryo-conserved cell lines were rapidly thawed in a water bath at 37 °C and transferred in a 50 ml Falcon tube. Pre-warmed culture medium was then added drop wise to the cell suspension before transferring it into a T25 flask for cultivation. Depending on growth, expansion in a T75 flask occurs two to three days later.

2.3.4 Transient production of scFv in mammalian cells

Murine anti-CD22 scFv RFB4 was transiently expressed in HEK-293-E cells and secreted in the cell culture supernatant. Two days before transfection, HEK-293-E cells were seeded with a cell density of $0.5x10^6$ cells/ml in F17 medium containing 0.1% Kolliphor P188, 4 mM Glutamin as well as 25 µg/ml G418 and incubated in a humidified shaker under constant conditions (120 rpm, 37 °C, 5% CO_2). Transfection reagent polyethylenimine (2 µg/ml final concentration) and endotoxin free plasmid DNA (1 µg/ml final concentration) were separately prepared in 1/20 of the final culture volume in F17 medium without G418. After mixing both preparations together, the solution was incubated at room temperature during a few minutes and added to HEK-293-E cells having a cell density of 1.7 - $2x10^6$ cells/ml. One day later, the cell suspension was supplemented with 0.5% (w/v) trypton N1. After 5 days, cells were centrifuged at 200 g for 20 min at 4 °C. Obtained supernatant was further clarified by a second centrifugation step (200 g, 20 min at 4 °C) and purified using an immobilized metal ion chromatography (method 2.4.1) and a size exclusion chromatography (method 2.4.2).

2.3.5 Determination of scFv stability

To determine the scFv stability, mammalian produced (method 2.3.4) antibody fragments (12 µg/ml) were incubated in 90% human serum or PBS over 7 days at 37 °C and 5% CO_2. At different time points, a sample was taken out and stored at -20 °C before analyzing its binding to antigen expressing cells.

To determine the binding of the antibody fragments, $5x10^5$ Raji cells were incubated with 100 µl of each stored scFv sample at 4 °C for 60 min. After several washing step with Fluorescence-Activated Cell Sorting (FACS) buffer, cells were resuspended with 100 µl of mouse anti c-myc antibody (5 µg/ml; Roche) and incubated at 4 °C for 45 min. To detect bound antibody fragments, cells were washed again and incubated with a FITC conjugated goat anti-mouse antibody (7.5 µg/ml; Jackson ImmunoResearch) at 4 °C for 30 min in the dark. Fluorescence of marked cells was measured with the FACSSuite software. For each sample, the fluorescence signal of the negative control (Raji cells incubated with the detection antibodies) was

subtracted from the calculated mean of fluorescence. All the values were standardized to the mean of fluorescence obtained for the time point 0 h corresponding to 100% scFv binding to Raji cells.

2.3.6 Measurement of the expressing CAR T cells by FACS

To determine the lentivirus titer and the transduction rate, the percentage of T cells expressing the CAR construct on their surface was determined by flow cytometry (FACS).

After removing the medium from the titration plate (method 2.5.2), cells were resuspended in 1 ml PBS and transferred into FACS tubes whereas 200 - 500 µl of the transduced cell suspension (method 2.5.3) was directly transferred into FACS tubes. Addition of 2 ml FACS buffer and centrifugation at 1400 rpm for 4 min allows washing the cells. After removing the supernatant, the cell pellet was resuspended in 2 ml FACS buffer for a second washing step. Once the supernatant discarded, cells were resuspended in 100 µl FACS buffer. Specific detection antibodies were added to the cells and the cell suspension further incubated for 30 min at 4 °C in the dark. In order to remove the antibody excess, cells in the FACS tubes were washed two times with FACS buffer as previously mentioned. After a final resuspension in 400 µl PBS, the expression of CAR T cells was measured by using the FACSCanto flow cytometer.

2.3.7 Apoptosis assay

The tumor cell lysis was determined with an Annexin V Apoptosis detection Kit (Becton Dickinson). In case of apoptosis, phosphatidylserine normally located along the cytoplasmic side of the membrane is translocated to the extracellular membrane and therefore detectable by the highly fluorescently conjugated protein annexin V. The vital stain propidium iodide (PI) is unable to enter living cells during early apoptosis but can bind the DNA during late apoptosis.

To evaluate the tumor cell lysis induced by CAR T cells, these effector cells were co-incubated with target positive and negative tumor cells. The fraction of positively

expressing CAR T cells varied from 0% to 60% between the CAR constructs and between the donors (method 2.3.6). Therefore, the amounts of transduced CAR T cells were adjusted to incubate the same quantity of positively expressing CAR T cells.

In a well of a 48 well plate, $1x10^5$ expressing CAR T cells (previously washed two times with PBS) were incubated with $1x10^5$ target positive or negative tumor cells in 1 ml RPMI-1640 with GlutaMAX supplemented with 10% fetal bovine serum, 100 U/ml penicillin and 100 mg/ml streptomycin for 48 h at 37 °C and 5% CO_2. As control, effector cells and tumor cells only were incubated in the same conditions. Every reaction was performed in triplicates.

After two days, plates were centrifuged at 1400 rpm for 4 min. The supernatant was removed and transferred in a new 48 well plate to determine the secreted amount of IFNγ with an IFNγ ELISA (method 2.4.8). The remaining cells were resuspended, transferred in FACS tubes and washed two times with 2 ml FACS buffer (centrifugation at 1400 rpm for 4 min). After discarding the supernatant of each tube, specific detection antibodies (Becton Dickinson) were incubated with the remaining 100 µl cell suspension. $CD3^+$ T cells as well as Jurkat cells were detected with Pacific Blue conjugated mouse anti-human CD3 antibody (0.2 mg/ml; Becton Dickinson), Nalm-6 and Raji cells with PE-Cy7 mouse anti-human CD19 antibody (dilution 1:40; Becton Dickinson) whereas the THP-1 cells were identified with PE-Cy7 mouse anti-human CD14 antibody (dilution 1:20; Becton Dickinson). After 30 min at 4 °C, cells were washed twice with FACS buffer as previously explained whereby the supernatant was completely removed after the last washing step. Cell pellets were resuspended with annexin V binding buffer (1x), centrifuged at 1400 rpm for 4 min and the supernatant again discarded. To the 100 µl remaining cell suspension, annexin V (dilution 1:20) and PI (dilution 1:20) were added and the solution vortex before an incubation of 15 min at room temperature in the dark. Annexin binding buffer (1x) and 10 µl Rainbow beads ($10x10^6$ particles/ml) were supplemented to the FACS tubes before analyzing the percentage of living tumor cells with the flow cytometer FACS Canto II (Becton Dickinson) and the FACSDiva software (Becton Dickinson).

2.3.8 Isolation of human T cells

Isolation of human T lymphocytes was performed in two distinct steps. Peripheral blood mononuclear cells (PBMCs) were first isolated from the blood of a healthy donor by Ficoll density gradient centrifugation. In a second step, isolation of human $CD3^+$ T cells by depletion of magnetically labeled cells was done using the Pan T cell isolation Kit (Miltenyi Biotech).

A buffy coat (25 ml) obtained from the Blutbank Heidelberg was divided into 6, diluted with PBS to a finale volume of 35 ml, slowly layered over 15 ml of Ficoll-Plaque and centrifuge at 2200 rpm for 20 min whereby the brake was switched off. After the centrifugation, upper phases corresponding to the plasma were discarded. The interphases containing the mononuclear cells were slowly removed and transferred in new falcon tubes. After diluting the interphases with PBS to a final volume of 50 ml, they were centrifuged at 1800 rpm for 10 min whereby the brake was switched on. The supernatants were then removed and each cell pellet was resuspended separately in 50 ml fresh PBS before a new centrifugation step at 1400 rpm for 10 min. After removing the supernatants, the six cell pellets were resuspended together in 50 ml fresh PBS in order to pursue the isolation of human T lymphocytes.

The Pan T cell isolation Kit was used according to the manufacturer's instruction. The method consists of a negative selection of $CD3^+$ T cells. Cell surface antigens of non-targeted cells are recognized by using a cocktail of biotin conjugated antibodies. The binding of anti-biotin MicroBeads to these antibodies allows to magnetically label the non-targeted cells which are retained on the magnetic separation column whereas the fraction of $CD3^+$ cells passed through the magnetic field.

2.3.9 Activation of human isolated T cells

Isolated $CD3^+$ T cells were cultivated in X-Vivo 20 medium with IL-2 (300 U/ml) and the agonistic anti-CD3 antibody OKT-3 (100 ng/ml). After 48 to 72 h, almost all the cells were in an active division phase which is a prerequisite for lentiviral gene transfer.

2.3.10 XTT assay

The potency of CAR T cells towards tumor cell killing was determined with the cell proliferation Kit II (Roche).

To evaluate the tumor cell lysis induced by CAR T cells, these effector cells were co-incubated with target positive tumor cells. The fraction of positively expressing CAR T cells varied from 0% to 60% between the CAR constructs and between the donors (method 2.3.6). Therefore, the amounts of transduced CAR T cells were adjusted to incubate the same quantity of positively expressing CAR T cells.

In a well of a 96 well plate, $5x10^4$ expressing CAR T cells (previously washed two times with PBS) were incubated with $5x10^4$ target positive tumor cells in 200 µl RPMI-1640 with GlutaMAX supplemented with 10% fetal bovine serum, 100 U/ml penicillin and 100 mg/ml streptomycin for 24 h at 37 °C and 5% CO_2. As control, effector cells and tumor cells only were incubated in the same conditions. Every reaction was performed in triplicates.

After one day, the plate was centrifuged at 1400 rpm for 4 min. The supernatant (150 µl) was removed and transferred in a new 96 well plate to determine the secreted amount of IFNγ with an IFNγ ELISA (method 2.4.8). The remaining cell suspension (50 µl) was mixed with 100 µl XTT labeling mixture and incubated for one hour in a humidified atmosphere. The mix was then blended again and the absorbance measured using a TECAN reader at 450 nm. To calculate the specific cytotoxicity, the difference between the means with and without the tumor cells was calculated, normalized to the mean of the medium alone (used as control).

2.4 Protein based methods

2.4.1 IMAC

Purification of the produced murine anti-CD22 scFv was performed with an immobilized metal ion chromatography (IMAC) on a FPLC system. The supernatant, containing the protein was first dialyzed over night against IMAC binding buffer at 4 °C (method 2.4.4). The next day, dialyzed solution was filtered using a 22 µm filter and loaded on a HIS Trap FF column with a flow rate of 1 ml/min. The bound scFv

fragments were eluted from the column with a linear increasing concentration of imidazol obtained by mixing the IMAC binding buffer (imidazol concentration of 10 mM) with IMAC elution buffer (imidazole concentration of 500 mM). The eluted protein fractions were separated by SDS-PAGE (method 2.4.5) and purity of the recombinant protein was subsequently analyzed by Coomassie blue staining (method 2.4.6) and western blot (method 2.4.7). Further purification of the murine scFv was performed by size exclusion chromatography.

2.4.2 Preparative size exclusion chromatography

Size exclusion chromatography was performed on a FPLC-system using the HiLoad 16/60 Superdex 75 column. To obtain a precise separation on the column, the IMAC purified protein was first concentrated with centrifugal filter units and then injected into a 5 ml loop. The separation was performed at a flow rate of 0.3 ml/min in PBS. Eluted protein fractions were then further analyzed by Coomassie blue staining (method 2.4.6) and western blot (method 2.4.7) after SDS-PAGE (method 2.4.5). The purified monomeric protein fractions without aggregates and unspecific proteins were pooled, concentrated if needed, sterile filtered and finally stored at 4 °C.

2.4.3 Analytical size exclusion chromatography

The oligomeric state of purified antibody fragments was analytically assessed on a FPLC-system with the Superdex 200 10/300 GL column that was previously calibrated with protein standards of known molecular size. 10 µg of protein were loaded on a 25 µl loop and separated at a flow rate of 0.25 ml/min in PBS.

2.4.4 Dialysis and protein concentration

For the dialysis and concentration of recombinant proteins, membranes with define sizes were utilized. In order to obtain complete protein retention, the exclusion size of the used membranes was at least three times bigger than the molecular size of the protein.

Buffer exchanges of protein solutions were performed by dialysis. For this purpose, the dialysis membrane was first rehydrated by incubating it into the new buffer. After loading the membrane with the protein solution, the dialysis occurred in the new buffer with an excess volume of a 100 times the protein solution volume, overnight at 4 °C under constant rotation.

Concentration of the purified protein solution was performed with centrifugal filter units. The solution was therefore centrifuged at 4000 g, 4 °C until reaching the desired concentration.

2.4.5 SDS-PAGE

According to their molecular weight, the protein samples were separated by sodium dodecyl sulfate polyacrylamide gel electrophoresis (SDS-PAGE). An SDS-PAGE gel consisting of a staking gel (5% acrylamide) and a separating gel (12% acrylamide) was poured. Protein samples were mixed with 5 µl of 4x reducing loading dye and 5 µl of a 1 M DTT solution, then denatured at 70 °C for 10 min and finally transferred in the corresponding well. The separation via gel electrophoresis was then performed at 185 volts for 45 min.

2.4.6 Coomassie blue staining

For the detection of protein bands with Coomassie blue, electrophoretically separated SDS-PAGE gels were washed several times with dH_2O and then stained in a Coomassie blue solution for one hour at room temperature. Distaining was performed with several washing step using dH_2O until the protein bands were clearly visible.

2.4.7 Western Blot

The SDS-PAGE gel and a nitrocellulose membrane were separately equilibrated for 10 min with the western-blot transfer buffer. The transfer of the protein bands from the gel to the nitrocellulose membrane occurred in a semi dry blotting system at 25 volts for 30 min. To detect these recombinant proteins, the membrane was first

blocked for one hour in PBS-T containing 2% (w/v) milk powder. The immunostaining occurred through incubation with HRP conjugated anti-his antibody (2 µg/ml; Santa Cruz) diluted in PBS with 2% (w/v) milk powder. Unspecific antibody was then removed by washing two times with PBS-T and three times with PBS. Specific antibody binding was finally detected after incubation in Pierce ECL Western Blotting Substrate by chemiluminiscence.

2.4.8 IFNγ and IL-2 ELISA

The fraction of positively expressing CAR T cells varied from 0% to 60% between the CAR constructs and among the donors (method 2.3.6). Therefore, the amounts of transduced CAR T cells were adjusted to incubate the same quantity of expressing CAR T cells.

A 1:2 serial dilution of CAR T cells (previously washed two times with PBS) starting at $3x10^4$ cells was performed and the cells further co-incubated with $3x10^4$ tumor cells over 48 h (at 37 °C and 5% CO_2) in 200 µl RPMI-1640 with GlutaMAX supplemented with 10% fetal bovine serum, 100 U/ml penicillin and 100 mg/ml streptomycin. In some experiments, instead of using tumor cells, hCD22-hFc and hFc antigens (3 µg/ml) were coated overnight on a 96 well plate at 4 °C and washed with PBS-T before starting the co-incubation with CAR T cells. As controls, effector cells and tumor cells alone were incubated in the same conditions. Every reaction was performed in triplicates.

To determine the amount of secreted IFNγ and IL-2 present in the supernatant after the induction of CAR T cell activation, an IFNγ and IL-2 ELISA kit was respectively used according to manufacturer´s instruction.

A half area 96 well plate was coated with capture antibody diluted in coating buffer and incubated overnight at 4 °C. After washing three times with PBS-T, blocking of the plate was performed with assay diluent for one hour at room temperature. After three further washing steps with PBS-T, 30 µl supernatant of the 48 h co-incubation and corresponding standard (99 ng/ml) was applied on the blocked plate and incubated in the dark for two hours at room temperature. Samples were then removed and the plate washed again five times with PBS-T. To detect the cytokines,

detection antibody and streptavidin conjugated HRP were mixed (1:1) in assay diluent and applied on the plate for one hour at room temperature. Unspecific antibody and streptavidin were removed by washing seven times with PBS-T. Specific detection antibody bind to HRP conjugated streptavidin was detected with TMB substrate reagent. After 30 min incubation, the reaction was stopped with sulfuric acid and the plate analyzed with a spectrophotometer.

2.5 Lentiviral gene transfer

2.5.1 Co-transfection of HEK-293T cells

The production of lentivirus in the cell culture supernatant was performed over five days by co-transfecting HEK-293T cells.

DAY 1:

On 15 cm culture plates, $6x10^6$ HEK-293T cells were seeded in 22 ml DMEM medium with 10% (v/v) FBS, 100 U/ml penicillin and 100 µg/ml streptomycin pro plate and incubated at 37 °C and 5% CO_2. After 48 h, cells were grown with a confluence of 80% which is optimal for co-transfection.

DAY 3:

For the transfection using polyethelinimine (PEI) as transfection reagent, DNA and PEI mixtures were separately prepared. The DNA preparation comprised DNA of the lentivirus vector of interest, helper plasmid #1 and #2 as well as NaCl and H_2O. The PEI preparation consisted of PEI, NaCl and H_2O. Amounts of the different components for the transfection of 5 and 10 plates are indicated in Table 21. The PEI mixture is added to the DNA preparation, the entire solution shortly vortex and incubated for 10 min at room temperature.

Table 21: Transfection components

Mix	Component	For 5 plates	For 10 plates
DNA mix	Lentiviral DNA plasmid of interest	112.5 µg	225 µg
	Helper plasmid #1	39.5 µg	79 µg
	Helper plasmid #2	73 µg	146 µg
	NaCl (300 mM)	3950 µl	7900 µl
	H_2O	3950 µl	7900 µ
PEI mix	PEI (7.5 mM)	1760 µl	3520 µl
	NaCl (300 mM)	3950 µl	7900 µl
	H_2O	2190 µ	4380 µl
Total		16025 µl	32050 µl

Transfection mix was added drop wise to the confluent cells, plates were then slowly rotated to spread the transfection mix over the cells and placed back in the incubator for 24 h at 37 °C and 5% CO_2.

DAY 4:

To enable the liberation of lentiviral particles in the supernatant, cell culture medium was removed and the cells washed with 5 ml PBS. Fresh DMEM medium (14 ml) with 100 U/ml penicillin and 100 µg/ml streptomycin but without FBS was slowly added on one side of the plate without removing the cells. Incubation over 24 h at 37 °C and 5% CO_2 allowing the secretion of lentivirus in the supernatant.

DAY 5:

Harvest and concentration of lentivirus secreted in the supernatant was performed with centricons Plus-70 Centrifugal Filter units.

Remaining cells were first removed by centrifuging the supernatant at 1800 rpm for 15 min. After transferring the supernatant into a centricon, centrifugation was performed at 3500 g for 30 min and the flow through discarded. Concentrated lentivirus was removed from the filter by centrifuging the reversed centricon at 1000 g for 2 min. The obtained volume was used for the titration, separated in aliquots and stored at -80 °C.

2.5.2 Lentiviral titration

One day before the titration, 6 wells of a 24 well plate were seeded with $5x10^4$ HEK-293T cells pro ml DMEM with 10% (v/v) FBS and 100 U/ml penicillin and 100 µg/ml streptomycin and incubated for 24 h at 37 °C and 5% CO_2.

Polybrene (8 µg/ml), a cationic polymer used to increase the efficiency of lentiviral gene transfer was mixed with different amount of lentivirus (3 µl, 1 µl, 0.3 µl, 0.1 µl) and added to the seeded HEK-293T cells. As a control, polybrene without the addition of lentivirus was used.

After 72 h of incubation at 37 °C and 5% CO_2, the titer of the lentivirus production was determined by flow cytometry (method 2.4.6). Therefore the percentage of target cells (100 000 cells) positively expressing the CAR on their surface was determined when adding 1 µl of lentivirus. The titer corresponding to the infection unit (IU) per ml was then calculated with the following formula:

$$\text{Titer (IU / ml)} = \frac{\text{Number of target cells } (10^5 \text{ cells}) \times (\% \text{ of positive cells} / 100)}{\text{Volume of added lentivirus (1µl)}} \times 10^3$$

2.5.3 Lentiviral transduction of activated T cells

Activated T cells were centrifuged at 1400 rpm for 4 min and resuspended in pre-warmed X-Vivo 20 medium with IL-2 (300 U/ml). A standing T25 or T75 cell culture flask was respectively used for the transduction of 4 to $5x10^6$ T cells or 1 to $4x10^7$ T cells. Lentivirus with a multiplicity of infection of 10 (MOI 10) and polybrene (8 µg/ml) were added to the cell suspension before an incubation period of 24 h at 37 °C. For the expansion of the transduced T cells, culture medium was removed, replaced by fresh X-Vivo 20 medium with IL-2 and the cell suspension incubated for further 24 h in the same conditions. Finally the efficiency of the CAR expression was determined by flow cytometry (method 2.4.6) and the transduced T cells used to perform an apoptosis or an ELISA assay.

2.6 Preliminary experiments in mice

2.6.1 Injection of tumor cells

Mice obtained from Envigo were six to eight weeks old. The animals were maintained in filtered cages in a day-night rhythm of 12 hours. Nalm-6 luciferase tumor cells were centrifuged at 100 g for 8 min. Obtained pellet was washed twice with PBS and then desired amount of cells ($1x10^6$ or $5x10^6$ cells) resuspended in 100 µl PBS. For the xenotransplantation, tumor cells were injected intravenously into the mice.

2.6.2 Bioluminescence measurement

Disseminated tumor growth of luciferase transfected tumor cells were followed *in vivo* by bioluminescence imaging. For this purpose, 3 mg of the luciferase substrate Luciferin-EF were diluted in 200 µl PBS and injected intraperitoneally in each mouse. Animals were anesthetized with 1.5% isoflurane and transferred in the photon-imager also connected to the anesthetic gas. Measurement was started 10 min after the luciferin injection and the emitted photons recorded during 2 min. After the measurement, a photography of the animals was superposed to the obtained bioluminescence signal and an equivalent region of interest was selected around each mouse. Based on this region, the number of emitted photons for each mouse was measured. For the quantitative analysis of the luciferase activity, the measured number of photons per minute was used.

2.7 Statistical analysis and graphical representation

Statistical analysis was performed with the GraphPad Prism 5.0 software. An unpaired, two-tailed T test was used to investigate the statistical significance between the specific tumor cell lysis and the cytokines secretion of the different CAR constructs. A $p\ value < 0.05$ was considered to be statistically significant. Graphs were created with the GraphPad Prism 5.0 software. Represented error bars showed the standard deviation applied to the means.

3 Results

Small format antibody fragments are characterized by high target specificity but may suffer from limited biophysical properties such as aggregation or low thermal stability. To increase their biophysical robustness, a linker peptide or a disulfide bridge, resulting in a single chain variable fragment (scFv) or a disulfide-bond stabilized Fv (dsFv), respectively, can be introduced.

In the present thesis, a new anti-CD22 CAR was developed and further optimized for clinical translation by mutagenesis. The targeting domain of the newly constructed CAR is composed of a humanized anti-CD22 (hCD22) scFv, which was generated by grafting the specificity of the clinically established murine anti-CD22 antibody named RFB4 to a phage display isolated stable human framework (Krauss et al., 2003b). The resulting antibody fragment shows high affinity for its target antigen CD22 as well as an exceptional high biophysical stability. Since the murine anti-CD22 (mCD22) scFv of RFB4 is used as control in the present work, we first investigated the stability of the mCD22 scFv targeting domain compared to the hCD22 scFv.

3.1 Stability of the murine and humanized anti-CD22 scFv targeting domain

3.1.1 Cloning of the murine anti-CD22 scFv

To compare the high thermal robustness of the hCD22 scFv at body temperature (Krauss et al., 2003b) to its murine counterpart, stability tests were performed. For the transient production of the mCD22 antibody fragment, DNA encoding the scFv fragment (purchased from Eurofins) was cloned into the mammalian expression vector pEE12.4 via a three step procedure involving the subcloning vector pEUC6B (Figure 7). To create matching overhangs for subcloning, the restriction sites PvuII and BamHI were introduced into the 5’ and 3’ end of the mCD22 gene sequence by PCR using the primer set RFB4_1 and RFB4_2 (method 2.2.6). Amplified PCR products and the subcloning vector were subsequently digested with both enzymes and ligated, resulting in a vector coding for the mCD22 scFv linked to a His_6- and c-myc tag. The sequence located at the 5’ end of the antibody fragment coded for the

IgG-VH leader peptide, which ensures the secretion of the expressed protein in the supernatant of transfected mammalian cells (Krauss et al., 2005a). Following control digestion and sequencing, which confirmed the correct integration of the insert, the gene cassette was cloned into the mammalian expression vector pEE12.4 using EcoRI restriction sites. After the identification of a clone with a sense oriented insert by enzymatic digestion, plasmid DNA was prepared in high amounts for transfection.

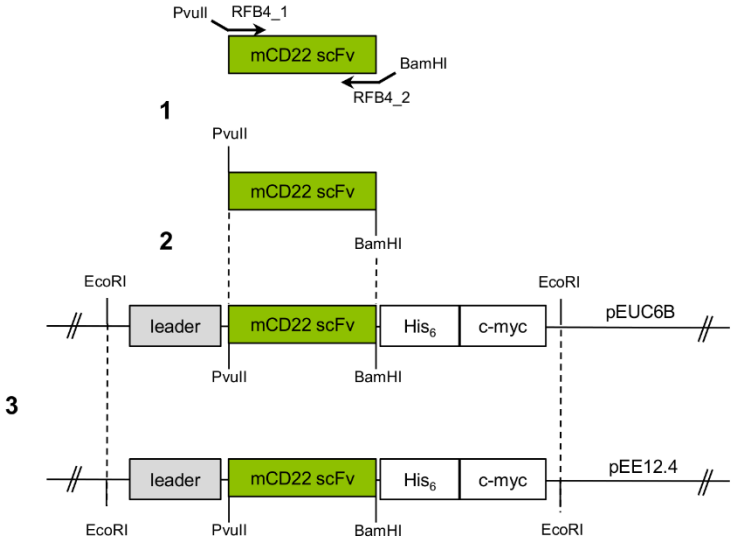

Figure 7: Schematic representation of the cloning strategy for the murine anti-CD22 scFv. mCD22 scFv was cloned into the expression vector pEE12.4 in three steps. **1:** Restriction sites PvuII and BamHI were respectively added to the 5' and 3' end of the mCD22 antibody fragment gene by PCR. **2:** The PCR product was inserted into the subcloning vector pEUC6B between the leader sequence and the His_6-tag using the restriction enzymes PvuII and BamHI. **3:** The gene cassette encoding the leader peptide, the mCD22 scFv, the His_6- and c-myc tag was finally cloned way into the expression vector pEE12.4 using EcoRI sites.

3.1.2 Expression and purification of the murine anti-CD22 scFv

The recombinant mCD22 scFv was produced by transiently transfected eukaryotic HEK-293-E cells (method 2.3.4). The purification of the antibody fragment from the cell culture supernatant was performed by IMAC (method 2.4.1) via the included His_6-tag sequence (Figure 8A). Unspecifically bound proteins were detached from the column with a buffer of low stringency (imidazole concentration of 10 mM). The scFv was eluted with a linear gradient of increasing imidazole concentrations. The subsequent analysis of the elution fractions via SDS-PAGE (Figure 8C; lane 3) revealed the desired scFv protein band at 28 kDa and some unspecific protein impurities. In a following purification step via size exclusion chromatography (SEC), the scFv containing IMAC fractions were pooled and loaded on a HiLoad Superdex 75 column to separate scFv from these impurities (method 2.4.2). The size exclusion chromatogram revealed two peaks (Figure 8B). Multimeric proteins and aggregates eluted at a volume of approximately 50 ml. The second peak with an apparent molecular mass of 28 kDa (volume = 70 ml) corresponded to the monomeric scFv. Coomassie blue stained SDS-PAGE (Figure 8C; lane 4) and western blot (Figure 8D; lane 4) confirmed the high purity of the monomeric antibody fraction. After purification, the protein yield obtained for the mCD22 antibody fragment was 0.9 mg/l. The purity of monomeric hCD22 scFv previously produced in our laboratory was confirmed in parallel to purified mCD22 scFv by analytical SEC using a Superdex 200 column (Figure 8E and 8F). Both antibody fragments eluted as one single peak at 16 ml corresponding to the purified monomeric fraction.

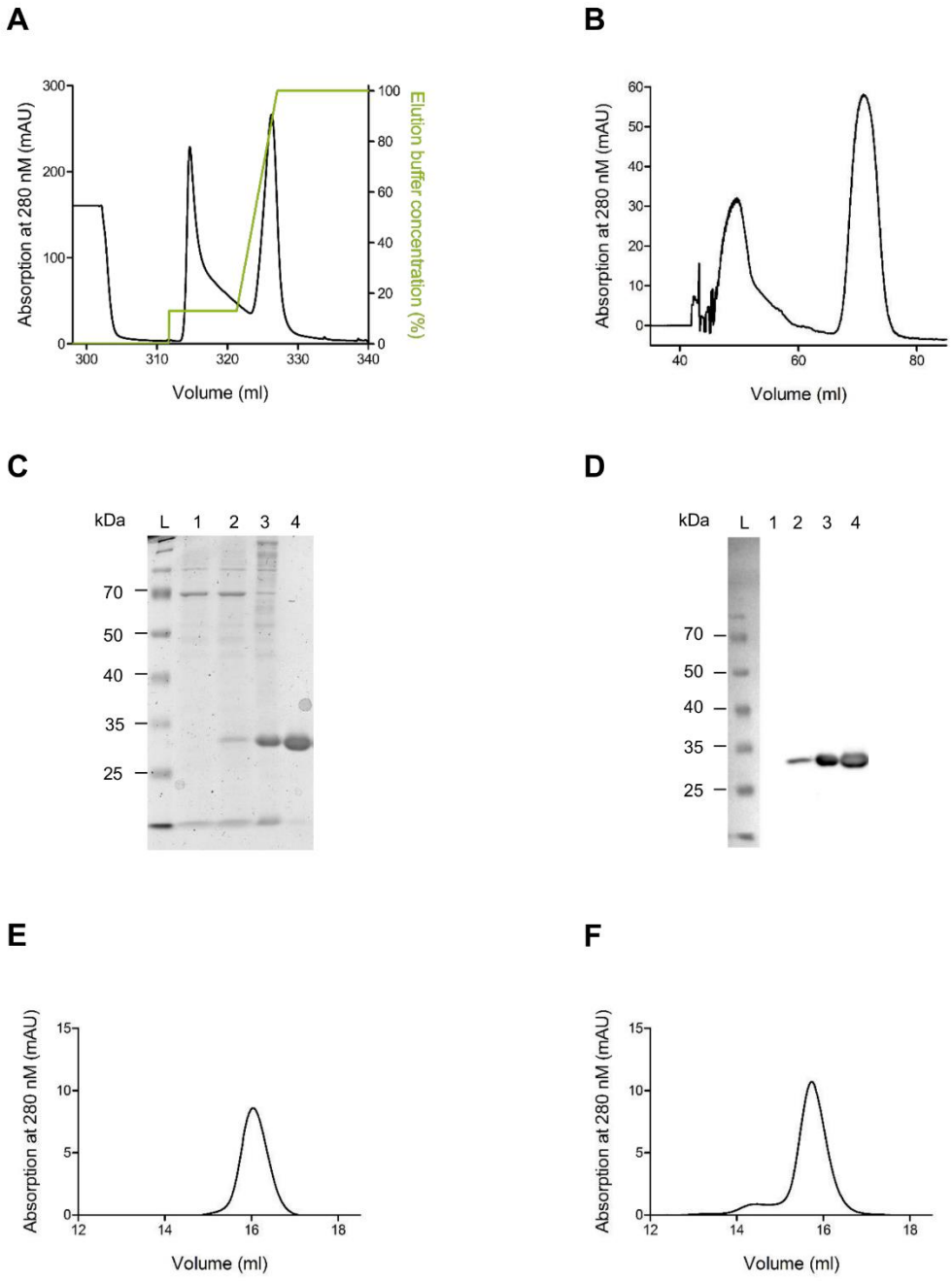

Figure 8: Purification of mCD22 scFv. A: IMAC purification chromatogram of the mCD22 scFv: the first peak contains unspecific proteins whereas the second peak corresponds to the eluted mCD22 scFv. **B:** Size exclusion chromatogram of the IMAC eluate using a Superdex 75 column: multimeric proteins and aggregates eluted within the first peak (volume=50 ml). The second peak corresponds to the monomeric mCD22 scFv. **C:** Detection by SDS-PAGE and coomassie blue staining of the IMAC flow through (1), IMAC peak 1 (2) and peak 2 (3) and final SEC purified mCD22 scFv (4). L: protein ladder. **D:** Western blot analysis with an anti His_6-tag antibody of the IMAC flow through (1), IMAC peak 1 (2) and peak 2 (3) and final SEC purified mCD22 scFv (4). L: protein ladder. **E:** Analytical SEC chromatogram of purified mCD22 scFv eluted in a single peak. **F:** Analytical SEC chromatogram of purified hCD22 scFv eluted in a single peak.

3.1.3 Stability test of the murine and humanized anti-CD22 scFv

The stability of purified mCD22 scFv and hCD22 scFv was assessed by flow cytometry, measuring their binding activity to living $CD22^+$ Raji cells after an incubation period of 7 days (168 h) at 37 °C in 90% human serum (method 2.3.5). At all-time points, high binding activity was detected for the hCD22 scFv as well as for its murine counterpart (Figure 9A). The analogue experiment performed in PBS revealed full binding activity for both scFvs throughout the whole experiment (Figure 9B).

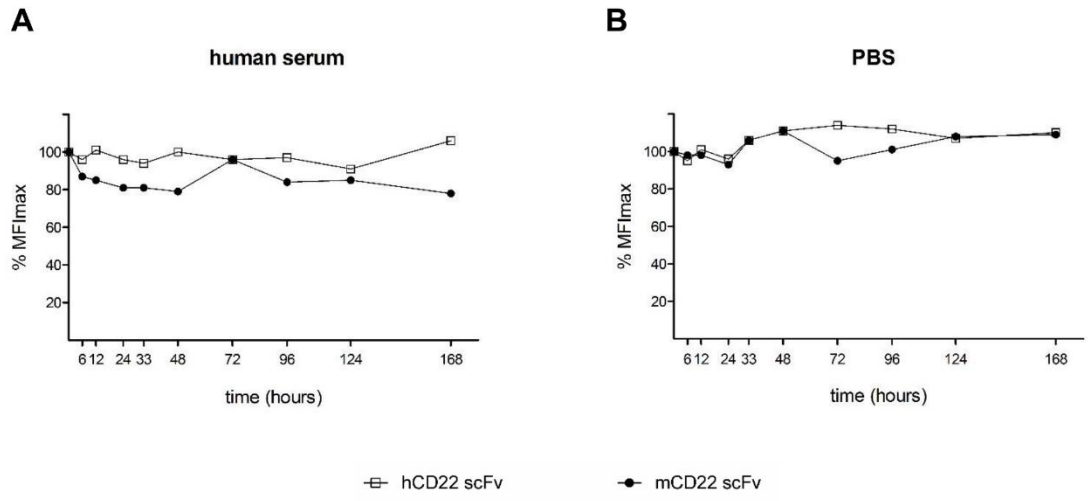

Figure 9: Serum and PBS stability of the humanized and murine anti-CD22 scFv. Binding activity of hCD22 scFv and mCD22 scFv to $CD22^+$ Raji cells, after 7 days incubation, at 37°C, in human serum (**A**) or PBS (**B**). Binding activity was measured by flow cytometry and indicated as percentage of initial median fluorescence intensity (MFImax).

3.2 Stability of derived CAR constructs

3.2.1 Generation and expression of the hCD22 scFv-(hFc-28BBz) CAR

The generation of the hCD22 scFv-(hFc-28BBz) CAR and its expression on T cells was chosen as an example to illustrate the construction of all the CAR constructs used in the present thesis.

The DNA cassette coding for the IgG-VH leader sequence and the hCD22 scFv was extracted from the subcloning vector pEUC6B by digestion with NcoI and BamHI and

further used as template for a PCR reaction with the primer pair hCD22_1 and hCD22_2 to replace the restriction site BamHI with NotI at the 3' end (Figure 10A). The amplified PCR product was then inserted into the pENTR vector 5' to the gene encoding the CAR backbone (hFc-28BBz) employing the restriction sites NcoI and NotI (Figure 10B). Transformed kanamycin resistant bacterial clones were analyzed by sequencing using the sequencing primers pENTR sense and pENTR AS. Plasmid DNA from one clone, presenting the correct sequence, was mixed to the DNA of the destination vector and a gateway reaction was performed using the LR clonase (method 2.2.8). The DNA sequence, located between the attL1 and attL2 sites, was in this way integrated into the destination vector between the attR1 and attR2 sites, resulting in a final expression clone. Success of this reaction was assessed by analytical digestion of the resulting carbenicillin resistant expression clones with KpnI via the detection of three distinct DNA fragments at 1462 bp, 2461 bp and 6332 bp (Figure 10C).

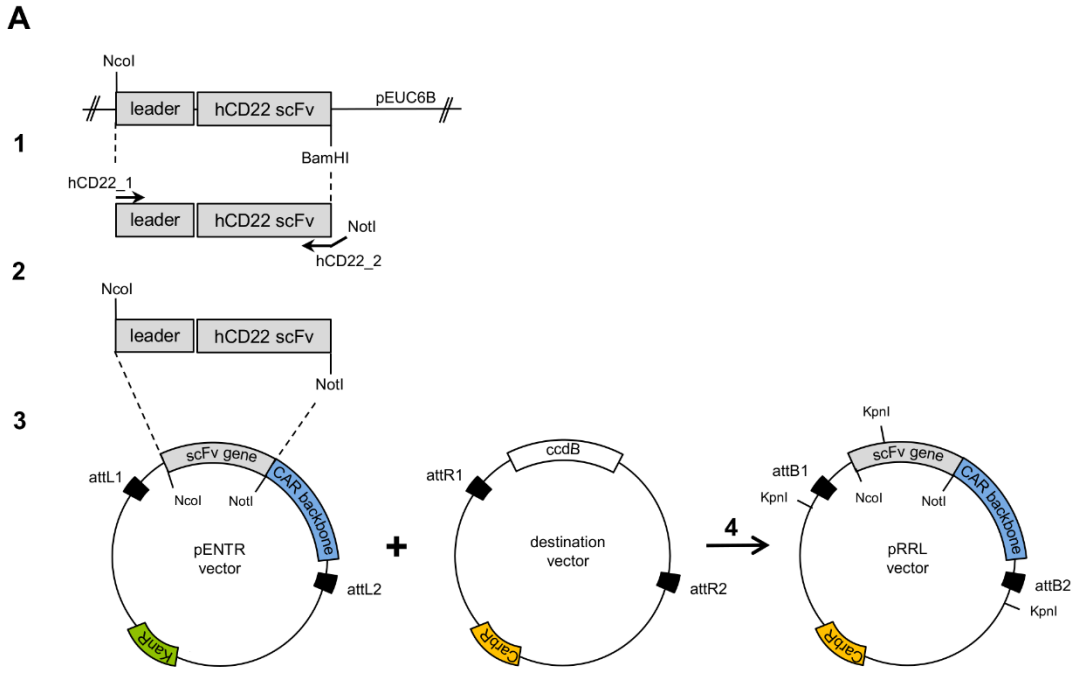

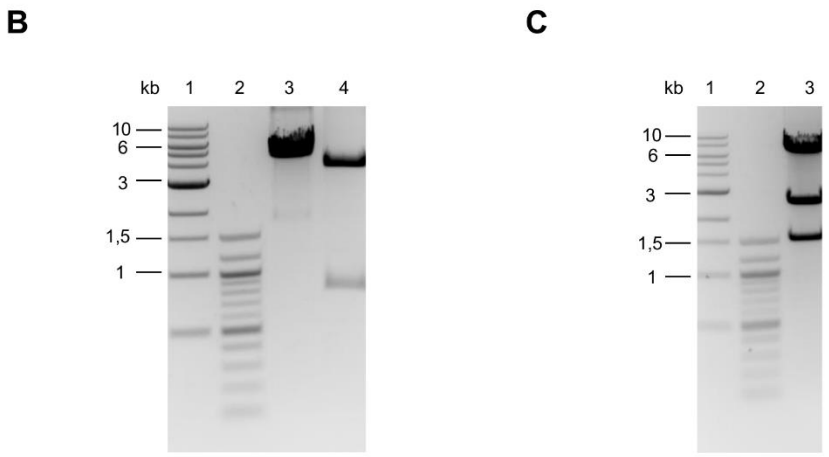

Figure 10: Cloning strategy for the hCD22 scFv-(hFc-28BBz) CAR. A: Schematic representation of the cloning strategy: the gene sequence encoding for the leader peptide and hCD22 scFv was extracted from the vector pEUC6B using NcoI and BamHI as restriction and ligation sites (1). The PCR reaction involving the primer pair hCD22_1 and hCD22_2 enables the replacement of the 3' restriction site BamHI by NotI (2). The amplified PCR product was cloned into the pENTR vector 5' to the gene encoding the CAR backbone employing NcoI and NotI. This cloning step resulted in the generation of the entry clone for the gateway reaction (3). DNA of the entry clone vector (pENTR) containing the CAR gene was combined with the destination vector to perform the gateway reaction via the LR clonase resulting in a final CAR expression clone (4). **B:** Agarose gel (1%) of the linearized (NcoI) (lane 3) and digested (NcoI/NotI) entry clone vector (pENTR) to confirm proper ligation of the scFv gene (lane 4), 1 kb marker (lane 1) and 100 bp marker (lane 2), before sequencing. **C:** Agarose gel (1%) showing the analytical digestion of the final hCD22 CAR expression clone with KpnI resulting in three distinct DNA bands: 1462 bp, 2461 bp and 6332 bp (3), 1 kb marker (1) and 100 bp marker (2).

For the expression of CAR constructs, T cells were freshly isolated from the blood of healthy donors and stimulated with the anti-CD3 antibody OKT-3 and the cytokine IL-2 (method 2.3.8 and 2.3.9). Activated T cells were then transduced with lentiviral particles containing the CAR gene with a multiplicity of infection (MOI) of 10 (method 2.5.3). Lentiviral particles were produced in the eukaryotic HEK-293T cell line which was transiently transfected with CAR DNA (pRRL vector) and the helper plasmids #1 and #2 (method 2.5.1). Transduction efficacy of T cells was assessed by flow cytometry after 48 h of culture, in the presence of IL-2 (method 2.3.6). The percentage of CAR expression on the surface of T cells was then compared to non-transduced T cells (mock). While a FITC conjugated anti-CD3 antibody enabled the detection of T cells, a phycoerythrin (PE) conjugated anti-human IgG (hFc

specific) antibody was used to detect the CAR. Dependent on the CAR construct, CAR T cell expression varied between 10% and 60%. The hCD22 CAR was expressed on 64% of T cells, corresponding to a very high expression rate (Figure 11).

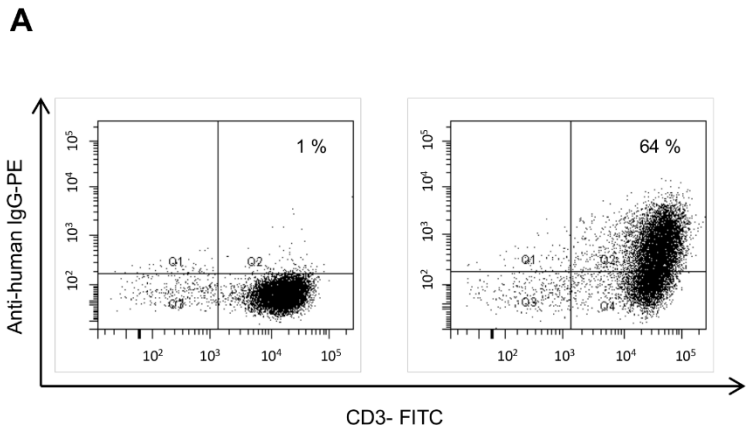

Figure 11: Flow cytometry analysis to detect the expression of hCD22 CAR on the surface of human T cells. T cells from a healthy donor were transduced with lentivirus encoding the hCD22 CAR expression vector. After 48 h, non-transduced (left) and CAR transduced T cells (right) were incubated with a PE conjugated anti-human IgG antibody, specifically binding the hFc spacer domain of the CAR, and a FITC conjugated anti-CD3 antibody. Specific antibody binding was measured by flow cytometry. Based on the total amount of T cells, the percentage indicates the proportion of T cells expressing the CAR.

3.2.2 Stability of the hCD22 scFv-(hFc-28BBz) and mCD22 scFv-(hFc-28BBz) CAR

The hCD22 scFv-(hFc-28BBz) and mCD22 scFv-(hFc-28BBz) CAR (Figure 12A) was generated for the investigation of CAR stability by measuring CAR mediated T cell activation towards a cell line expressing the antigen CD22. Secretion of IFNγ in the supernatant of the co-culture was used as readout of the T cell activation. Due to the difference of positively expressing hCD22 and mCD22 CAR T cell fractions, the amount of transduced CAR T cells was adjusted in order to incubate the same quantity of positively expressing CAR T cells.

Activation of T cells through hCD22 and mCD22 CAR was induced by co-incubating CAR positive T cells with the CD22 positive human cell line Raji. The amount of

secreted IFNγ present in the supernatant of the co-culture was measured after 48 h by ELISA (method 2.4.8). To show specificity, transduced T cells were also incubated with CD22 negative Jurkat cells.

The amount of IFNγ release obtained after the incubation of transduced T cells without target cells (Figure 12B) was subtracted from the co-culture conditions before plotting. At an effector-to-target ratio of 1:2 both mCD22 and hCD22 CAR T cells were able to induce a significant IFNγ secretion compared to non-transduced T cells (mock) when incubated with Raji cells (Figure 12C). However, the IFNγ release of mCD22 CAR T cells was three fold higher than for hCD22 CAR T cells. When cultivated with Jurkat cells, mCD22 and hCD22 CAR T cells induced no IFNγ secretion.

Both, hCD22 and mCD22 CARs show high specificity for their target CD22. Human T cells expressing these constructs are specifically activated when stimulated by CD22 positive cells. Besides CD22, Raji cells also express the human Fc receptor on their surface. Therefore, off-target activation of CD22 CAR T cells can occur through binding of the hFc spacer domain of the CAR to the hFc receptor expressed on Raji cells and influence the observed IFNγ secretion.

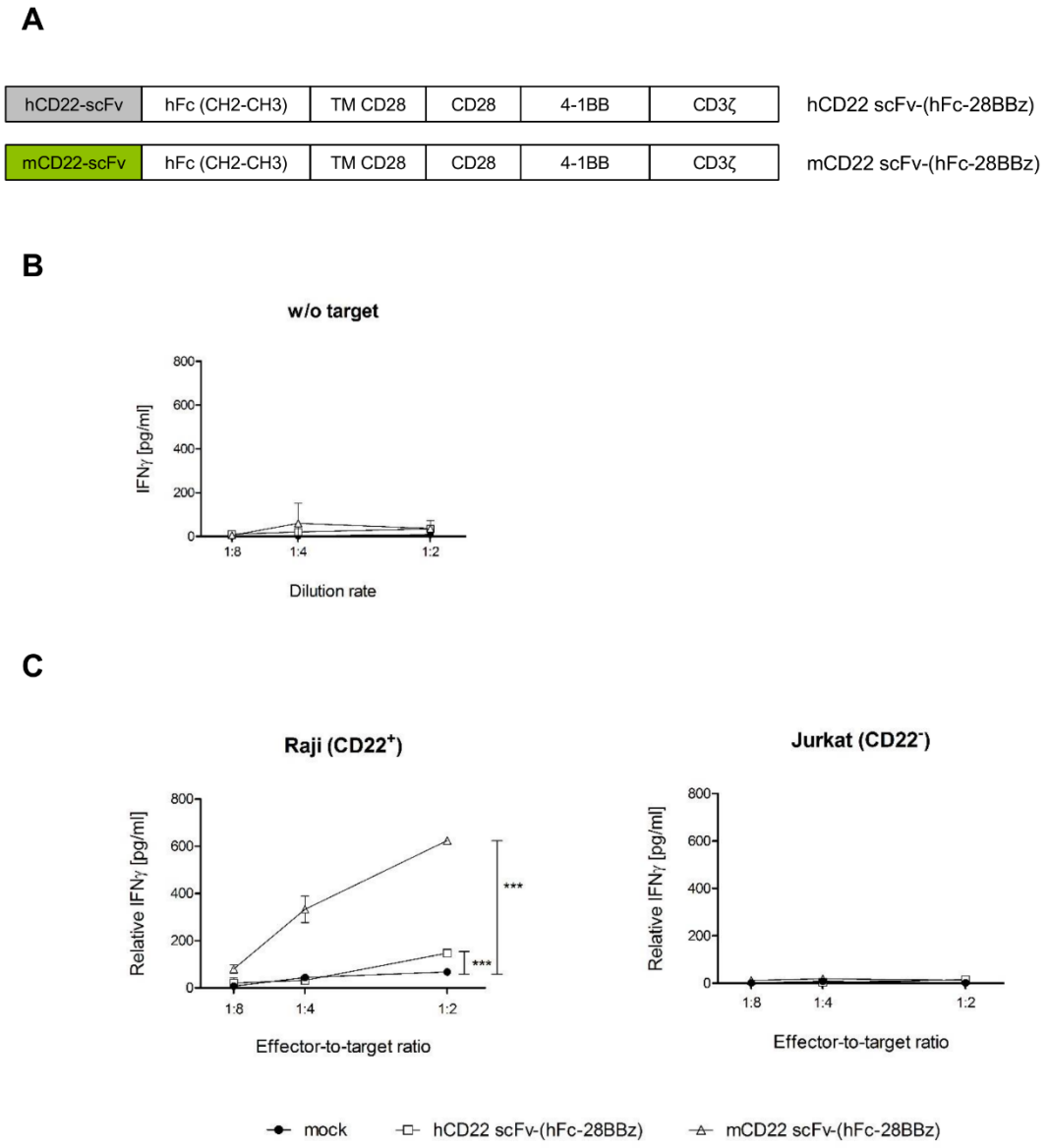

Figure 12: Activation of hCD22 scFv-(hFc-28BBz) and mCD22 scFv-(hFc-28BBz) CAR T cells. A: Schematic representation of the hCD22 and mCD22 CAR. **B:** Through lentiviral gene transfer, isolated T cells from a healthy donor were equipped with the hCD22 or the mCD22 CAR. As control, hCD22 CAR and mCD22 CAR transduced T cells and non-transduced T cells (mock; $0.375x10^4$ - $3x10^4$ cells per well) were incubated without target cells. IFNγ secretion was used as read out for CAR T cell activation and measured by ELISA in the supernatant of the co-culture. **C:** To assess specific CAR T cell activation, hCD22 CAR and mCD22 CAR transduced T cells and non-transduced T cells ($0.375x10^4$ - $3x10^4$ cells per well) were co-incubated with Raji cells (left) or Jurkat cells (right, $3x10^4$ cells per well). Amount of secreted IFNγ obtained for transduced and non-transduced T cells only was subtracted before plotting. Data represent the mean of triplicates ± standard deviation. * $P < 0.05$; ** $P < 0.01$; *** $P < 0.001$.

To avoid off-target activation and to enable the stability analysis by measuring the specific hCD22 and mCD22 CAR T cell, the hFc spacer was replaced by a CD8 spacer domain resulting in two new constructs: hCD22 scFv-(CD8-28BBz) CAR and mCD22 scFv-(CD8-28BBz) CAR (Figure 13A). Furthermore, Raji cells were replaced by the tumor cell line Nalm-6, which expresses CD22 but lacks the hFc receptor.

CAR generation was performed, as previously described, by using a destination vector encoding for a CAR backbone with CD8 as spacer domain. Transduction efficacy was assessed by flow cytometry using a FITC conjugated anti-CD3 antibody to detect T cells and a biotin-alexa 488 conjugated streptavidin detection system to identify the variable light chain of the scFv present on the CAR.

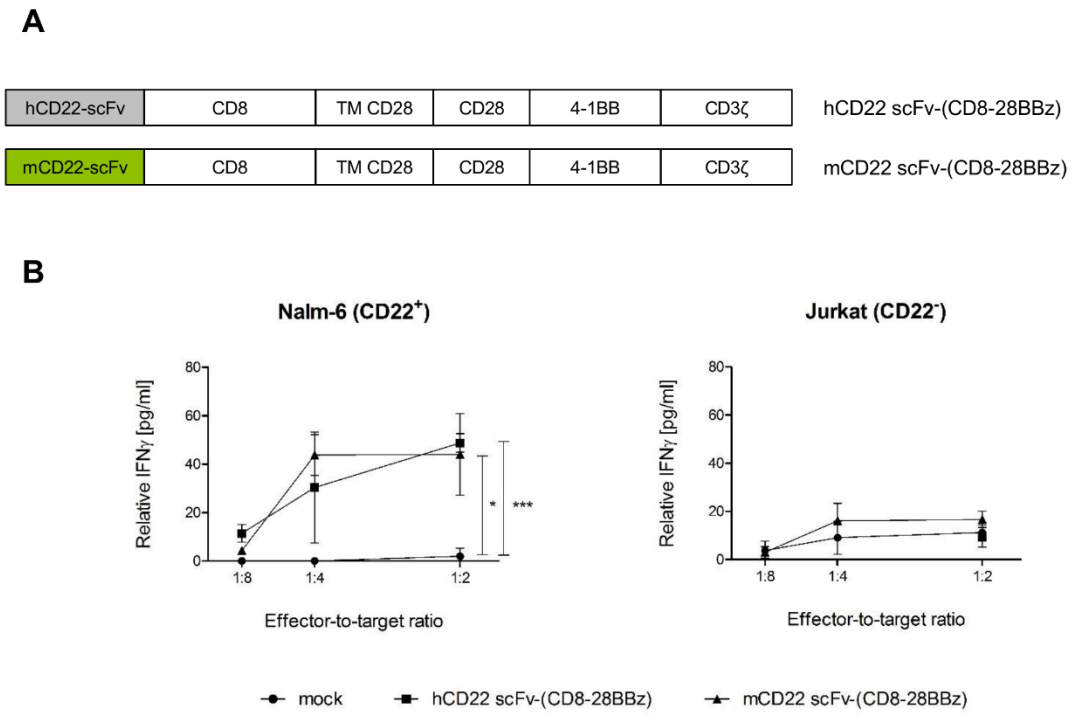

Figure 13: Activation of hCD22 scFv-(CD8-28BBz) and mCD22 scFv-(CD8-28BBz) CAR T cells. **A:** Schematic representation of the hCD22 and mCD22 CAR with the CD8 spacer domain instead of the hFc spacer. **B:** Through lentiviral gene transfer, isolated T cells from a healthy donor were equipped with the hCD22 or the mCD22 CAR. To assess specific CAR T cell activation, hCD22 CAR and mCD22 CAR transduced T cells and non-transduced T cells ($0.375x10^4$ - $3x10^4$ cells per well) were co-incubated with Nalm-6 cells (left) or Jurkat cells (right, $3x10^4$ cells per well). IFNγ secretion was used as read out for CAR T cell activation and measured by ELISA in the supernatant of the co-culture. Data represent the mean of triplicates ± standard deviation. * $P < 0.05$; ** $P < 0.01$; *** $P < 0.001$.

At an effector-to-target ratio of 1:2, significantly increased IFNγ amounts were detected in the supernatant of activated murine and humanized CD22 CAR transduced T cells in comparison to non-transduced T cells after 48 h of cultivation with Nalm-6 cells (Figure 13B). Co-cultured with Jurkat cells, T cells equipped with the murine and humanized CD22 CAR showed no increase in IFNγ secretion. The specific activation of T cells expressing the murine and humanized CD22 CAR was triggered by CD22 positive Nalm-6 cells, demonstrating biophysical stability of both scFv derived CARs.

3.3 Optimization of the hCD22 scFv-(hFc-28BBz) CAR by mutagenesis

3.3.1 Generation of two single and a double mutant of hCD22 scFv-(hFc-28BBz) CAR

The success of ongoing clinical trials shows that, CAR engineered T cells are potent and in general well tolerated. However, for their broader use, new approaches have to be developed to prevent serious adverse events, such as cytokine release syndrome or on-target, off-tumor toxicity (Brentjens et al., 2011b; Morgan et al., 2010). To increase CAR safety, solutions such as improved tumor selectivity by combinatorial signaling (Kloss et al., 2013), a deeper understanding of cytokine storms, the development of trigger and elimination mechanisms or the implementation of on/off switching systems (Juillerat et al., 2016) are currently emerging. Another approach is to focus on the CAR design itself (Maus and Powell, 2015). The use of different components or specific mutations inside CAR domains allows the development of highly effective tumor-specific T cells with an optimal activation.

To enhance the safety of the parental hCD22 scFv-(hFc-28BBz) CAR (hCD22 CAR), the Fcγ receptors (FcγR) and LCK binding domains were mutated/inactivated by site-directed mutagenesis of the hFc spacer and the CD28 co-stimulatory domain, resulting in two mutants referred to as hCD22 scFv-(ΔhFc-28BBz) CAR (simplified as ΔFc hCD22 CAR) and hCD22 scFv-(hFc-Δ28BBz) CAR (simplified as ΔCD28 hCD22 CAR) and one double mutant hCD22 scFv-(ΔhFc-Δ28BBz) CAR

(simplified as ΔFc-ΔCD28 hCD22 CAR) in which both mutations were simultaneously expressed (Figure 14).

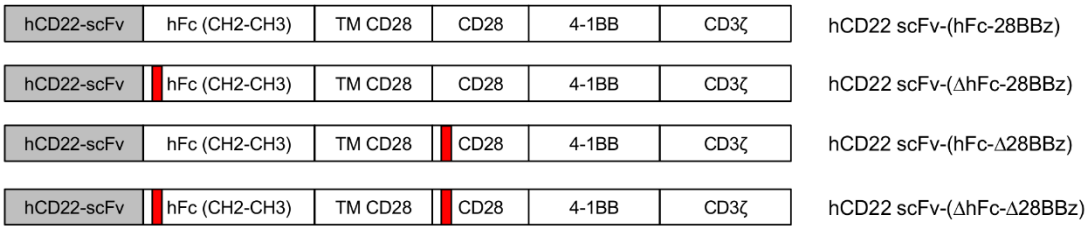

Figure 14: Schematic representation of parental and mutated hCD22 CAR sequences. The hCD22 scFv-(ΔhFc-28BBz) CAR is mutated in the CH2 domain of the hFc spacer to prevent off-target activation of innate immune cells. The deletion of the LCK binding region in the hCD22 scFv-(hFc-Δ28BBz) CAR blocks IL-2 secretion. The hCD22 scFv-(ΔhFc-Δ28BBz) CAR combines both mutations in one construct.

To generate the ΔFc hCD22 CAR and ΔCD28 hCD22 CAR variants, mutations were introduced by site-directed mutagenesis using the parental hCD22 entry clone vector (pENTR) as template with either the mutagenic primer combination CD28_Lck-Fw and CD28_Lck-Rev or hIgG1_CH2-Fw and hIgG1_CH2-Rev (method 2.2.7). DNA modification of transformed kanamycin resistant bacterial clones was confirmed by sequencing using the primers pENTR sense and pENTR AS and further used for the gateway reaction. The sequence of the resulting carbenicillin resistant expression clone was confirmed by analytical digestion. The double mutated hCD22 scFv-(ΔhFc-Δ28BBz) CAR carrying both single mutations was generated by site-directed mutagenesis with hIgG1_CH2-Fw and hIgG1_CH2-Rev as mutagenic primer pair and DNA of the CD28 single mutated hCD22 entry clone as template.

3.3.2 T cell activation of the mutated CAR variants *in vitro*

3.3.2.1 Impact of the mutation within the hFc domain

To assess the impact of mutating the CH2 domain of the IgG1 Fc spacer, specific tumor cell lysis and IFNγ release induced by CAR T cell activation were measured by an XTT assay and by ELISA, respectively. For this purpose, the parental, the ΔhFc

and ΔFc-ΔCD28 hCD22 CAR T cells were co-incubated with THP-1 cells which express the Fcγ receptor (FcγR) but lack CD22 expression. After 24 h, the supernatants of the co-cultures were removed for IFNγ measurement and the remaining cells were used to quantify CAR T cell mediated tumor cell lysis by XTT assay (method 2.3.10). Non-transduced T cells served as controls (mock).

In contrast to the parental hCD22 CAR, ΔhFc and ΔFc-ΔCD28 hCD22 CAR T cells were not activated by binding to THP-1 cells and thus lacked specific tumor cell lysis (Figure 15A). Low amounts of IFNγ were observed for the ΔhFc hCD22 CAR T cells when incubated with FcγR$^+$ THP-1 cells (Figure 15B). Secretion of this cytokine was six times higher for the parental hCD22 CAR T cells in comparison to CAR T cells harboring the hFc mutation.

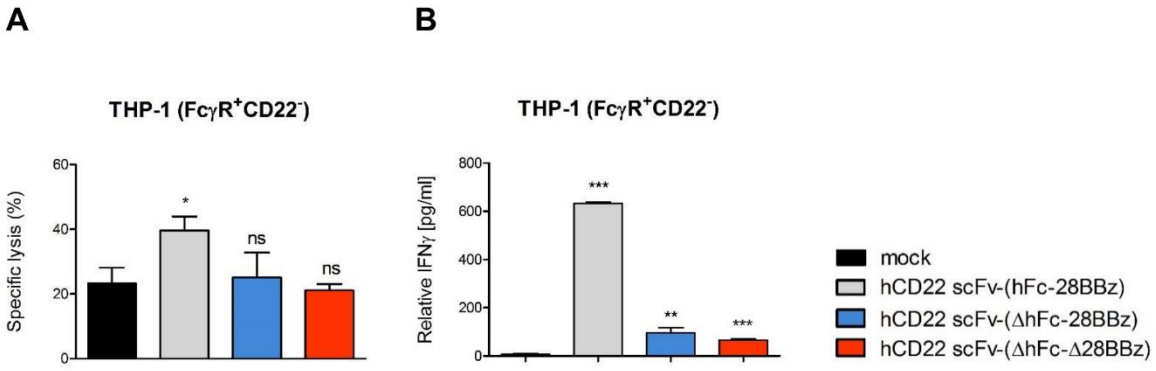

Figure 15: Specific activation by FcγR binding of parental, ΔhFc and ΔhFc-ΔCD28 hCD22 CAR T cells. A: Freshly isolated T cells from a healthy donor were equipped with one of the three hCD22 CAR variants by lentiviral gene transfer and cultured (1x10^5 cells per well) with THP-1 cells (1x10^5 cells per well). After 24 h, cytotoxicity against THP-1 cells was recorded by XTT assay. **B:** Concentration of secreted IFNγ was quantified by ELISA. Data represent the mean of triplicates ± standard deviation. * P < 0.05; ** P < 0.01; *** P < 0.001.

3.3.2.2 Impact of the mutation within the CD28 domain

The impact of mutating the intracellular CD28 LCK binding moiety was assessed by measuring the amount of secreted IFNγ and IL-2 by ELISA after CAR T cell activation (method 2.4.8). IL-2 abrogation is expected to be observed for activated ΔCD28 and ΔFc-ΔCD28 hCD22 CAR T cells but not for those with the parental and ΔhFc hCD22 CARs. While CAR T cell activation (measured by IFNγ release) was observed for all

CAR variants, surprisingly, IL-2 could not be detected by ELISA in the supernatant of the parental and ΔhFc hCD22 CAR T cells co-cultured with CD22 expressing Nalm-6 cells (Data not shown). To understand the absence of IL-2 secretion, a previously characterized carcinoembryonic antigen (CEA) scFv-(hFc-28zOX40) CAR inducing the secretion of IL-2 in high amounts was used as a reference for the following experiment.

3.3.2.2.1 T cell activation of CEA scFv-(hFc-28zOX40) and CEA scFv-(hFc-28BBz) *in vitro*

The CEA scFv-(hFc-28zOX40) CAR harbors a CEA antibody fragment as targeting moiety on the extracellular site and OX40 as second co-stimulatory domain instead of 4-1BB which was used in the hCD22 CAR variants in this thesis. To investigate the impact of the second co-stimulatory domains OX40 and 4-1BB on IL-2 secretion, a new CEA scFv-(hFc-28BBz) CAR including 4-1BB instead of OX40 was generated (Figure 16A). NcoI-NotI digested CEA scFv was ligated to the similar digested parental hCD22 CAR entry clone encoding for the CAR backbone with 4-1BB. After sequencing and performing the gateway reaction with the correct DNA sequence, final carbenicillin resistant expression clones were confirmed by analytical digestion. After isolation, $CD3^+$ T cells were equipped with both CEA CARs by lentiviral gene transfer.

Activation of transduced T cells was assessed after 48 h of co-incubation with CEA expressing MCF-7 cells by quantifying the amount of IFNγ and IL-2 secreted into the supernatant of the co-culture. To control the specificity of the activation, CEA CAR T cells were incubated with CEA negative HEK-293T cells. In comparison to non-transduced T cells, significantly increased IFNγ amounts were detected in the supernatant of CEA CAR T cells co-incubated with MCF-7 cells at an effector-to-target ratio of 1:1 (Figure 16B). Secretion of this cytokine was three times higher for activated CEA CAR T cells harboring the OX40 domain than for T cells equipped with the CEA CAR comprising 4-1BB.

As expected, no IFNγ release was induced by transduced T cells incubated with antigen negative control cells (HEK-293T). When cultivated with MCF-7 cells, IL-2

secretion was only observed in the supernatant of CEA CAR T cells harboring the OX40 domain but not for those carrying 4-1BB as second costimulatory signal (Figure 16C). No IL-2 was secreted by T cells and CEA CAR T cells after being co-incubated with CEA negative HEK-293T cells.

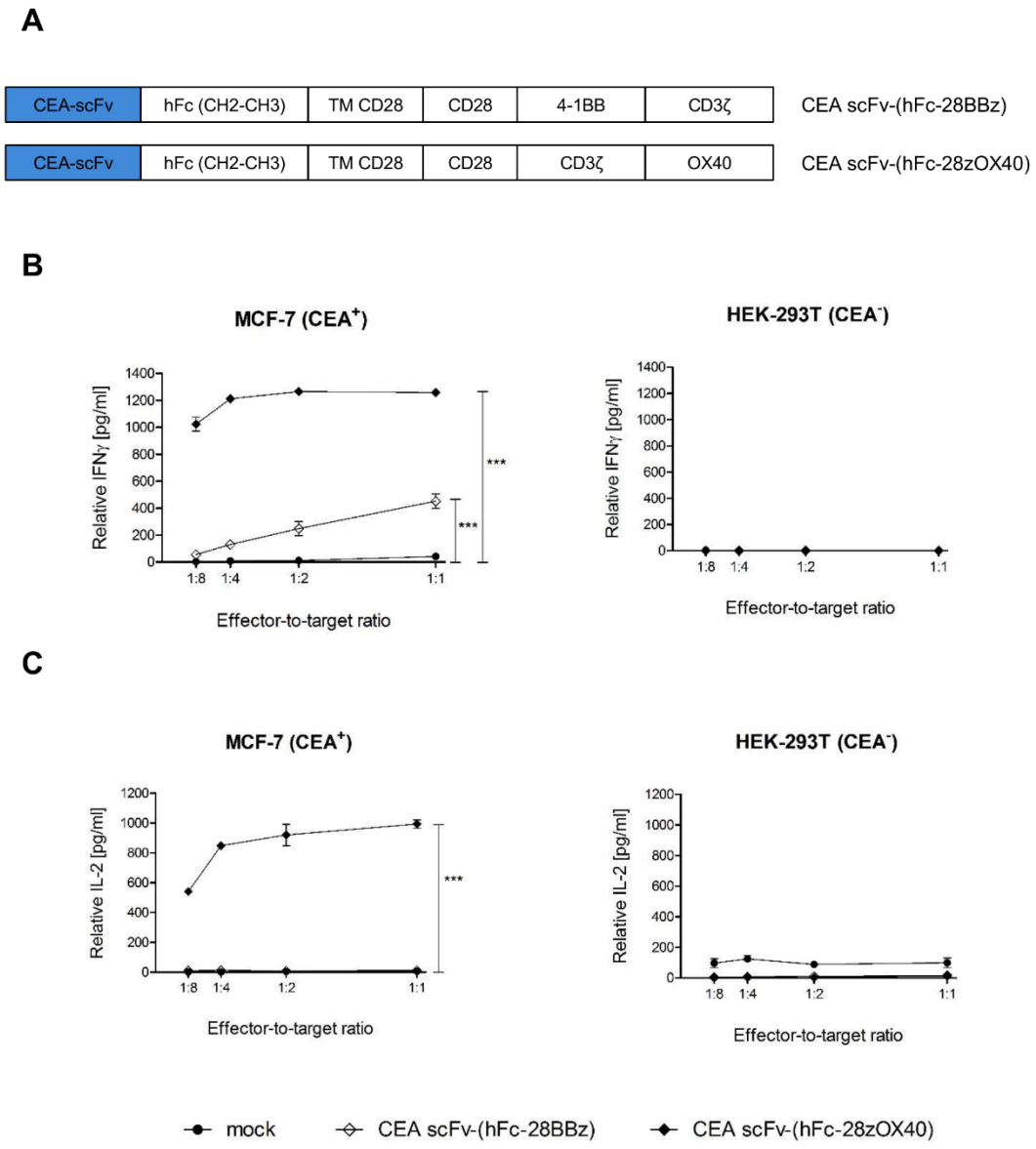

Figure 16: Activation of CEA scFv-(hFc-28BBz) and CEA scFv-(hFc-28zOX40) CAR T cells. A: Schematic representation of the CEA CAR constructs incorporating either 4-1BB or OX40 as second co-stimulatory domain. **B:** $CD3^+$ cells were transduced with lentiviral particles containing the CEA CAR DNA. MCF-7 cells (left) and HEK-293T cells (right, $3x10^4$ cells per well) were co-cultured for 48 h with CEA CAR T cells and non-transduced T cells ($0.375x10^4$ - $3x10^4$ cells per well) to analyze the specific CAR T cell activation. IFNγ levels in the supernatant were measured by ELISA as a read out for CAR T cell activation. **C:** IL-2 levels present in the supernatant were quantified by ELISA. Data represent the mean of triplicates ± standard deviation. * $P < 0.05$; ** $P < 0.01$; *** $P < 0.001$.

At an effector-to-target ratio of 1:1, the significantly increased IFNγ secretion confirmed the specific activation of both CEA CAR T cells by the CEA antigen. While the co-stimulatory domain CD28, responsible for IL-2 secretion, is integrated in both tested CEA CARs, the type of second-co-stimulatory domain seems to have a direct impact on the IL-2 release. The presence of OX40 in combination with CD28 might promote the IL-2 secretion compared to 4-1BB.

3.3.2.2.2 T cell activation of hCD22 scFv-(hFc-28zOX40) *in vitro*

To investigate if IL-2 secretion is specific to CEA scFv-(hFc-28zOX40) CAR T cells or is induced by the presence of the combination CD28-OX40, independently of the scFv targeting domain, the hCD22 scFv-(hFc-28zOX40) CAR incorporating the hCD22 scFv and the co-stimulatory domains CD28 and OX40 was generated (Figure 17 A).

Isolated T cells equipped with hCD22 CAR harboring either the OX40 or 4-1BB domain were compared to each other by analyzing the IFNγ and IL-2 levels present in the supernatant after binding to CD22 (method 2.4.8). For this purpose, transduced T cells were incubated with coated recombinant hCD22-hFc proteins. After 48 h, the level of secreted cytokines was measured by ELISA. To control for non-specific activation, hCD22 CAR T cells were also incubated in a control plate coated with the hFc protein (Figure 17B). The resulting unspecific activation was subtracted before plotting. When incubated on a plate coated with hCD22-hFc, hCD22 CAR T cells containing either OX40 or 4-1BB were specifically activated by binding the hCD22 protein and high IFNγ amounts were detected in the supernatant in comparison to T cells without CAR (Figure 17C). Significant IL-2 levels were measured in the supernatant of hCD22 CAR T cells presenting OX40 as co-stimulatory domain in comparison to non-transduced T cells. No IL-2 was secreted from hCD22 CAR T cells containing the 4-1BB domain.

For CEA scFv-(hFc-28zOX40) and hCD22 scFv-(hFc-28zOX40) CAR T cells, the combination of the intracellular co-stimulatory domains seems to be decisive for a detectable IL-2 secretion whereas the targeting domain has no influence.

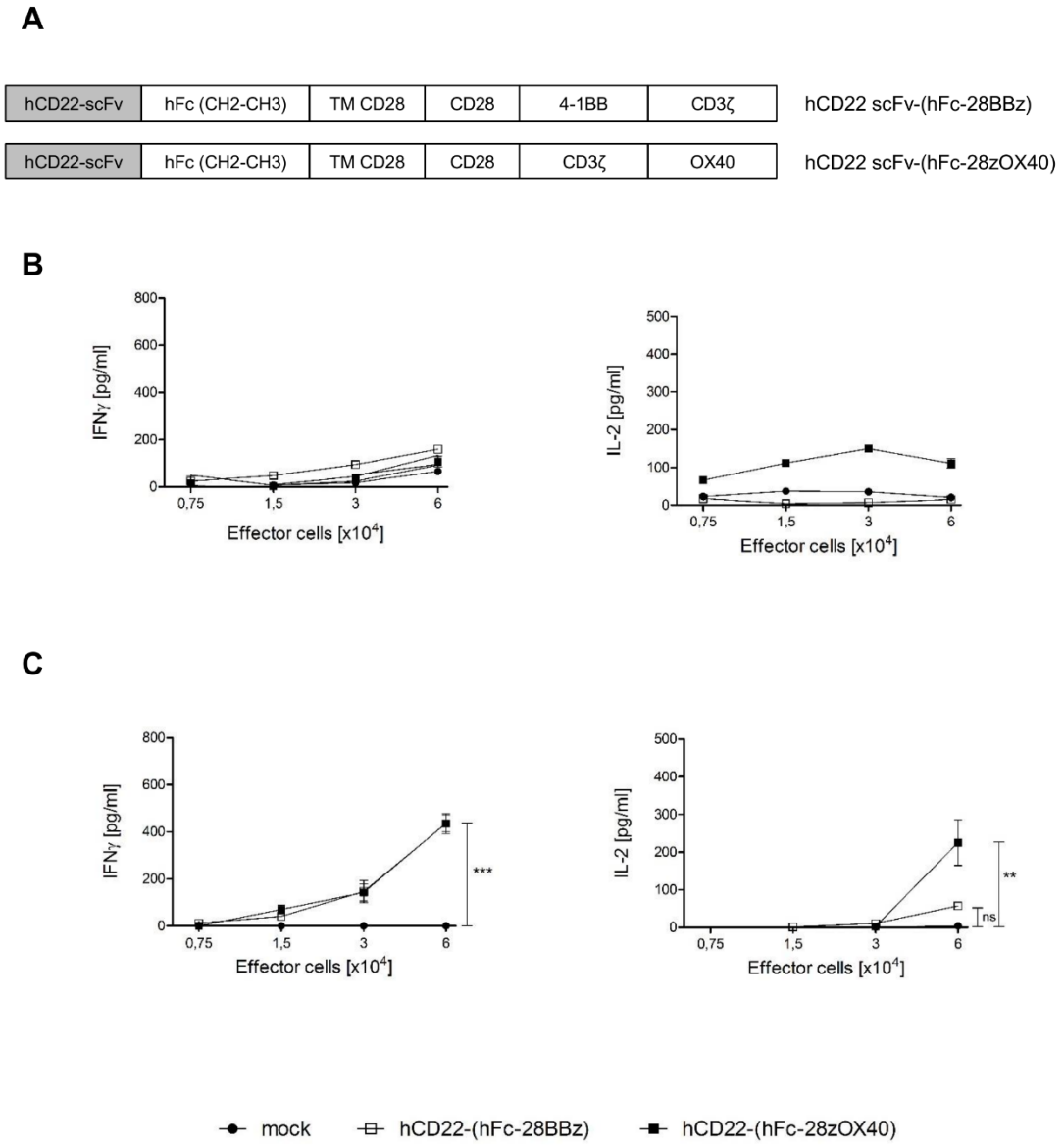

Figure 17: Activation of hCD22 scFv-(hFc-28BBz) and hCD22 scFv-(hFc-28zOX40) CAR T cells. **A:** Schematic representation of the hCD22 CAR containing either OX40 or 4-1BB as second co-stimulatory domain. **B:** Through lentiviral gene transfer, isolated T cells from a healthy donor were equipped with the hCD22 CARs. To control the specificity, hCD22 CAR transduced T cells and non-transduced T cells ($0.75x10^4$ - $6x10^4$ cells) were incubated for 48 h with coated hFc proteins. Specific CAR T cell activation was assessed by measuring the amount of secreted IFNγ (left) and IL-2 (right) by ELISA. **C:** To assess specific CAR T cell activation, hCD22 CAR transduced T cells and non-transduced T cells ($0.75x10^4$ - $6x10^4$ cells) were incubated for 48 h with coated hCD22-hFc proteins. Amount of secreted IFNγ and IL-2 obtained for transduced and non-transduced T cells incubated with coated hFc proteins was deduced before plotting. Data represent the mean of triplicates ± standard deviation. * $P < 0.05$; ** $P < 0.01$; *** $P < 0.001$.

3.3.2.3 *In vitro* cytotoxicity analysis of the mutated CAR variants

In this approach, the T cell activation of parental and mutated hCD22 CARs was characterized *in vitro* in order to select the lead candidate for further *in vivo* studies. An IFNγ ELISA was performed to assess if CAR T cells are specifically activated through CD22 positive Nalm-6 cells and an apoptosis assay allowed the investigation of target induced tumor cell lysis. Taking into account natural T cell variability, T cells from three healthy donors were tested independently.

Purified donor T cells were modified *ex vivo* by lentiviral gene transfer with either the parental, the ΔhFc, the ΔCD28 or the ΔFc-ΔCD28 hCD22 CARs. Expression of the four different CAR variants on the surface of T cells was determined by flow cytometry with an APC conjugated anti-CD3 antibody, recognizing $CD3^+$ T cells, and a PE-conjugated IgG1 antibody detecting the parental and the mutated hFc spacer domain of the CAR.

The relative number of T cells expressing the hCD22 CAR variants differed for each donor within a range from 10% to 60% (Table 22). The highest expressing hCD22 CAR T cells were obtained for donor 1 whereas the relative CAR expression on T cells from donor 3 was the lowest. Within each donor, the expression levels among the different CAR constructs varied around 10%.

Table 22: Expression of hCD22 CAR variants on the surface of T cells from three donors.

	Relative CAR expression (%)		
hCD22 CAR variants	Donor 1	Donor 2	Donor 3
hCD22 scFv-(hFc-28BBz)	48,2	39,2	14,7
hCD22 scFv-(ΔhFc-28BBz)	59,4	43,1	10
hCD22 scFv-(hFc-Δ28BBz)	60	40,7	10,5
hCD22 scFv-(ΔhFc-Δ28BBz)	51,5	33,6	18,4

For each donor, the different hCD22 CAR T cells were incubated with the CD22 positive target cell line Nalm-6 at an effector-to-target ratio of 1:1 to measure the specific CAR T cell activation. To enable a comparison among the hCD22 CAR variants while their expression levels are different, the amounts of hCD22 CAR T cells were adjusted to incubate the same quantity of positively expressing CAR T cells. To assess the specific activation, CAR T cells were also cultivated alone (w/o) and with target negative Jurkat cells. After 24 h or 48 h, the supernatant of the co-culture was removed for IFNγ measurement and the remaining cells were used to quantify CAR T cell mediated tumor cell lysis by flow cytometry (method 2.3.7). CD22 positive Nalm-6 cells were identified by a PE-Cy7 conjugated anti-CD19 antibody and both T cells as well as Jurkat cells by a pacific-blue conjugated anti-CD3 antibody. Nalm-6 cell death was detected by the combination of the apoptotic markers, namely FITC conjugated annexin V and propidium iodide (PI) for the first and second donor and by caspase 3 for the third donor in order to validate cytotoxicity via a second detection system.

For donor 1, all three hCD22 CAR T cell variants triggered the lysis of CD22 positive Nalm-6 but had no cytotoxic effect on CD22 negative Jurkat cells (Figure 18A). T cells transduced with the parental hCD22 CAR induced 20% higher tumor cell lysis than ΔhFc and ΔCD28 hCD22 CAR T cells. $CD3^+$ cells expressing the double mutant ΔFc-ΔCD28 hCD22 construct showed the lowest lytic activity. Significantly more IFNγ was detected in the supernatant of T cells with the parental CAR after cultivation with Nalm-6 cells compared to the supernatant of mutated CAR T cells (Figure 18B). Double mutant ΔFc-ΔCD28 hCD22 CAR T cells induced the lowest cytokine release.

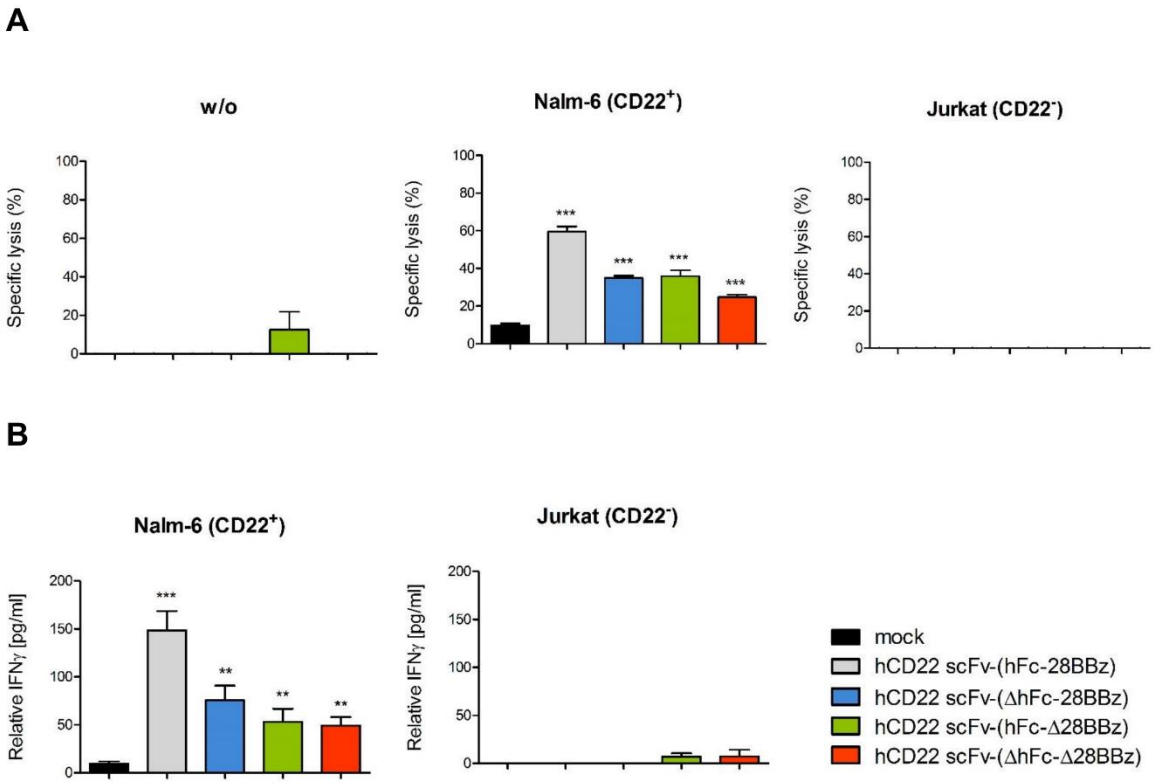

Figure 18: Specific activation of parental and mutated hCD22 CAR expressing T cells from donor 1. A: Freshly isolated T cells from donor 1 were transduced with lentivirus particles containing one of the four hCD22 CAR variant genes and cultured ($1x10^5$ cells per well) either alone (w/o; left), with Nalm-6 (middle) or with Jurkat cells (right; $1x10^5$ cells per well). After 48 h, co-cultivated cells were stained with an anti-CD19 antibody, an anti-CD3 antibody, annexin V and PI to determine tumor cell lysis by flow cytometry. **B:** The concentration of IFNγ present in the supernatant was measured by ELISA. Data represent the mean of triplicates ± standard deviation. * $P < 0.05$; ** $P < 0.01$; *** $P < 0.001$.

For the second donor, Nalm-6 cell lysis was mediated by T cells equipped with each of the four hCD22 CAR variants whereas no lytic activity was observed after co-incubation with Jurkat cells (Figure 19A). T cells expressing either the parental, the ΔhFc or the ΔCD28 hCD22 CARs showed a similar lytic activity. The hCD22 CAR T cells carrying a mutated spacer and a mutated CD28 domain lysed a lower amount of tumor cells. IFNγ secretion was detected for all hCD22 CAR variant T cells co-incubated with Nalm-6 cells (Figure 19B). For this donor and contrary to donor 1, a relatively high amount of IFNγ was measured for non-transduced T cells (mock)

when incubated with Nalm-6 cells which is probably due to alloreactive T cells. When incubated with Jurkat cells, no IFNγ secretion was detected.

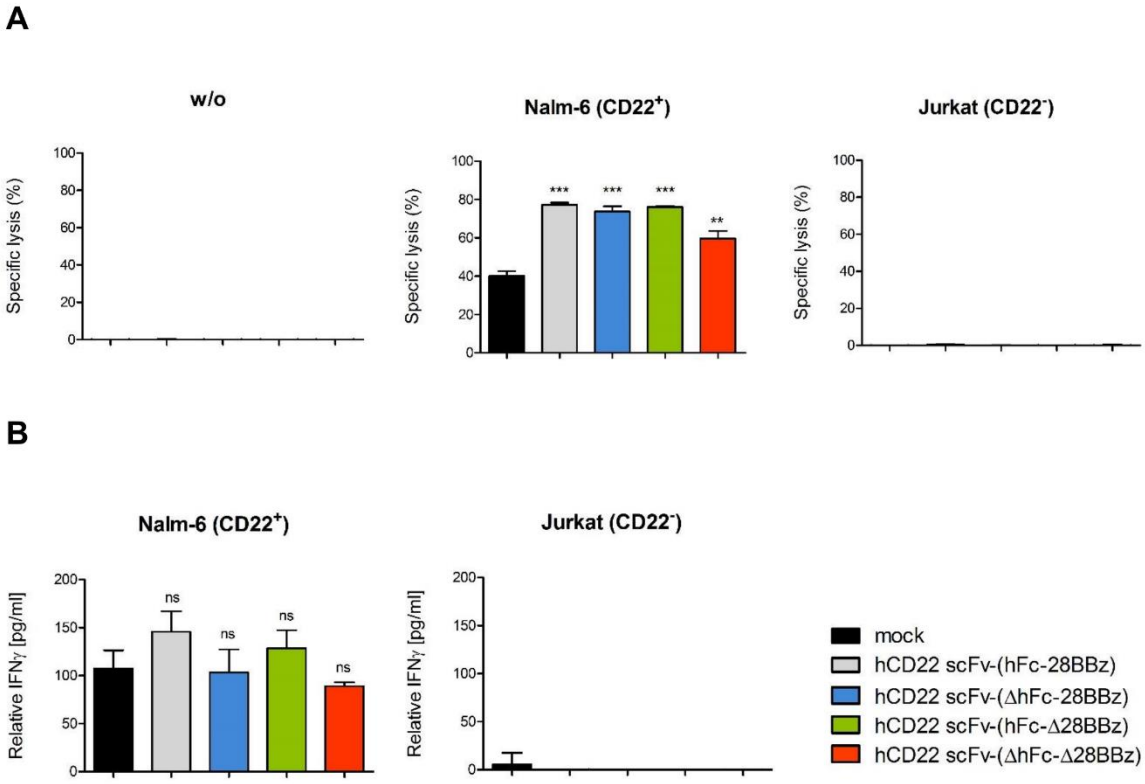

Figure 19: Specific activation of parental and mutated hCD22 CAR expressing T cells from donor 2. A: Isolated T cells from donor 2 were equipped with one of the four hCD22 CAR variants by lentiviral gene transfer. CAR T cells ($1x10^5$ cells per well) were cultured either alone (w/o; left), with Nalm-6 (middle) or with Jurkat cells (right; $1x10^5$ cells per well). After 48 h, tumor cell lysis was assessed by flow cytometry. Cultivated cells were stained with an anti-CD19 antibody, an anti-CD3 antibody, annexin V and PI. **B:** Secretion of IFNγ in the supernatant was evaluated by ELISA. Data represent the mean of triplicates ± standard deviation. * $P < 0.05$; ** $P < 0.01$; *** $P < 0.001$.

For the third donor, specific tumor cell lysis was assessed by the IntelliCyt HTFC screening system measuring the apoptotic marker caspase 3. Mutated hCD22 CAR T cells triggered a specific Nalm-6 cell lysis compared to T cells without CAR (Figure 20A). For this donor, the lytic activity of the ΔFc-ΔCD28 double mutated hCD22 CAR T cells was as high as for the ΔFc and for the ΔCD28 mutated CAR T cells. T cells transduced with the parental hCD22 CAR showed no significant tumor cell lysis in comparison to non-transduced T cells. An alloreaction of these original T cells might be responsible for the high level of observed cytotoxicity. In the

supernatant of mutated hCD22 CAR T cells incubated with Nalm-6 cells, high amounts of IFNγ were measured (Figure 20B). When incubated with $CD22^+$ tumor cells, no significant cytokine levels were detected for T cells expressing the parental CAR variant in comparison to T cells without CAR.

Parental hCD22 CAR T cell activation has already been shown in earlier experiments through specific tumor cell lysis for donor 1 and 2 as well as through IFNγ secretion. Therefore, for this donor, the lack of a significant activation is probably due to a combination of alloreactive T cells and a problem in the experimental progress.

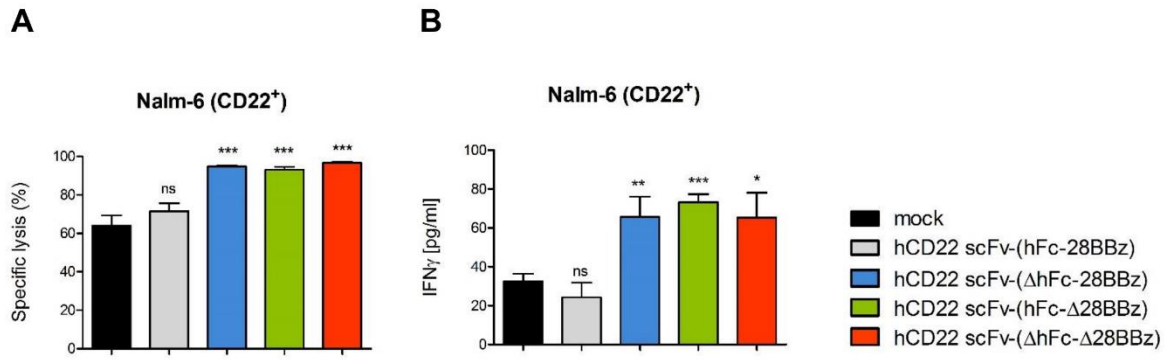

Figure 20: Specific activation of parental and mutated hCD22 CAR expressing T cells from donor 3. A: Freshly isolated T cells from donor 3 were equipped with the four hCD22 CAR variants by lentiviral gene transfer and cultured ($1x10^5$ cells per well) with Nalm-6 cells ($1x10^5$ cells per well). After 24 h, specific tumor cell lysis was determined via the IntelliCyt HTFC Screening System by measuring the apoptotic marker caspase 3. **B:** Concentration of secreted IFNγ was quantified by the IntelliCyt HTFC Screening System. Data represent the mean of triplicates ± standard deviation. * $P < 0.05$; ** $P < 0.01$; *** $P < 0.001$.

Using two distinct detection methods, T cell activation mediated by the parental and the mutated hCD22 CARs was confirmed with T cells from different donors. Introduction of the mutation in the hFc or the CD28 domain had no influence on the capacity of hCD22 CAR T cells to induce lytic activity against CD22 positive tumor cells. Nevertheless, by mutating the spacer and the domain responsible for IL-2 secretion, the lytic activity of the double mutated ΔFc-ΔCD28 hCD22 CAR was reduced in comparison to the ΔFc or ΔCD28 mutated ones.

Successful clinical development of a CAR T cell therapy is strongly related to the prevention and management of unwanted CAR toxicity (Bonifant et al., 2016). To improve CAR safety, toxic effects following CAR T cell infusion have to be minimized. Therefore, based on its lower lytic activity and on its innovative aspect by combining the hFc and CD28 mutations, the hCD22 scFv-(ΔhFc-Δ28BBz) CAR is selected as lead candidate for further *in vivo* studies.

3.4 Characterization of the lead candidate and preliminary *in vivo* studies

3.4.1 Selection of a CAR lead candidate for *in vivo* studies

3.4.1.1 Generation of the hCD22 (L36Y) scFv-(ΔhFc-Δ28BBz) CAR

Previously, for the generation of an anti-CD22 derived dimeric immunoenzyme, a hCD22 diabody was created by reducing the size of the linker peptide (Krauss et al., 2005b). Early bacterial production of this hCD22 diabody resulted in high aggregation levels. Due to the formation of multimeric molecules, the soluble expression and purification of the diabody-RNase fusion protein was difficult (Krauss et al., 2005b). To overcome this problem, the V_H-V_L interface of the hCD22 diabody was engineered by mutating the leucine residue at position 36 to tyrosine, a common human amino acid at this location. This amino acid exchange also resulted in enhanced solubility and stability of the bivalent molecules.

Since the properties of the antibody fragment directly affect CAR T cell activation, we investigated if the stability of the hCD22 CAR can be enhanced by engineering the associated scFv. For this purpose, the engineered hCD22 (L36Y) scFv-(ΔhFc-Δ28BBz) CAR (simplified as L36Y engineered ΔFc-ΔCD28 hCD22 CAR) was generated (Figure 21A). The mutation at position 36 of the V_H-V_L interface was introduced by site directed mutagenesis using hCD22_LY-Fw and hCD22_LY-Rev as primer set and the non-engineered double mutant ΔFc-ΔCD28 hCD22 CAR entry clone vector (pENTR) as template. The final expression clone was confirmed by analytical digestion and further used to produce the corresponding lentiviral particles.

3.4.1.2 T cell activation of hCD22 (L36Y) scFv-(∆hFc-∆28BBz) *in vitro*

To assess the stability of the L36Y engineered ΔFc-ΔCD28 hCD22 CAR in comparison to the ΔFc-ΔCD28 construct, IFNγ secretion was measured after CAR T cell activation. T cells isolated from the blood of three healthy donors were used as biological triplicates to account for T cell variability. After lentiviral gene transfer, transduced T cells were incubated for 48 h on a plate coated with the recombinant hCD22-hFc protein. The IFNγ concentration, in the supernatant, was detected by ELISA. To analyze unspecific activation, L36Y engineered ΔFc-ΔCD28 and ΔFc-ΔCD28 hCD22 CAR T cells were also incubated on a control plate coated with the hFc protein only. The resulting unspecific activation was deduced before plotting.

For the first donor, both hCD22 CAR T cells induced IFNγ release after binding to the hCD22 antigen in comparison to T cells without CAR. A higher cytokine concentration was measured for T cells expressing the L36Y engineered ΔFc-ΔCD28 hCD22 CAR (Figure 21B).

For the second and third donor, IFNγ secretion was only detected for ΔFc-ΔCD28 CAR T cells. L36Y engineered CAR T cells did not induce secretion of this cytokine when compared to ordinary T cells.

The mutation in the hCD22 scFv did not enhance the activation of the corresponding CAR T cells. The double mutant ΔFc-ΔCD28 hCD22 CAR was therefore kept as lead candidate for further *in vivo* studies.

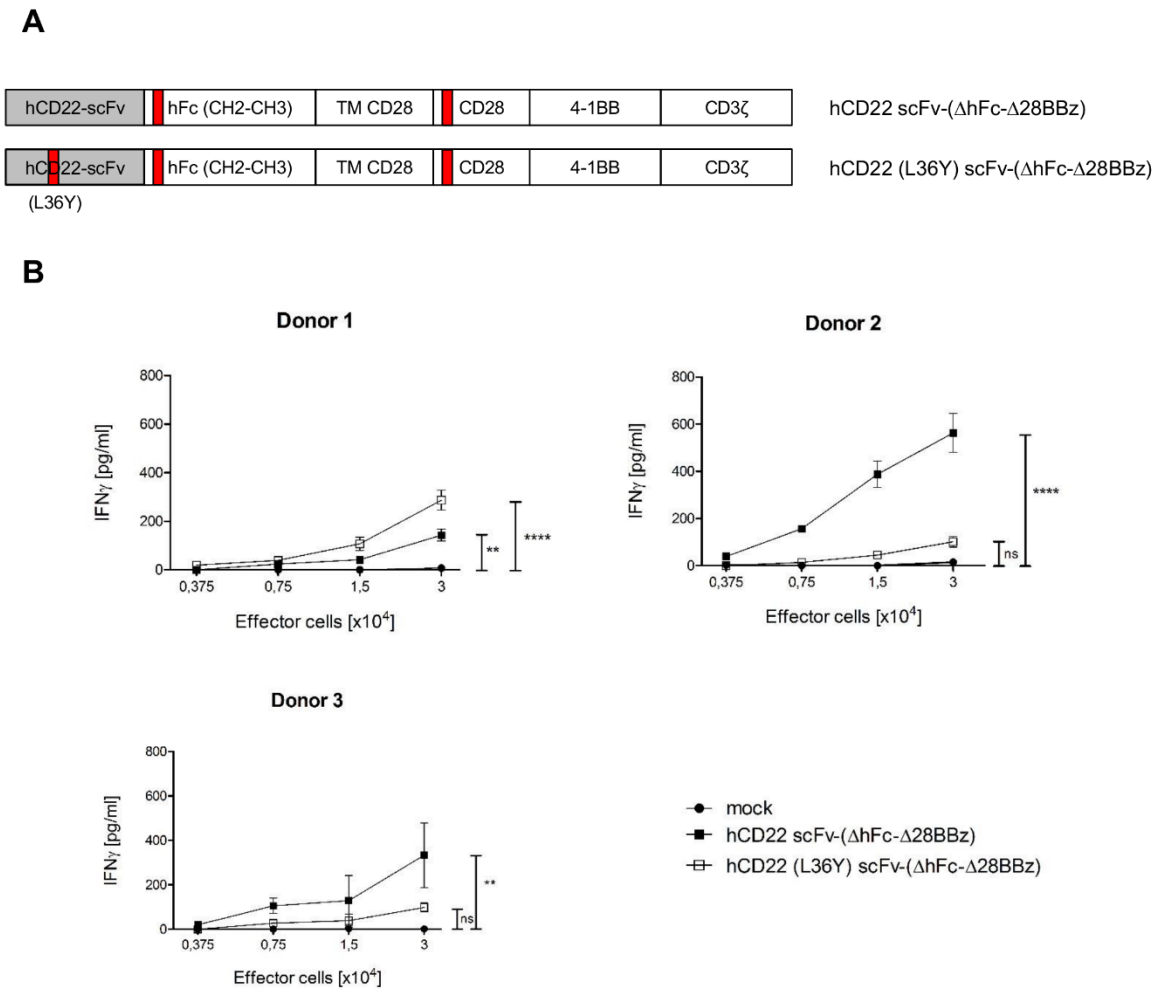

Figure 21: Specific activation of hCD22 scFv-(ΔhFc-Δ28BBz) and hCD22 (L36Y) scFv-(ΔhFc-Δ28BBz) CAR T cells. A: Schematic representation of the ΔFc-ΔCD28 and L36Y engineered ΔFc-ΔCD28 hCD22 CAR. **B:** Freshly isolated T cells from the blood of three healthy donors were transduced with lentiviral particles containing the ΔFc-ΔCD28 or L36Y engineered ΔFc-ΔCD28 CAR gene. These CAR T cells and non-transduced T cells ($0.75x10^4$ - $3x10^4$ cells) were incubated for 48 h on a plate coated with hCD22-hFc protein. Specific activation of CAR T cells was assessed by measuring the amount of secreted IFNγ for donor 1 (top left), donor 2 (right) and donor 3 (bottom left) present in the supernatant of the co-cultures via ELISA.

3.4.2 Generation and T cell activation of mCD22 scFv-(ΔhFc-Δ28BBz) and HSV scFv-(ΔhFc-Δ28BBz) *in vitro*

After completion of the *in vitro* characterization of the double mutant ΔFc-ΔCD28 hCD22 CAR, the aim was to characterize the *in vivo* the efficacy of the construct using a xenograft mouse model. As the hCD22 antibody fragment is derived from the mCD22 scFv (Krauss et al., 2003b), a double mutant mCD22 CAR (mCD22 scFv-(ΔhFc-Δ28BBz)) (ΔFc-ΔCD28 mCD22 CAR) was created and included in the experiments for direct comparison (Figure 22A). To control the scFv-independent effect of the CAR backbone itself, a double mutant CAR comprising a non-relevant anti-herpes simplex virus (HSV) scFv (HSV scFv-(ΔhFc-Δ28BBz)) (ΔFc-ΔCD28 HSV CAR) was generated and used as control.

The new double mutant ΔFc-ΔCD28 mCD22 and HSV CARs were built by replacing the hCD22 scFv with the corresponding antibody moiety in the double mutant entry clone. Final expression clones obtained after the gateway reaction were used for lentiviral gene transfer.

Specific activation of double mutant ΔFc-ΔCD28 mCD22 CAR T cells against CD22 expressing Nalm-6 cells was assessed by measuring induced tumor cell lysis and IFNγ secretion. Double mutant ΔFc-ΔCD28 HSV CAR T cells were tested in parallel. After lentiviral gene transfer, the same amount of CAR expressing T cells was co-incubated with Nalm-6 cells. To control for non-specific CAR mediated activation, double mutant ΔFc-ΔCD28 mCD22 and HSV CAR T cells were also cultured alone or with target negative Jurkat cells. After 48 h, the concentration of IFNγ in the supernatant was determined and the remaining cells were analyzed by flow cytometry to quantify CAR T cell mediated tumor cell lysis. CD22 positive Nalm-6 cells were identified by a PE-Cy7 conjugated anti-CD19 antibody, T cells and Jurkat cells by a pacific-blue conjugated anti-CD3 antibody. Lysis of Nalm-6 cells was detected by the apoptotic marker combination FITC conjugated annexin V / PI.

When incubated with CD22 positive Nalm-6 cells, specific tumor cell lysis was observed for double mutant ΔFc-ΔCD28 mCD22 CAR T cells in comparison to T cells transduced with the ΔFc-ΔCD28 HSV CAR (Figure 22B). No lytic activity was detected for double mutant ΔFc-ΔCD28 mCD22 and HSV CAR T cells incubated with Jurkat cells confirming the specificity of the ΔFc-ΔCD28 mCD22 CAR. Detected IFNγ

levels were significantly higher for double mutant ΔFc-ΔCD28 mCD22 CAR T cells than for HSV CAR T cells when co-incubated with Nalm-6 cells (Figure 22C). No cytokine secretion was observed for both CAR T cells after co-cultivation with Jurkat cells.

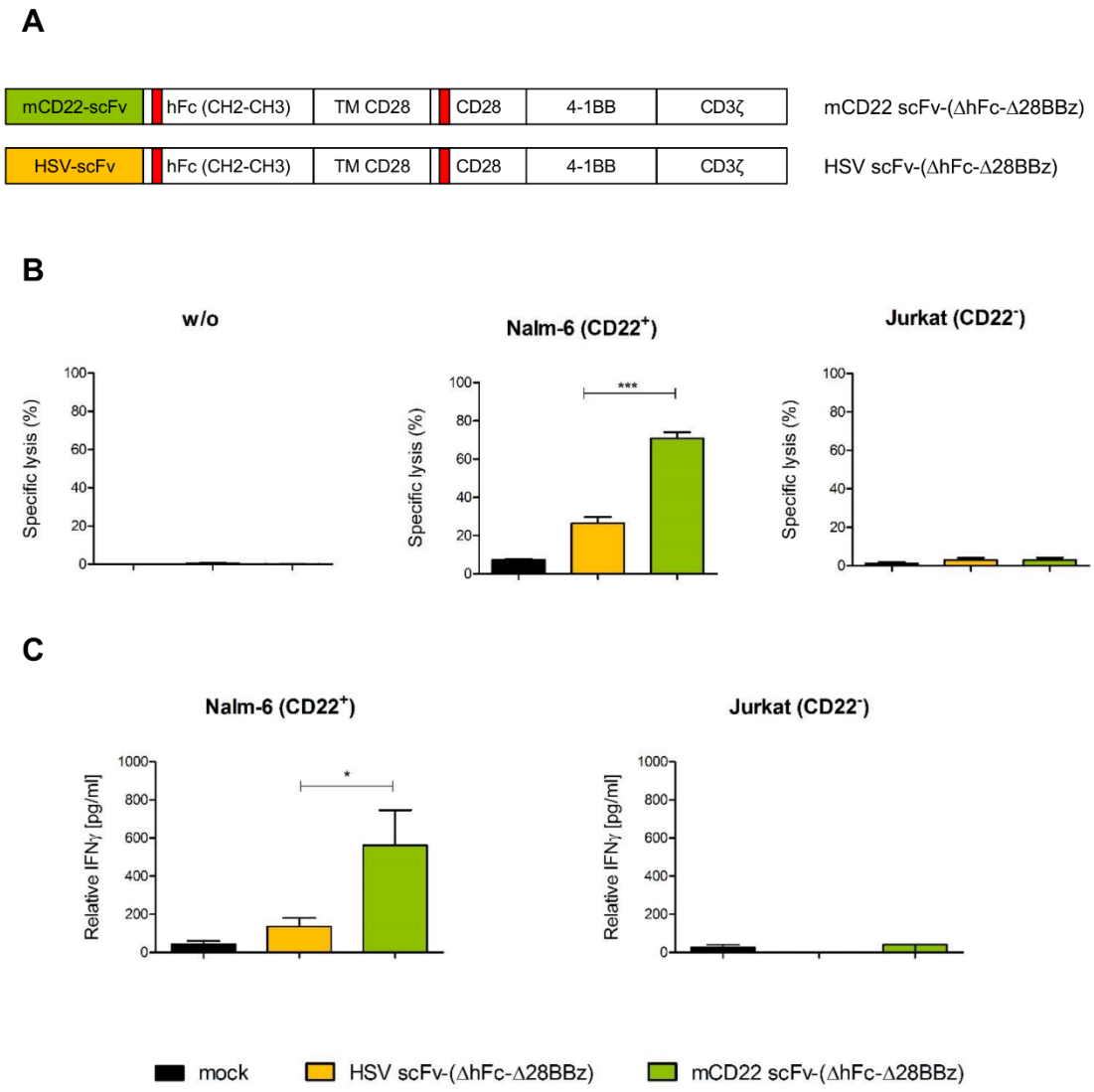

Figure 22: *In vitro* characterization of double mutant mCD22 and HSV CAR expressing T cells. **A:** Schematic representation of the double mutant mCD22 and the double mutant HSV CAR. **B:** $CD3^+$ isolated T cells were transduced with lentivirus encoding either the double mutant mCD22 or HSV CAR. CAR T cells ($1x10^5$ cells per well) were cultured either alone (w/o; left), with Nalm-6 cells (middle) or with Jurkat cells (right; $1x10^5$ cells per well). After 48 h, tumor cell lysis was assessed by flow cytometry. Cultivated cells were stained with PE-Cy7 conjugated anti-CD19 antibody, the pacific-blue conjugated anti-CD3 antibody, FITC conjugated annexin V and PI. **C:** The concentration of secreted IFNγ was determined by ELISA.

3.4.3 Preliminary *in vivo* studies: establishment of a leukemia xenograft in NOD-SCID mice

In order to assess the therapeutic *in vivo* efficacy of double mutant ΔFc-ΔCD28 hCD22 and mCD22 CAR T cells in NOD/SCID mice, a disseminated model of pre-B-cell acute lymphoblastic leukemia, the CD22 positive Nalm-6 cell line, was used.

Engraftment of tumor cells was first investigated in a preliminary *in vivo* test. The use of stably luciferase transfected Nalm-6 cells (Nalm-6-Luc cells), previously generated by Tobias Weber (PhD, University of Heidelberg) allowed the monitoring of the tumor progression by non-invasive bioluminescent measurements. Mice with a body weight loss of more than 20% or showing tumor related paralysis symptoms were sacrificed.

Six female NOD/SCID mice (6 - 8 weeks old) were separated into two groups and received either $1x10^6$ or $5x10^6$ Nalm-6-Luc cells intravenously. Disseminated tumor engraftment was monitored one to two times per week by bioluminescence imaging. This non-invasive method is based on light emission resulting from the oxidation of D-luciferin by the luciferase enzyme expressed in the tumor cells. Intraperitoneal injection of 3 mg of D-luciferin substrate per mouse is followed, after 10 min, by light measurement of luciferase transfected leukemia cells. Measured luciferase activity is presented as the number of photons detected per minute.

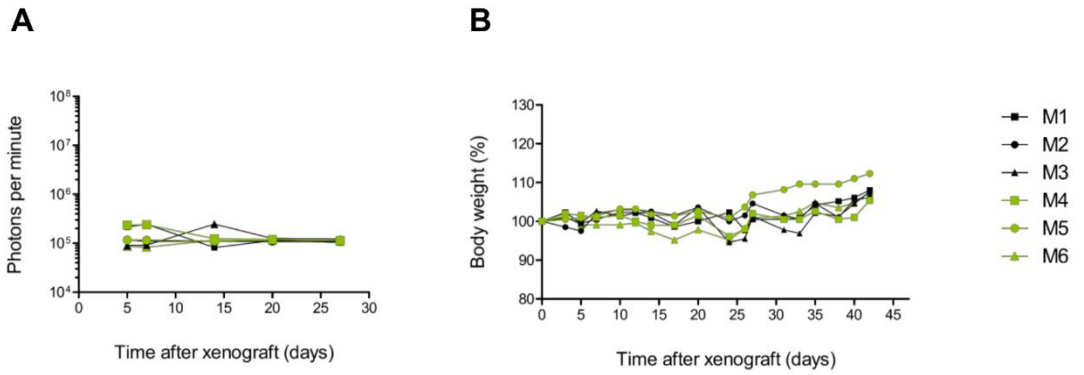

Figure 23: Preliminary *in vivo* test with a disseminated Nalm-6 xenograft model. Each NOD/SCID mouse (M1-M6) received an intravenous injection of $1x10^6$ (black) or $5x10^6$ (green) Nalm-6-Luc cells. **A:** Number of photons detected per minute. Luciferase activity was measured one to two times per week starting at day 5. **B:** Weight progression of each animal.

The first bioluminescence imaging was performed five days after xenotransplantation (Figure 23A). Until day 27, no tumor progression was observed for all six mice. The body weight of the animals, regularly measured after xenotransplantation, remained stable over time (Figure 23B). No tumor engraftment could be observed in the NOD/SCID mice.

4 Discussion

4.1 CD22 as target for a CAR based therapy

Over the last decade, the adoptive T cell transfer with chimeric antigen receptor (CAR) engineered T cells emerged as a clinically effective therapy to treat hematological malignancies. A CAR consists of at least two functional components: an extracellular single chain variable fragment (scFv) specifically binding a tumor-associated antigen (TAA) and an intracellular T cell receptor (TCR) derived signaling domain, initiating T cell activation upon target engagement (Eshhar, 2008; Gross et al., 1989). To ensure high anti-tumor efficacy and at the same time a low toxicity, the target antigen has to be carefully chosen when developing a CAR therapy.

Nowadays, the most investigated target is CD19 due to its presence in most B cell malignancies. Its B cell lineage limited expression (Li et al., 1996) restricts the potential of off-target complications. Apart from malignant cells, healthy B cells expressing CD19 are likewise destroyed as seen during CD19 CAR T cell therapy, resulting in B cell aplasia and hypogammaglobulinemia (Kochenderfer et al., 2012b; Porter et al., 2011). This side effect can fortunately be managed by γ-globulin infusion as replacement. Unlike CD19, an unwanted outcome occurred with CAR T cells therapy targeting the carbonic anhydrase IX (CAIX), a target overexpressed on the surface of clear cell renal carcinoma (Lamers et al., 2006). Due to unexpected target expression in the biliary tract, for which CAIX transduced CAR T cells showed reactivity, liver toxicity was observed in treated patients after therapy.

In the field of CAR therapy, two second generation CD19 CARs, harboring either the co-stimulatory domain CD28 or 4-1BB in addition to CD3ζ have been mainly investigated. Preclinical studies showed enhanced antitumor activity compared to the CD19 CAR without co-stimulatory domains (Brentjens et al., 2007; Milone et al., 2009) and the efficacy of both CARs was confirmed in the clinic. A milestone was achieved in 2012 with a phase I clinical trial using CD19 CAR T cells carrying the co-stimulatory domain 4-1BB when lasting remissions were observed in relapsed acute lymphoblastic leukemia patients (Maude et al., 2014). Further phase I clinical trials were performed in three independent centers and the treatment of pediatric and adult B-ALL patients using CD19 CAR T cells showed complete remission rates

within a range of 67 to 90% (Brentjens et al., 2013; Davila et al., 2014; Lee et al., 2015; Maude et al., 2014). This number is particularly impressive when considering the poor prognosis of relapsed ALL patients. Indeed, relapse after CD19 CAR T cell therapy remains a challenge in B-ALL. At this stage of treatment, not only CD19 positive but also CD19 negative blast cells have been observed and their progression is a concern. In a recent trial, target loss occurring under selective pressure was observed in one child with relapsed and refractory pre-B-ALL after CD19 CAR T cell therapy (Grupp et al., 2013). These results are in accordance with earlier studies suggesting that CD19 negative variants are already present at low levels in some patients with ALL at the time of treatment (Hotfilder et al., 2005; Sotillo et al., 2015; Le Viseur et al., 2009). The CD19 epitope is lost from leukemia cells in 10 to 20% of pediatric B-ALL treated with anti-CD19 antibody based therapy (Sotillo et al., 2015). The enrichment of CD19 negative blast cells might be a direct consequence of CD19 CAR therapy leading to a decrease in CD19 CAR T cells efficiency and consequently to ALL relapse. To overcome CD19 antigen loss in relapsed ALL patients, alternative CAR therapies, targeting new antigens, need to emerge.

Like CD19, the cell surface antigen CD22 has a B cell restricted expression and is essential in B lineage differentiation (Nitschke, 2009; Tedder et al., 2005). Within a range of 50 - 100% in adult (Hoelzer and Gökbuget, 2012; Piccaluga et al., 2011; Raponi et al., 2011) and around 90% in pediatric acute lymphoblastic leukemia (ALL) (Iwamoto et al., 2011; Raetz et al., 2008), CD22 is frequently expressed on B-ALL. Complete remission was observed in phase II clinical trials using the humanized anti-CD22 monoclonal antibody Epratuzumab in combination with chemotherapy in adult ALL patients (Advani et al., 2014; Chevallier et al., 2015) and in a phase I dose-escalation trial of the anti-CD22 recombinant immunotoxin HA22 in relapsed and refractory hairy cell leukemia patients (Kreitman et al., 2012). Another anti-CD22 monoclonal antibody-based therapies, an anti-CD22 CAR (Haso et al., 2013) are currently being developed. The CD22 expression profile and the clinical success of related therapies confirm CD22 as an important therapeutic target in B cell malignancies.

A therapy based on the currently developed double mutant hCD22 scFv-(ΔhFc-Δ28BBz) CAR would therefore be an ideal and promising therapeutic option to treat CD22 positive pediatric and adult B-ALL patients. This kind of treatment could

be used as a single therapy or in combination with CD19 CAR T cells for refractory and relapsed ALL patients to overcome the loss of the CD19 epitope (Grupp et al., 2013). Indeed, this could especially prevent the emergence and growth of CD19 negative blasts as well as ALL relapse.

Besides ALL, sustainable remission was also observed in patients with relapsed and refractory non-Hodgkin's lymphoma (NHL), especially with diffuse large B-cell lymphoma, when treated with ^{90}Y-epratuzumab tetraxetan, an anti-CD22 radioimmunotherapy (Kraeber-Bodere et al., 2016; Morschhauser et al., 2010). Concerning the treatment of lymphoma with CARs, the clinical efficacy appears more modest than for ALL but highly encouraging partial and complete responses were observed with CD19 CAR or CD20 CAR therapies (Kochenderfer et al., 2015; Till et al., 2008; Wang et al., 2014).

4.2 Evaluation of the hCD22 scFv-(ΔhFc-Δ28BBz) CAR with regard to safety

4.2.1 Stability of the hCD22 and mCD22 targeting domains and derived CARs

Choosing a selectively expressed tumor target and a single chain variable fragment (scFv) with high target affinity is crucial for CAR development as both contribute substantially to the safety of such a therapy. The incorporated antibody fragment has to specifically recognize its target antigen to avoid off-target toxicity. Another important scFv requirement is a high thermal stability (Willuda et al., 1999). Indeed, for the use in patients, the activity of the therapeutic antibody fragment has to be retained for several hours or days at 37°C in the serum without degradation. However, some high affinity scFvs were shown to be unstable with the tendency to denature and aggregate, limiting their activity and clinical application (Willuda et al., 1999; Wörn and Plückthun, 1999). To reduce thermal instability without affecting the affinity, a linker peptide or an interdomain disulfide bond can be introduced forming a scFv or a stabilized antibody fragment (dsFv), respectively (Wörn and Plückthun, 2001; Zhao et al., 2011). This stabilization measure was performed for the anti-B3 immunotoxin B3(dsFv), and, resulted in the prevention of the dissociation of the variable chain and reduced the tendency to aggregate (Brinkmann et al., 1993).

In the present thesis, a highly stable, humanized anti-CD22 (hCD22) scFv was used for the development of an anti-CD22 CAR therapy against CD22 positive leukemia and lymphoma. Derived from the clinically established murine anti-CD22 IgG1 RFB4 antibody (Campana et al., 1985), the hCD22 targeting moiety was generated by grafting the specificity-determining regions of the murine RFB4 antibody to a human framework, pre-selected for stability from a phage display library (Krauss et al., 2003b).

In earlier studies, a disulfide stabilized RFB4 derived anti-CD22 immunotoxin linked to PE38, a truncated version of Pseudomonas Exotoxin (PE) was generated (Mansfield et al., 1997a). A phase II clinical trial using this anti-CD22 RFB4(dsFv)-PE38 immunotoxin (called BL22) showed a high response rate with complete remissions in patients with hairy cell leukemia (Kreitman et al., 2009). A BL22-dsFv derived phage display affinity mutant immunotoxin HA22 showed improved binding affinity to CD22 and an enhanced cytotoxic activity *in vitro* in B-lineage ALL cells (Mussai et al., 2010; Salvatore et al., 2002; Wayne et al., 2010). To develop anti-CD22 CARs, the scFv portion of HA22, recognizing a proximal epitope of CD22 (Ig domain 3) was used as binding domain and compared to a fully human, phage display isolated scFv (m971) targeting a more membrane proximal epitope (Ig domains 5 - 7). Although the derived CARs mediated anti-tumor activity *in vitro* in ALL cells, a higher therapeutic efficacy was achieved *in vivo* with the m971 CAR (Haso et al., 2013). Based on these results, Haso *et al.,* concluded that the selection of target antigen epitope has a major impact on CAR efficacy and consequently on potent CAR development. However, we hypothesized that the low therapeutic activity observed for the HA22 derived *CARs in vivo* is rather due to a biophysical instability of the murine anti-CD22 dsFv, resulting in less antigen binding, than due to an inferior epitope accessibility.

In this context, we investigated the stability of the murine anti-CD22 scFv fragment of RFB4 (mCD22) with a linker peptide instead of an interdomain disulfide bond as is the case for RFB4(dsFv) included in BL22 and HA22. Surprisingly, both the hCD22 scFv and the mCD22 scFv displayed the same stability in human serum and PBS throughout seven days at 37°C (result 3.1). When expressed in the CAR format with either the IgG1 Fc or CD8 spacer domain, CAR T cells with either the mCD22 or the hCD22 scFv led to T cell activation (result 3.2). These results demonstrate that

antibody fragments (dsFv and scFv) derived from the parental murine anti-CD22 IgG display a sufficient stability. Earlier studies also showed the stability of the immunotoxin RFB4(scFv)-PE38 after 24 h incubation at 37 °C (Mansfield et al., 1997b). The disulfide stabilized BL22 showed, similar to the RFB4 IgG, a nine-fold improvement in binding affinity to CD22 compared to RFB4(scFv)-PE38 (Reiter et al., 1996). Taking all together, for the development of BL22, HA22 and derived CARs, the disulfide bonds were probably introduced to improve the scFv binding affinities and not their stabilities. Furthermore, several studies supported the finding of Haso *et al*., that the efficacy of activated CAR T cells is dependent on the epitope position and its distance to the membrane (Hombach et al., 2007; James et al., 2008). To further investigate the importance of epitope localization on CD22 CAR T cell activation, a direct comparison between the currently developed hCD22 CAR and the m971 CAR from Haso *et al*. could be performed as both scFvs are phage display selected but bind different CD22 epitopes. To conclude, despite high thermal stability observed for both the hCD22 and mCD22 as scFv but also as CAR, the humanized antibody fragment is preferred to its murine counterpart for the development of antibody-based therapy. Due to its reduced immunogenicity, the humanized target moiety is a safer therapeutic antibody (Kim et al., 2005).

In previous studies, a strong tendency to aggregate was observed for a CD22 diabody, derived from the hCD22 scFv, complicating the production and purification of this molecule (Krauss et al., 2005b). A decrease in aggregation was obtained by engineering the variable heavy (V_H) and light (V_L) chain interface of the diabody resulting in improved antibody solubility and interdomain stability. Since the stability of the hCD22 scFv is essential for specific and efficient target binding and consequently for full CAR T cell activation, the optimization induced by engineering the V_H-V_L interface of the hCD22 scFv-(ΔhFc-Δ28BBz) CAR was investigated. Taking together the results of three independently tested healthy donors, no significant improvement in T cell activation was observed for the engineered hCD22 (L36Y) scFv-(ΔhFc-Δ28BBz) CAR when compared to the hCD22 scFv-(ΔhFc-Δ28BBz) CAR (result 3.4.1.2). The hCD22 scFv-(ΔhFc-Δ28BBz) CAR T cells displayed more efficient activation, probably by the higher binding affinity of the wildtype hCD22 scFv compared to the engineered hCD22 (L36Y) scFv. In fact, after replacing the leucine

residue at position 36 of the variable light chain with tyrosine the binding affinity of the engineered hCD22 (L36Y) scFv was reduced by 4,8 fold (Krauss et al., 2005b).

4.2.2 Optimization of hCD22 scFv-(ΔhFc-Δ28BBz) CAR T cell activation by mutagenesis

The large number of developed CD19 CARs and ongoing CD19 CAR phase I and II clinical trials treating acute and chronic lymphoblastic leukemia patients confirm the success of CAR therapies (Oluwole and Davila, 2016). However, they also reveal the need to improve the CAR safety by developing new approaches to continuously reduce the CAR T cell induced unspecific toxicity. For their broader use, the risk of causing adverse events such as cytokine release syndrome (Tisoncik et al., 2012) or “on-target, off-tumor” toxicity (Brentjens et al., 2011b; Lamers et al., 2006; Morgan et al., 2010) must be prevented. To enhance clinical CAR efficacy while reducing these kind of toxicities, new strategies in CAR design are emerging (Maus and Powell, 2015). In this context, our newly developed hCD22 scFv-(hFc-28BBz) CAR was optimized by mutagenesis to prevent unwanted toxicity. The Fcγ receptors (FcγR) binding domain in the IgG1 Fc spacer and of the LCK binding domain in the CD28 co-stimulatory domain were mutated in the CAR.

Previous studies showed that for an optimal and full functional CAR T cell response, a spacer domain is mandatory for some but not all chimeric immune receptors (Guest et al., 2005b; Moritz and Groner, 1995). The Fc spacer, localized between the scFv and the transmembrane domain binds target-independently to FcγR expressed on innate immune cells (Hombach et al., 2010). This binding causes off-target activation of CAR T cells leading to the lysis of monocytes and natural killer cells and cytokine release. In addition to these effects, CAR off-target activation might quickly reduce anti-tumor activity due to activation-induced cell death. To overcome unspecific CD22 CAR T cell activation, the domain responsible for FcγR binding in the hFc domain was mutated, resulting in the hCD22 scFv-(ΔhFc-28BBz) CAR. IgG1 amino acids indispensable for binding IgG1-FcγR were exchanged with IgG2 amino acids (Hombach et al., 2010). By mutating this region, the interaction of the hCD22 scFv-(ΔhFc-28BBz) and the double mutated hCD22 scFv-(ΔhFc-Δ28BBz) CAR T cells with $FcγR^+$ THP-1 cells and the target independent activation of these cells could be

successfully prevented (result 3.3.2.1). Consequently, our results obtained for both hCD22 CAR variants confirmed those achieved with an anti-CD30 CAR presenting the same mutated FcγR binding domain (Hombach et al., 2010). Most importantly, the introduced hFc mutation had no impact on the efficacy of CD22 CAR T cell activation as observed for three individual donors (result 3.3.2.3).

The co-stimulatory domain CD28 is required for full CAR T cell activation, characterized by enhanced anti-tumor activity and cytokine release such as IFNγ and IL-2 as well as improved proliferation and persistence of CAR T cells, both *in vitro* and *in vivo* (Kowolik et al., 2006; Maher et al., 2002; Savoldo et al., 2011). Furthermore, CD28 co-stimulatory domain is essential for the activation-induced interleukin-2 (IL-2) secretion (Hombach et al., 2001b) which plays an important role in the maintenance of regulatory T (T reg) cells (Brandenburg et al., 2008; Thornton et al., 2004). It has been previously demonstrated that the anti-tumor activity of CD28-CD3ζ CAR T cells, attended by a rising amount of tumor infiltrating T reg cells, is less efficient compared to CD3ζ CAR T cells (Kofler et al., 2011). It was shown that mutating the CD28 binding domain of the LCK enzyme blocks IL-2 secretion *in vitro* without affecting T cell specific tumor cell lysis and IFNγ release, induced by activated CAR T cells (Kofler et al., 2011).

Our results confirm these observations using three healthy donors demonstrating that for the hCD22 scFv-(hFc-Δ28BBz) and the double mutated hCD22 scFv-(ΔhFc-Δ28BBz) CAR T cells, the introduced CD28 mutation did not alter the ability to induce specific tumor cell lysis and IFNγ release (result 3.3.2.3). Unexpectedly, no IL-2 secretion was observed for these two hCD22 CAR variants, however, we surprisingly also found an IL-2 abolishment for the parental and the hCD22 scFv-(ΔhFc-28BBz) CAR T cells as well as for parental CEA CAR T cells (result 3.3.2.2). Several studies confirmed the variability of IL-2 secretion by CAR T cells including the CD28 and 4-1BB domain. Indeed, for CD19 CAR T cells harboring the same intracellular regions, the amount of produced IL-2 was different from donor to donor (Tammana et al., 2010). Although the IFNγ release is consistent, only CD19 CAR T cells from two donors released IL-2 whereas effector cells from a third donor lacked IL-2 secretion after activation by CD19 positive Daudi cells. The absence of IL-2 release was also observed in two other studies, using third generation CAR T cells (with CD28 and 4-1BB) targeting either mesothelin or the CD22 antigen (Carpenito et

al., 2009; Haso et al., 2013). Furthermore, for the mesothelin CAR as well as for another third generation CD19 CAR also including CD28 and 4-1BB, transduced $CD4^+$ and $CD8^+$ T cells were analyzed separately, demonstrating that only $CD4^+$ CAR T cells were able to induce IL-2 secretion while no cytokine release was observed for $CD8^+$ CAR T cells (Carpenito et al., 2009; Milone et al., 2009). For T cell cultivation, we used X-Vivo 20 medium which sustains the proliferation of $CD8^+$ T cells but not of $CD4^+$ T cells. This might influence the IL-2 levels observed for activated parental and mutated hCD22 scFv-(ΔhFc-28BBz) CAR T cells. However, this would rather explain a decrease in IL-2 secretion than a full suppression of this cytokine. High amounts of IL-2 were produced by T cells transduced with a CEA CAR harboring CD28 and the co-stimulatory OX40 domain instead of 4-1BB (Hombach and Abken, 2011). Nevertheless, in this study, while IFNγ was secreted, no IL-2 release was observed for second generation CEA CAR T cells including only OX40, thus demonstrating that this co-stimulatory domain has no impact on IL-2 release (Hombach and Abken, 2011). Since our results (result 3.3.2.2.1) confirmed the observation of Hombach and Abken concerning the activation-induced IL-2 release of T cells carrying the third generation CEA CAR including the CD28 and OX40 domains, this CAR was taken as reference for the following experiment. By replacing the co-stimulatory domain 4-1BB of our parental hCD22 CAR with OX40 while keeping the CD28 domain responsible for IL-2 secretion, activation-induced production of IL-2 could be observed (result 3.3.2.2.2). As a next step, to confirm the observations of Kofler *et al.*, it would be interesting to investigate if by mutating the CD28 LCK binding domain in the hCD22 CAR variant with CD28 and OX40, IL-2 release could be blocked after CAR T cell activation.

T reg cells are necessary to sustain immune cell homeostasis by regulating other immune cells in a dominant negative fashion. In fact, T reg cells prevent autoimmune diseases by suppressing immune responses to tumor, allo- and autoantigens. However, they are also able to suppress T cell proliferation *in vitro* and *in vivo* (Shevach, 2002) thus acting against T cell persistence, proliferation and activation on which CAR therapies are based. The amount and the functions of T reg cells need to be controlled. Interleukin-2 cytokine is essential for the peripheral balance of T reg cells by mediating their survival and for the activation of their T cell suppressive function (Brandenburg et al., 2008; Thornton et al., 2004). Maintaining a low number

of T reg cells by blocking the secretion of IL-2 by mutating the CD28 LCK binding domain of the CAR is therefore of therapeutic relevance for CAR therapies. In the presence of T reg cells, an enhanced anti-tumor response was obtained *in vivo* for mutated CD28 CAR T cells compared to parental CAR T cells (Kofler et al., 2011). In this context, even if IL-2 is absent for all types of hCD22 CAR T cells with 4-1BB as co-stimulatory domain, the CD28 mutation was kept in the selected lead candidate to ensure the highest level of safety in further studies. Since the Fc and CD28 mutations, introduced for safety and efficacy reasons, did not affect the ability to induce CAR T cell activation, the hCD22 scFv-(ΔhFc-Δ28BBz) CAR, was selected as lead candidate. This CAR displayed efficient CAR T cell activation and its lack of activation-induced IL-2 release suggests excellent properties for preclinical and clinical development.

To assess the therapeutic efficacy of double mutant hCD22 scFv-(ΔhFc-Δ28BBz) CAR T cells *in vivo*, the NOD/SCID mouse model was chosen based on earlier results demonstrating the successful engraftment of the human acute lymphoblastic leukemia (ALL) cell line Nalm-6 in SCID mice with $1*10^6$ cells (Seifert et al., 2008). Since improved engraftment of human cells was observed in NOD/SCID mice compared to SCID mice (Belizário, 2009; Greiner et al., 1998), NOD/SCID mice were chosen as a suitable model for hCD22 CAR T cells *in vivo* studies. Surprisingly, no ALL leukemia engraftment was observed in NOD/SCID mice even with a high amount of Nalm-6-luciferase tumor cells ($5*10^6$ cells) (result 3.4.3). The NOD/SCID/Gamma mouse model (NSG), corresponding to a hybrid model crossing NOD/SCID mice with *IL2rg*$^{-/-}$ deficient mice, features an improved efficacy for human tumor cell engraftment (Ishikawa et al., 2005; Ito et al., 2002). In this model, leukemia xenograft transplantation could be performed by injection of $1*10^6$ Nalm-6 luciferase cells (Barrett et al., 2011). In this study, for the control group lacking treatment, fatal leukemia was observed after 22 to 25 days and the disease was reliably detected by bioluminescence imaging seven days after tumor cell injection. This confirmed that Nalm-6 luciferase cells could be used for leukemia engraftment whereas the NOD/SCID mouse model might not be suitable for this xenograft transplantation.

4.3 Conclusion and outlook

Within the present thesis, four distinct humanized CD22 CARs were developed to treat CD22 positive leukemia and lymphoma. Optimization by mutating the FcRγ and LCK binding domain was performed to prevent adverse events caused by unwanted toxicities while maintaining successful and specific hCD22 CAR T cell activation. Because of its efficient T cell activation, its high tumor specific cytotoxicity and its reduced immunogenicity, the double mutated hCD22 scFv-(ΔhFc-Δ28BBz) CAR constitutes a promising effector molecule for potential clinical applications as a novel CD22-targeted CAR therapy.

The upcoming preclinical study in a suitable xenograft mouse model, will give us information about the *in vivo* efficacy of hCD22 scFv-(ΔhFc-Δ28BBz) CAR T cells. A complementary safety check of this therapy will be further performed in transgenic mice expressing the human CD22 antigen to investigate potential cross reactivity. To further reduce CAR toxicity effects, several emerging strategies in CAR design to turn off conventional CAR T cells might be applicable. Switching CAR T cells on and off can be performed, for example, by introducing an engineered hinge domain into the CAR (Juillerat et al., 2016) or by using the UniCAR system in which external specific scFv-epitope molecules are added to modulate the activity of a permanent anti-epitope CAR (Cartellieri et al., 2016).

Due to the B cell lineage restricted expression profile of CD22, this anti-CD22 antibody based CAR therapy represents a promising alternative to currently investigated CD19 CAR T cell therapies (Khalil et al., 2016). A CD22 CAR therapy could also be used in combination with a previous CD19 CAR treatment for CD19 negative refractory and relapsed ALL patients who retained the expression of CD22. While the present thesis focused on the development of a new CAR therapy for CD22 positive leukemia and lymphoma, this approach might be extended to treat other CD22 expressing tumors including solid tumors such as lung cancers (Tuscano et al., 2012).

5 Bibliography

5.1 References

Abken, H. (2014). Engineering CARs : How the idea of redirecting an immune response takes the front seat. MACS&more *16*, 32–36.

Advani, A., McDonough, S., Coutre, S., Wood, B.L., Radich, J., Mims, M.P., O'Donnell, M., Elkins, S., Becker, M., Othus, M., et al. (2014). SWOG S0910: A Phase 2 Trial of Clofarabine/Cytarabine/ Epratuzumab for Relapsed/Refractory Acute Lymphocytic Leukaemia. Br J Haematol *165*, 504–509.

Ai, J., and Advani, A. (2015). Current status of antibody therapy in ALL. Br. J. Haematol. *168*, 471–480.

Annesley, C.E., and Brown, P. (2015). Novel agents for the treatment of childhood acute leukemia. Ther. Adv. Hematol. *6*, 61–79.

Baeuerle, P.A., and Reinhardt, C. (2009). Bispecific T-Cell Engaging Antibodies for Cancer Therapy. Cancer Res. *69*, 4941–4944.

Barrett, D.M., Zhao, Y., Liu, X., Jiang, S., Carpenito, C., Kalos, M., Carroll, R.G., June, C.H., and Grupp, S.A. (2011). Treatment of Advanced Leukemia in Mice with mRNA Engineered T Cells. Hum. Gene Ther. *22*, 1575–1586.

Belizário, J.E. (2009). Immunodeficient Mouse Models: An Overview. Open Immunol. J. *2*, 79–85.

Bird, R.E., Hardman, K.D., Jacobson, J.W., Johnson, S., Kaufman, B.M., Lee, S.-M., Timothy, L., Pope, S.H., Riordan, G.S., and Whitlow, M. (1988). Single-Chain Antigen-Binding Proteins. Science (80-.). *242*, 423–426.

Bonifant, C.L., Jackson, H.J., Brentjens, R.J., and Curran, K.J. (2016). Toxicity and management in CAR T-cell therapy. Mol. Ther. Oncolytics *3*.

Brandenburg, S., Takahashi, T., de la Rosa, M., Janke, M., Karsten, G., Muzzulini, T., Orinska, Z., Bulfone-Paus, S., and Scheffold, A. (2008). IL-2 induces in vivo suppression by CD4+CD25+Foxp3+ regulatory T cells. Eur. J. Immunol. *38*, 1643–1653.

Brentjens, R., Davila, M.L., Riviere, I., Park, J., Wang, X., Cowell, L.G., Bartido, S., Stefanski, J., Taylor, C., Olszewska, M., et al. (2013). CD19-targeted T cells rapidly induce molecular remissions in adults with chemotherapy-refractory acute lymphoblastic leukemia. Sci Transl Med *5*.

Brentjens, R.J., Santos, E., Nikhamin, Y., Yeh, R., Matsushita, M., La Perle, K., Quintás-Cardama, A., Larson, S.M., and Sadelain, M. (2007). Genetically targeted T cells eradicate systemic acute lymphoblastic leukemia xenografts. Clin. Cancer Res. *13*, 5426–5435.

Brentjens, R.J., Rivière, I., Park, J.H., Davila, M.L., Wang, X., Stefanski, J., Taylor, C., Yeh, R., Bartido, S., Borquez-Ojeda, O., et al. (2011a). Safety and persistence of adoptively transferred autologous CD19-targeted T cells in patients with relapsed or chemotherapy refractory B-cell leukemias. Blood *118*, 4817–4828.

Brentjens, R.J., Rivière, I., Park, J.H., Davila, M.L., Wang, X., Stefanski, J., Taylor, C., Yeh, R., Bartido, S., Borquez-Ojeda, O., et al. (2011b). Safety and persistence of adoptively transferred autologous CD19-targeted T cells in patients with relapsed or chemotherapy refractory B-cell leukemias. Blood *118*, 4817–4828.

Brinkmann, U., Reiter, Y., Jung, S.-H., Lee, B., and Pastan, I. (1993). A recombinant immunotoxin containing a disulfide-stabilized Fv fragment. Immunology *90*, 7538–7542.

Campana, D., Janossy, G., Bofill, M., Trejdosiewicz, L.K., Ma, D., Hoffbrand, A.V., Mason, D.Y., Lebacq, A.-M., and Forster, H.K. (1985). Human B cell development. I. Phenotypic differences of B lymphocytes in the bone marrow and peripheral lymphoid tissue. J. Immunol. *134*, 1524–1530.

Campo, E., Swerdlow, S.H., Harris, N.L., Pileri, S., Stein, H., and Jaffe, E.S. (2011). The 2008 WHO classification of lymphoid neoplasms and beyond: Evolving concepts and practical applications. Blood *117*, 5019–5032.

Carpenito, C., Milone, M.C., Hassan, R., Simonet, J.C., Lakhal, M., Suhoski, M.M., Varela-Rohena, A., Haines, K.M., Heitjan, D.F., Albelda, S.M., et al. (2009). Control of large, established tumor xenografts with genetically retargeted human T cells containing CD28 and CD137 domains. PNAS *106*, 3360–3365.

Cartellieri, M., Feldmann, A., Koristka, S., Arndt, C., Loff, S., Ehninger, A., von Bonin, M., Bejestani, E.P., Ehninger, G., and Bachmann, M.P. (2016). Switching CAR T cells on and off: a novel modular platform for retargeting of T cells to AML blasts. Blood Cancer J. *6*.

Chevallier, P., Francoise, H., Emmanuel, R., Etienne, A., Leguay, T., Isnard, F., Robillard, N., Guillaume, T., Delaunay, J., Charbonnier, A., et al. (2015). Vincristine, dexamethasone and epratuzumab for older relapsed/refractory CD22+ B-acute lymphoblastic leukemia patients: a phase II study. Hematologica.

Chmielewski, M., Hombach, A.A., and Abken, H. (2011). CD28 cosignalling does not affect the activation threshold in a chimeric antigen receptor-redirected T-cell attack. Gene Ther. *18*, 62–72.

Cooper, S.L., and Brown, P.A. (2015). Treatment of Pediatric Acute Lymphoblastic Leukemia. Pediatr Clin North Am *62*, 61–73.

Curran, K.J., Pegram, H.J., and Brentjens, R.J. (2012). Chimeric Antigen Receptors for T cell Immunotherapy: Current Understanding and Future Direction. J Gene Med *14*, 405–415.

Dai, H., Wang, Y., Lu, X., and Han, W. (2016). Chimeric antigen receptors modified T-cells for cancer therapy. J. Natl. Cancer Inst. *108*.

Davila, M.L., Riviere, I., Wang, X., Bartido, S., Park, J., Curran, K., Chung, S.S., Stefanski, J., Borquez-Ojeda, O., Malgorzata, O., et al. (2014). Efficacy and Toxicity Management of 19-28z CAR T Cell Therapy in B Cell Acute Lymphoblastic Leukemia. Sci Transl Med *6*.

Dinner, S., Lee, D., and Liedtke, M. (2014). Current therapy and novel agents for relapsed or refractory acute lymphoblastic leukemia. Leuk. Lymphoma *55*, 1715–1724.

Dotti, G., Gottschalk, S., Savoldo, B., and Brenner, M.K. (2014). Design and Development of Therapies using Chimeric Antigen Receptor-Expressing T cells. Immunol Rev *257*.

Dudley, M.E., and Rosenberg, S.A. (2003). Adoptive-cell-transfer therapy for the treatment of patients with cancer. Nat. Rev. Cancer *3*, 666–675.

Dudley, M.E., Wunderlich, J.R., Robbins, P.F., Yang, J.C., Hwu, P., Schwartzentruber, D.J., Topalian, S.L., Sherry, R., Restifo, N.P., Hubicki, A.M., et al. (2002). Cancer Regression and Autoimmunity in Patients After Clonal Repopulation with Antitumor Lymphocytes. Science (80-.). *298*, 850–854.

Dudley, M.E., Wunderlich, J.R., Shelton, T.E., Even, J., and Rosenberg, S.A. (2003). Generation of Tumor-Infiltrating Lymphocyte Cultures for Use in Adoptive Transfer Therapy for Melanoma Patients. J Immunother *26*, 332–342.

Dudley, M.E., Wunderlich, J.R., Yang, J.C., Sherry, R.M., Topalian, S.L., Restifo, N.P., Royal, R.E., Kammula, U., White, D.E., Mavrouskakis, S.A., et al. (2005). Adoptive Cell Transfer Therapy Following Non-Myeloablative but Lymphodepleting Chemotherapy for the Treatment of Patients With Refractory Metastatic Melanoma. J Clin Oncol *23*, 2346–2357.

Eshhar, Z. (2008). The T-body approach: Redirecting T cells with antibody specificity. Handb. Exp. Pharmacol. *181*, 329–342.

Eshhar, Z., Waks, T., Gross, G., and Schindler, D.G. (1993). Specific activation and targeting of cytotoxic lymphocytes through chimeric single chains consisting of antibody-binding domains and the gamma or zeta subunits of the immunoglobulin and T-cell receptors. Proc. Natl. Acad. Sci. U. S. A. *90*, 720–724.

Essig, N.Z., Wood, J.F., Howard, A.J., Raag, R., and Whitlow, M. (1993). Crystallization of Single-Chain Fv Proteins. J. Mol. Biol. *234*, 897–901.

Finney, H.M., Lawson, A.D.G., Bebbington, C.R., and Weir, A.N.C. (1998). Chimeric receptors providing both primary and costimulatory signaling in T cells from a single gene product. J. Immunol. *161*, 2791–2797.

Frenzel, A., Hust, M., and Schirrmann, T. (2013). Expression of recombinant antibodies. Front. Immunol. *4*.

Gacerez, A.T., Arellano, B., and Sentman, C.L. (2016). How Chimeric Antigen Receptor Design Affects Adoptive T Cell Therapy. J. Cell. Physiol. *231*, 2590–2598.

Garcia-Lora, A., Algarra, I., and Garrido, F. (2003). MHC class I antigens, immune surveillance, and tumor immune escape. J. Cell. Physiol. *195*, 346–355.

Gattinoni, L., Powell, D.J., Rosenberg, S.A., and Restifo, N.P. (2006). Adoptive immunotherapy for cancer: building on success. Nat. Rev. Immunol. *6*, 383–393.

Greiner, D.L., Hesselton, R.A., and Shultz, L.D. (1998). SCID mouse models of human stem cell engraftment. Stem Cells *16*, 166–177.

Gross, G., Gorochov, G., Waks, T., and Eshhar, Z. (1989). Generation of Effector T Cells Expressing Chimeric T cell Receptor with Antibody Type-Specificity. Transplant. Proc. *21*, 127–130.

Grupp, S. a, Kalos, M., Barrett, D., Aplenc, R., Porter, D.L., Rheingold, S.R., Teachey, D.T., Chew, A., Hauck, B., Wright, J.F., et al. (2013). Chimeric antigen receptor-modified T cells for acute lymphoid leukemia. N. Engl. J. Med. *368*, 1509–1518.

Guest, R.D., Hawkins, R.E., Kirillova, N., Cheadle, E.J., Arnold, J., O'Neill, A., Irlam, J., Chester, K.A., Kemshead, J.T., Shaw, D.M., et al. (2005a). The role of extracellular spacer regions in the optimal design of chimeric immune receptors: evaluation of four different scFvs and antigens. J Immunother *28*, 203–211.

Guest, R.D., Hawkins, R.E., Kirillova, N., Cheadle, E.J., Arnold, J., O'Neill, A., Irlam, J., Chester, K.A., Kemshead, J.T., Shaw, D.M., et al. (2005b). The role of extracellular spacer regions in the optimal design of chimeric immune receptors: evaluation of four different scFvs and antigens. J. Immunother.

Haso, Lee, and Orentas (2013). Anti-CD22 chimeric antigen receptors targeting B-cell precursor acute lymphoblastic leukemia. Blood.

Hoelzer, D., and Gökbuget, N. (2012). Chemoimmunotherapy in acute lymphoblastic leukemia. Blood Rev. *26*, 25–32.

Hombach, A.A., and Abken, H. (2011). Costimulation by chimeric antigen receptors revisited: the T cell antitumor response benefits from combined CD28-OX40 signalling. Int. J. Cancer *129*, 2935–2944.

Hombach, A., Wieczarkowiecz, A., Marquardt, T., Heuser, C., Usai, L., Pohl, C., Seliger, B., and Abken, H. (2001a). Tumor-Specific T Cell Activation by Recombinant Immunoreceptors: CD3ζ Signaling and CD28 Costimulation Are Simultaneously Required for Efficient IL-2 Secretion and Can Be Integrated Into One Combined CD28/CD3ζ Signaling Receptor Molecule. J. Immunol. *167*, 6123–6131.

Hombach, A., Sent, D., Schneider, C., Heuser, C., Koch, D., Pohl, C., Seliger, B., and Abken, H. (2001b). T-cell activation by recombinant receptors: CD28 costimulation is required for interleukin 2 secretion and receptor-mediated T-cell proliferation but does not affect receptor-mediated target cell lysis. Cancer Res. *61*, 1976–1982.

Hombach, A., Hombach, A., and Abken, H. (2010). Adoptive immunotherapy with genetically engineered T cells: modification of the IgG1 Fc “spacer” domain in the extracellular moiety of chimeric antigen receptors avoids “off-target” activation and unintended initiation of an innate immune response. Gene Ther. *17*, 1206–1213.

Hombach, A.A., Schildgen, V., Heuser, C., Finnern, R., Gilham, D.E., and Abken, H. (2007). T Cell Activation by Antibody-Like Immunoreceptors: The Position of the Binding Epitope within the Target Molecule Determines the Efficiency of Activation of Redirected T Cells. J. Immunol. *178*, 4650–4657.

Hotfilder, M., Röttgers, S., Rosemann, A., Schrauder, A., Schrappe, M., Pieters, R., Jürgens, H., Harbott, J., and Vormoor, J. (2005). Leukemic Stem Cells in Childhood High-Risk ALL / t (9 ; 22) and t (4 ; 11) Are Present in Primitive Lymphoid-Restricted CD34 + CD19 – Cells. Cancer Res. *65*, 1442–1449.

Ishikawa, F., Yasukawa, M., Lyons, B., Yoshida, S., Miyamoto, T., Yoshimoto, G., Watanabe, T., Akashi, K., Shultz, L.D., and Harada, M. (2005). Development of functional human blood and immune systems in NOD/SCID/IL2 receptor gamma chain null mice. Blood *106*, 1565–1573.

Ito, M., Hiramatsu, H., Kobayashi, K., Suzue, K., Kawahata, M., Hioki, K., Ueyama, Y., Koyanagi, Y., Sugamura, K., Tsuji, K., et al. (2002). NOD/SCID/gammac null mouse: an excellent recipient mouse model for engraftment of human cells. Blood *100*, 3175–3182.

Iwamoto, S., Deguchi, T., Ohta, H., Kiyokawa, N., Tsurusawa, M., Yamada, T., Takase, K., Fujimoto, J., Hanada, R., Hori, H., et al. (2011). Flow cytometric analysis of de novo acute lymphoblastic leukemia in childhood: Report from the Japanese Pediatric Leukemia/Lymphoma Study Group. Int. J. Hematol. *94*, 185–192.

Jackson, H.J., Rafiq, S., and Brentjens, R.J. (2016). Driving CAR T-cells forward. Nat. Rev. Clin. Oncol. *13*, 370–383.

James, S.E., Greenberg, P.D., Jensen, M.C., Lin, Y., Wang, J., Till, B.G., Raubitschek, A., Forman, S.J., and Press, O.W. (2008). Antigen sensitivity of CD22-specific chimeric T cell receptors is modulated by target epitope distance from the cell membrane. J.Immunol. *180*, 7028–7038.

Jefferis, R. (2012). Isotype and glycoform selection for antibody therapeutics. Arch. Biochem. Biophys. *526*, 159–166.

Johnson, P., and Glennie, M. (2003). The mechanisms of action of rituximab in the elimination of tumor cells. Semin. Oncol. *30*, 3–8.

Juillerat, A., Marechal, A., Filhol, J.-M., Valton, J., Duclert, A., Poirot, L., and Duchateau, P. (2016). Design of chimeric antigen receptors with integrated controllable transient functions. Sci. Rep. *6*.

Kalos, M., Levine, B.L., Porter, D.L., Katz, S., Grupp, S.A., Bagg, A., and June, C.H. (2011). T Cells with Chimeric Antigen Receptors Have Potent Antitumor Effects and Can Establish Memory in Patients with Advanced Leukemia. Sci Transl Med *3*.

Kershaw, M.H., Westwood, J.A., Parker, L.L., Wang, G., Zelig, E., Mavroukakis, S.A., White, D.E., Wunderlich, J.R., Carnevari, S., Rogers-Freezer, L., et al. (2006). A Phase I Study on Adoptive Immunotherapy Using Gene- Modified T Cells for Ovarian Cancer. Clin Cancer Res *12*, 6106–6115.

Khalil, D.N., Smith, E.L., Brentjens, R.J., and Wolchok, J.D. (2016). The future of cancer treatment: immunomodulation, CARs and combination immunotherapy. Nat. Rev. Clin. Oncol. *13*, 273–290.

Kim, S.J., Park, Y., and Hong, H.J. (2005). Antibody engineering for the development of therapeutic antibodies. Mol. Cells *20*, 17–29.

Kloss, C.C., Condomines, M., Cartellieri, M., Bachmann, M., and Sadelain, M. (2013). Combinatorial antigen recognition with balanced signaling promotes selective tumor eradication by engineered T cells. Nat. Biotechnol. *31*, 71–75.

Kochenderfer, J.N., Dudley, M.E., Feldman, S.A., Wilson, W.H., Spaner, D.E., Maric, I., Stetler-Stevenson, M., Phan, G.Q., Hughes, M.S., Sherry, R.M., et al. (2012a). B-cell depletion and remissions of malignancy along with cytokine-associated toxicity in a clinical trial of anti-CD19 chimeric-antigen-receptor-transduced T cells.

Kochenderfer, J.N., Dudley, M.E., Feldman, S.A., Wilson, W.H., Spaner, D.E., Maric, I., Stetler-Stevenson, M., Phan, G.Q., Hughes, M.S., Sherry, R.M., et al. (2012b). B-cell depletion and remissions of malignancy along with cytokine-associated toxicity in a clinical trial of anti-CD19 chimeric-antigen-receptor-transduced T cells. Blood *119*, 2709–2720.

Kochenderfer, J.N., Dudley, M.E., Kassim, S.H., Somerville, R.P.T., Carpenter, R.O., Maryalice, S.S., Yang, J.C., Phan, G.Q., Hughes, M.S., Sherry, R.M., et al. (2015). Chemotherapy-refractory diffuse large B-cell lymphoma and indolent B-cell malignancies can be effectively treated with autologous T cells expressing an anti-CD19 chimeric antigen receptor. J. Clin. Oncol. *33*, 540–549.

Koehler, P., Schmidt, P., Hombach, A.A., Hallek, M., and Abken, H. (2012). Engineered T cells for the adoptive therapy of b-cell chronic lymphocytic leukaemia. Adv. Hematol. *2012*.

Kofler, D.M., Chmielewski, M., Rappl, G., Hombach, A., Riet, T., Schmidt, A., Hombach, A.A., Wendtner, C.M., and Abken, H. (2011). CD28 costimulation Impairs the efficacy of a redirected t-cell antitumor attack in the presence of regulatory t cells which can be overcome by preventing Lck activation. Mol Ther *19*, 760–767.

Kohler, G., and Milstein, C. (1975). Continuous cultures of fused cells secreting antibody of predifined specificity. Nature *256*, 495–497.

Kowolik, C.M., Topp, M.S., Gonzalez, S., Pfeiffer, T., Olivares, S., Gonzalez, N., Smith, D.D., Forman, S.J., Jensen, M.C., and Cooper, L.J.N. (2006). CD28 costimulation provided through a CD19-specific chimeric antigen receptor enhances in vivo persistence and antitumor efficacy of adoptively transferred T cells. Cancer Res. *66*, 10995–11004.

Kraeber-Bodere, F., Pallardy, A., Maisonneuve, H., Campion, L., Moreau, A., Soubeyran, I., Le Gouill, S., Tournilhac, O., Daguindau, E., Jardel, H., et al. (2016). Consolidation anti-CD22 fractionated radioimmunotherapy with 90Y-epratuzumab tetraxetan following R-CHOP in elderly patients with diffuse large B-cell lymphoma: a prospective, single group, phase 2 trial. Lancet Haematol. *4*.

Krauss, J., Arndt, M.A.E., Martin, A.C.R., Liu, H., and Rybak, S.M. (2003a). Specificity grafting of human antibody frameworks selected from a phage display library: generation of a highly stable humanized anti-CD22 single-chain Fv fragment. Protein Eng. *16*, 753–759.

Krauss, J., Arndt, M.A., Martin, A.C., Liu, H., and Rybak, S.M. (2003b). Specificity grafting of human antibody frameworks selected from a phage display library: generation of a highly stable humanized anti-CD22 single-chain Fv fragment. Protein Eng *16*, 753–759.

Krauss, J., Arndt, M.A.E., Vu, B.K., Newton, D.L., and Rybak, S.M. (2005a). Targeting malignant B-cell lymphoma with a humanized anti-CD22 scFv-angiogenin immunoenzyme. Br. J. Haematol.

Krauss, J., Arndt, M.A.E., Vu, B.K., Newton, D.L., Seeber, S., and Rybak, S.M. (2005b). Efficient killing of CD22+ tumor cells by a humanized diabody-RNase fusion protein. Biochem. Biophys. Res. Commun. *331*, 595–602.

Kreitman, R.J., Stetler-Stevenson, M., Margulies, I., Noel, P., FitzGerald, D.J.P., Wilson, W.H., and Pastan, I. (2009). Phase II trial of recombinant immunotoxin RFB4(dsFv)-PE38 (BL22) in patients with hairy cell leukemia. J. Clin. Oncol. *27*, 2983–2990.

Kreitman, R.J., Tallman, M.S., Robak, T., Coutre, S., Wilson, W.H., Stetler-Stevenson, M., FitzGerald, D.J., Lechleider, R., and Pastan, I. (2012). Phase I trial of anti-CD22 recombinant immunotoxin moxetumomab pasudotox (CAT-8015 or HA22) in patients with hairy cell leukemia. J. Clin. Oncol. *30*, 1822–1828.

Lamers, C.H.J., Sleijfer, S., Vulto, A.G., Kruit, W.H.J., Kliffen, M., Debets, R., Gratama, J.W., Stoter, G., and Oosterwijk, E. (2006). Treatment of metastatic renal cell carcinoma with autologous T-lymphocytes genetically retargeted against carbonic anhydrase IX: first clinical experience. J. Clin. Oncol. *24*, e20–e22.

Lee, D.W., Kochenderfer, J.N., Stetler-Stevenson, M., Cui, Y.K., Delbrook, C., Feldman, S.A., Fry, T.J., Orentas, R., Sabatino, M., Shah, N.N., et al. (2015). T cells expressing CD19 chimeric antigen receptors for acute lymphoblastic leukaemia in children and young adults: A phase 1 dose-escalation trial. Lancet *385*, 517–528.

Li, Y.S., Wasserman, R., Hayakawa, K., and Hardy, R.R. (1996). Identification of the earliest B lineage stage in mouse bone marrow. Immunity *5*, 527–535.

Locatelli, F., Schrappe, M., Bernardo, M.E., and Rutella, S. (2012). How I treat relapsed childhood acute lymphoblastic leukemia. Blood *120*, 2807–2816.

Maher, J., Brentjens, R.J., Gunset, G., Rivière, I., and Sadelain, M. (2002). Human T-lymphocyte cytotoxicity and proliferation directed by a single chimeric TCRzeta /CD28 receptor. Nat. Biotechnol. *20*, 70–75.

Mansfield, E., Amlot, P., Pastan, I., and FitzGerald, D.J. (1997a). Recombinant RFB4 immunotoxins exhibit potent cytotoxic activity for CD22-bearing cells and tumors. Blood *90*, 2020–2026.

Mansfield, E., Chiron, M.F., Amlot, P., Pastan, I., and FitzGerald, D.J. (1997b). Recombinant RFB4 single-chain immunotoxin that is cytotoxic towards CD22-positive cells. Biochem. Soc. Trans. *25*, 709–714.

Maude, S.L., Frey, N. V., Shaw, P.A., Aplenc, R., Barrett, D.M., Bunin, N.J., Chew, A., Gonzalez, V.E., Zheng, Z., Lacey, S.F., et al. (2014). Chimeric Antigen Receptor T Cells for Sustained Remissions in Leukemia. N Engl J Med *371*, 1507–1517.

Maus, M. V., and Powell, D.J. (2015). CAR T Cells: New Approaches to Improve Their Efficacy and Reduce Toxicity. Cancer J. *21*, 475–479.

Maus, M. V., Grupp, S.A., Porter, D.L., and June, C.H. (2014). Antibody-modified T cells: CARs take the front seat for hematologic malignancies. Blood Rev. *123*, 2625–2635.

Milone, M.C., Fish, J.D., Carpenito, C., Carroll, R.G., Binder, G.K., Teachey, D., Samanta, M., Lakhal, M., Gloss, B., Danet-Desnoyers, G., et al. (2009). Chimeric receptors containing CD137 signal transduction domains mediate enhanced survival of T cells and increased antileukemic efficacy in vivo. Mol Ther *17*, 1453–1464.

Morgan, R.A., Dudley, M.E., Wunderlich, J.R., Hughes, M.S., Yang, J.C., Sherry, R.M., Royal, R.E., Topalian, S.L., Kammula, U.S., Restifo, N.P., et al. (2006). Cancer regression in patients after transfer of genetically engineered lymphocytes. Science (80-.). *314*, 126–129.

Morgan, R.A., Yang, J.C., Kitano, M., Dudley, M.E., Laurencot, C.M., and Rosenberg, S.A. (2010). Case report of a serious adverse event following the administration of T cells transduced with a chimeric antigen receptor recognizing ERBB2. Mol. Ther. *18*, 843–851.

Moritz, D., and Groner, B. (1995). A spacer region between the single chain antibody- and the CD3ζ-chain domain of chimeric T cell receptor components is required for efficient ligand binding and signaling activity. Gene Ther. *2*, 539–546.

Morrison, S.L., Johnson, M.J., Herzenberg, L.A., and Oi, V.T. (1984). Chimeric human antibody molecules: mouse antigen-binding domains with human constant region domains. Proc. Natl. Acad. Sci. U. S. A. *81*, 6851–6855.

Morschhauser, F., Kraeber-Bodéré, F., Wegener, W.A., Harousseau, J.L., Petillon, M.O., Huglo, D., Trümper, L.H., Meller, J., Pfreundschuh, M., Kirsch, C.M., et al. (2010). High rates of durable responses with anti-CD22 fractionated radioimmunotherapy: Results of a multicenter, phase I/II study in non-Hodgkin's lymphoma. J. Clin. Oncol. *28*, 3709–3716.

Mussai, F., Campana, D., Bhojwani, D., Stetler-Stevenson, M., Steinberg, S.M., Wayne, A.S., and Pastan, I. (2010). Cytotoxicity of the anti-CD22 immunotoxin HA22 (CAT-8015) against paediatric acute lymphoblastic leukaemia. Br. J. Haematol. *150*, 352–358.

Muul, L.M., Spiess, P.J., Director, E.P., and Rosenberg, S.A. (1987). Identification of specific cytolytic immune responses against autologous tumor in humans bearing malignant melanoma. J.Immunol. *138*, 989–995.

Nitschke, L. (2009). CD22 and Siglec-G: B-cell inhibitory receptors with distinct functions. Immunol. Rev. *230*, 128–143.

Oluwole, O.O., and Davila, M.L. (2016). At The Bedside: Clinical review of chimeric antigen receptor (CAR) T cell therapy for B cell malignancies. J. Leukoc. Biol. *100*.

Pandey, M., and Mahadevan, D. (2014). Monoclonal antibodies as therapeutics in human malignancies. Futur. Oncol. *10*, 609–636.

Piccaluga, P.P., Arpinati, M., Candoni, A., Laterza, C., Paolini, S., Gazzola, A., Sabattini, E., Visani, G., and Pileri, S.A. (2011). Surface antigens analysis reveals significant expression of candidate targets for immunotherapy in adult acute lymphoid leukemia. Leuk. Lymphoma *52*, 325–327.

Piper, W. (2012). Innere Medizin, 2. Auflage.

Porter, D.L., Levine, B.L., Kalos, M., Bagg, A., and June, C.H. (2011). Chimeric antigen receptor-modified T cells in chronic lymphoid leukemia. N. Engl. J. Med. *365*, 725–733.

Porter, D.L., Hwang, W., Frey, N. V., Lacey, S.F., Shaw, P.A., Loren, A.W., Bagg, A., Marcucci, K.T., Shen, A., Gonzalez, V., et al. (2015). Chimeric antigen receptor T cells persist and induce sustained remissions in relapsed refractory chronic lymphocytic leukemia. Sci Transl Med *7*, 303ra139.

Raetz, E.A., Cairo, M.S., Borowitz, M.J., Blaney, S.M., Krailo, M.D., Leil, T.A., Reid, J.M., Goldenberg, D.M., Wegener, W.A., Carroll, W.L., et al. (2008). Chemoimmunotherapy reinduction with epratuzumab in children with acute lymphoblastic leukemia in marrow relapse: A children's oncology group pilot study. J. Clin. Oncol. *26*, 3756–3762.

Raponi, S., De Propris, M.S., Intoppa, S., Milani, M.L., Vitale, A., Elia, L., Perbellini, O., Pizzolo, G., Foá, R., and Guarini, A. (2011). Flow cytometric study of potential target antigens (CD19, CD20, CD22, CD33) for antibody-based immunotherapy in acute lymphoblastic leukemia: analysis of 552 cases. Leuk. Lymphoma *52*, 1098–1107.

Redman, J., Hill, E., AlDeghaither, D., and Weiner, L. (2015). Mechanisms of Action of Therapeutic Antibodies for Cancer. Mol Immunol *67*, 28–45.

Reichert, J.M. (2017). Antibodies to watch in 2017. MAbs *0*, 1–15.

Reiter, Y., Brinkmann, U., Lee, B., and Pastan, I. (1996). Engineering antibody Fv fragments for cancer detection and therapy: Disulfide-stabilized Fv fragments. Nat. Biotechnol. *14*, 1239–1245.

Ribatti, D. (2014). From the discovery of monoclonal antibodies to their therapeutic application: An historical reappraisal. Immunol. Lett. *161*, 96–99.

Rosenberg, S.A., Yannelli, J.R., Yang, J.C., Topalian, S.L., Schwartzentruber, D.J., Weber, J.S., Parkinson, D.R., Seipp, C.A., Einhorn, J.H., and White, D.E. (1994). Treatment of Patients With Metastatic Melanoma With autologous tumor-infiltrating Lymphocytes and Interleukin 2. J. Natl. Cancer Inst. *86*, 1159–1166.

Rosenberg, S.A., Restifo, N.P., Yang, J.C., Morgan, R.A., and Mark, E. (2008). Adoptive cell transfer: a clinical path to effective cancer immunotherapy. *8*, 299–308.

Sadelain, M., Brentjens, R., and Rivière, I. (2013). The basic principles of chimeric antigen receptor (CAR) design. Cancer Discov. *3*, 388–398.

Salvatore, G., Beers, R., Margulies, I., Kreitman, R.J., and Pastan, I. (2002). Improved Cytotoxic Activity toward Cell Lines and Fresh Leukemia Cells of a Mutant Anti-CD22 Immunotoxin Obtained by Antibody Phage Display. *8*, 995–1002.

Satta, A., Mezzanzanica, D., Turatti, F., Canevari, S., and Figini, M. (2013). Redirection of T-cell effector functions for cancer therapy: bispecific antibodies and chimeric antigen receptors. Futur. Oncol. *9*, 527–539.

Savoldo, B., Ramos, C.A., Liu, E., Mims, M.P., Keating, M.J., Carrum, G., Kamble, R.T., Bollard, C.M., Gee, A.P., Mei, Z., et al. (2011). CD28 costimulation improves expansion and persistence of chimeric antigen receptor-modified T cells in lymphoma patients. J. Clin. Invest. *121*, 1822–1826.

Schrama, D., Reisfeld, R.A., and Becker, J.C. (2006). Antibody targeted drugs as cancer therapeutics. Nat. Rev. Drug Discov. *5*, 147–159.

Seifert, G., Jesse, P., Laengler, A., Reindl, T., Lüth, M., Lobitz, S., Henze, G., Prokop, A., and Lode, H.N. (2008). Molecular mechanisms of mistletoe plant extract-induced apoptosis in acute lymphoblastic leukemia in vivo and in vitro. Cancer Lett. *264*, 218–228.

Seliger, B., Maeurer, M.J., and Ferrone, S. (1997). TAP off -tumors on. Immunol. Today *18*.

Shah, N.N., Stevenson, M.S., Yuan, C.M., Richards, K., Delbrook, C., Kreitman, R.J., Pastan, I., and Wayne, A.S. (2015). Characterization of CD22 Expression in Acute Lymphoblastic Leukemia. Pediatr Blood Cancer *62*, 964–969.

Shevach, E.M. (2002). CD4+ CD25+ suppressor T cells: more questions than answers. Nat. Rev. Immunol. *2*, 389–400.

Sotillo, E., Barrett, D.M., Black, K.L., Bagashev, A., Oldridge, D., Wu, G., Sussman, R., Lanauze, C., Ruella, M., Gazzara, M.R., et al. (2015). Convergence of Acquired Mutations and Alternative Splicing of CD19 Enables Resistance to CART-19 Immunotherapy. Cancer Discov. *5*, 1282–1295.

Stamova, S., Koristka, S., Keil, J., Arndt, C., Feldmann, A., Michalk, I., Bartsch, H., Bippes, C.C., Schmitz, M., Cartellieri, M., et al. (2012). Cancer Immunotherapy by Retargeting of Immune Effector Cells via Recombinant Bispecific Antibody Constructs. Antibodies *1*, 172–198.

Stewart-Jones, G., Wadle, A., Hombach, A., Shenderov, E., Held, G., Fischer, E., Kleber, S., Stenner-Liewen, F., Bauer, S., Mcmichael, A., et al. (2009). Rational development of high-affinity T-cell receptor-like antibodies. PNAS *106*, 5784–5788.

Strebhardt, K., and Ullrich, A. (2008). Paul Ehrlich ' s magic bullet concept : 100 years of progress. Nat. Rev. Cancer *8*, 473–480.

Tam, C.S., O'Brien, S., Wierda, W., Kantarjian, H., Wen, S., Do, K., Thomas, D.A., Cortes, J., Lerner, S., and Keating, M.J. (2008). Long-term results of the fludarabine, cyclophosphamide, and rituximab regimen as initial therapy of chronic lymphocytic leukemia. Blood *112*, 975–981.

Tammana, S., Huang, X., Wong, M., Milone, M.C., Ma, L., Levine, B.L., June, C.H., Wagner, J.E., Blazar, B.R., and Zhou, X. (2010). 4-1BB and CD28 signaling plays a synergistic role in redirecting umbilical cord blood T cells against B-cell malignancies. Hum. Gene Ther. *21*, 75–86.

Tedder, T.F., Poe, J.C., and Haas, K.M. (2005). CD22: A multifunctional receptor that regulates B lymphocyte survival and signal transduction. Adv. Immunol. *88*, 1–50.

Thornton, A.M., Donovan, E.E., Piccirillo, C.A., and Shevach, E.M. (2004). Cutting Edge: IL-2 Is Critically Required for the In Vitro Activation of CD4+CD25+ T Cell Suppressor Function. J. Immunol. *172*, 6519–6523.

Till, B.G., Jensen, M.C., Wang, J., Chen, E.Y., Wood, B.L., Greisman, H.A., Qian, X., James, S.E., Raubitschek, A., Forman, S.J., et al. (2008). Adoptive immunotherapy for indolent non-hodgkin lymphoma and mantle cell lymphoma using genetically modified autologous CD20-specific T cells. Blood *112*, 2261–2271.

Tisoncik, J.R., Korth, M.J., Simmons, C.P., Farrar, J., Martin, T.R., and Katze, M.G. (2012). Into the eye of the cytokine storm. Microbiol. Mol. Biol. Rev. *76*, 16–32.

Tu, X., LaVallee, T., and Lechleider, R. (2011). CD22 as a target for cancer therapy. J. Exp. Ther. Oncol. *9*, 241–248.

Tuscano, J.M., Kato, J., Pearson, D., Xiong, C., Newell, L., Ma, Y., Gandara, D.R., and O'Donnell, R.T. (2012). CD22 antigen is broadly expressed on lung cancer cells and is a target for antibody-based therapy. Cancer Res. *72*, 5556–5565.

Le Viseur, C., Hotfilder, M., Bomken, S., Wilson, K., Röttgers, S., Schrauder, A., Rosemann, A., Irving, J., Stam, R.W., Schultz, L.D., et al. (2009). In childhood acute lymphoblastic leukemia, blasts at different stages of immunophenotypic maturation have stem cell properties. Cancer Cell *14*, 47–58.

Wang, Y., Zhang, W., Han, Q., Liu, Y., Dai, H., Guo, Y., Bo, J., Fan, H., Zhang, Y., Zhang, Y., et al. (2014). Effective response and delayed toxicities of refractory advanced diffuse large B-cell lymphoma treated by CD20-directed chimeric antigen receptor-modified T cells. Clin. Immunol. *155*, 160–175.

Wayne, A.S., Kreitman, R.J., Findley, H.W., Lew, G., Delbrook, C., Steinberg, S.M., Stetler-Stevenson, M., FitzGerald, D.J., and Pastan, I. (2010). Anti-CD22 immunotoxin RFB4(dsFv)-PE38 (BL22) for CD22-positive hematologic malignancies of childhood: Preclinical studies and phase I clinical trial. Clin. Cancer Res. *16*, 1894–1903.

Willuda, J., Honegger, A., Waibel, R., Schubiger, P.A., Stahel, R., Zangemeister-Wittke, U., and Plü Ckthun, A. (1999). High Thermal Stability Is Essential for Tumor Targeting of Antibody Fragments: Engineering of a Humanized Anti-epithelial Glycoprotein-2 (Epithelial Cell Adhesion Molecule) Single-Chain Fv Fragment. Cancer Res. *59*, 5758–5767.

Wörn, A., and Plückthun, A. (1999). Different equilibrium stability behavior of scFv fragments: Identification, classification, and improvement by protein engineering. Biochemistry *38*, 8739–8750.

Wörn, A., and Plückthun, A. (2001). Stability engineering of antibody single-chain Fv fragments. J. Mol. Biol. *305*, 989–1010.

Wu, Y., Jiang, S., and Ying, T. (2016). From therapeutic antibodies to chimeric antigen receptors (CARs): making better CARs based on antigen-binding domain. Expert Opin. Biol. Ther. *16*, 1469–1478.

Yao, X., Ahmadzadeh, M., Lu, Y.-C., Liewehr, D.J., Dudley, M.E., Liu, F., Schrump, D.S., Steinberg, S.M., Rosenberg, S.A., and Robbins, P.F. (2012). Levels of peripheral CD4 +FoxP3 + regulatory T cells are negatively associated with clinical response to adoptive immunotherapy of human cancer. Blood *119*, 5688–5696.

Yokota, T., Milenic, D.E., Whitlow, M., and Schlom, J. (1992). Rapid Tumor Penetration of a Single-Chain Fv and Comparison with Other Immunoglobulin Forms. Cancer Res. *52*, 3402–3408.

Zhao, J.X., Yang, L., Gu, Z.N., Chen, H.Q., Tian, F.W., Chen, Y.Q., Zhang, H., and Chen, W. (2011). Stabilization of the single-chain fragment variable by an interdomain disulfide bond and its effect on antibody affinity. Int. J. Mol. Sci. *12*, 1–11.

5.2 Internet sources

[A] Gesellschaft der epidemiologischen Krebsregister e.V. (GEKID)

Zentrum für Krebsregisterdaten (ZfKD)

Robert-Koch-Institut (2015)

Krebs in Deutschland 2011/2012, 10. Ausgabe, 2015

URL:

http://www.krebsdaten.de/Krebs/DE/Content/Publikationen/Krebs_in_Deutschland/kid_2015/kid_2015_c00_97_krebs_gesamt.pdf?__blob=publicationFile

[B] Gesellschaft der epidemiologischen Krebsregister e.V. (GEKID)

Zentrum für Krebsregisterdaten (ZfKD)

Robert-Koch-Institut (2015)

Krebs in Deutschland 2011/2012, 10. Ausgabe, 2015

URL:

http://www.krebsdaten.de/Krebs/DE/Content/Publikationen/Krebs_in_Deutschland/kid_2015/kid_2015_c00_97_krebs_gesamt.pdf?__blob=publicationFile

6 Annexes

6.1 Vectors

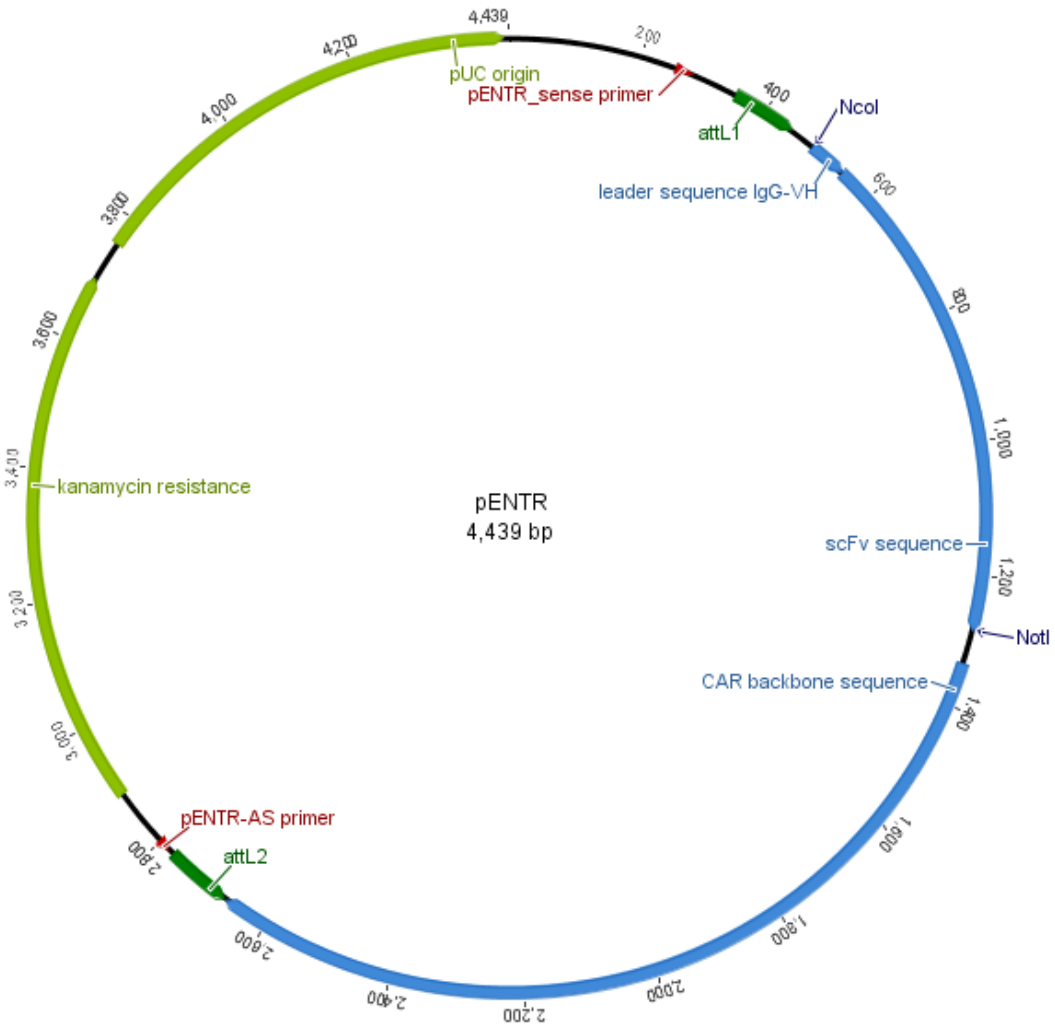

Figure 24: Map of the entry vector pENTR.

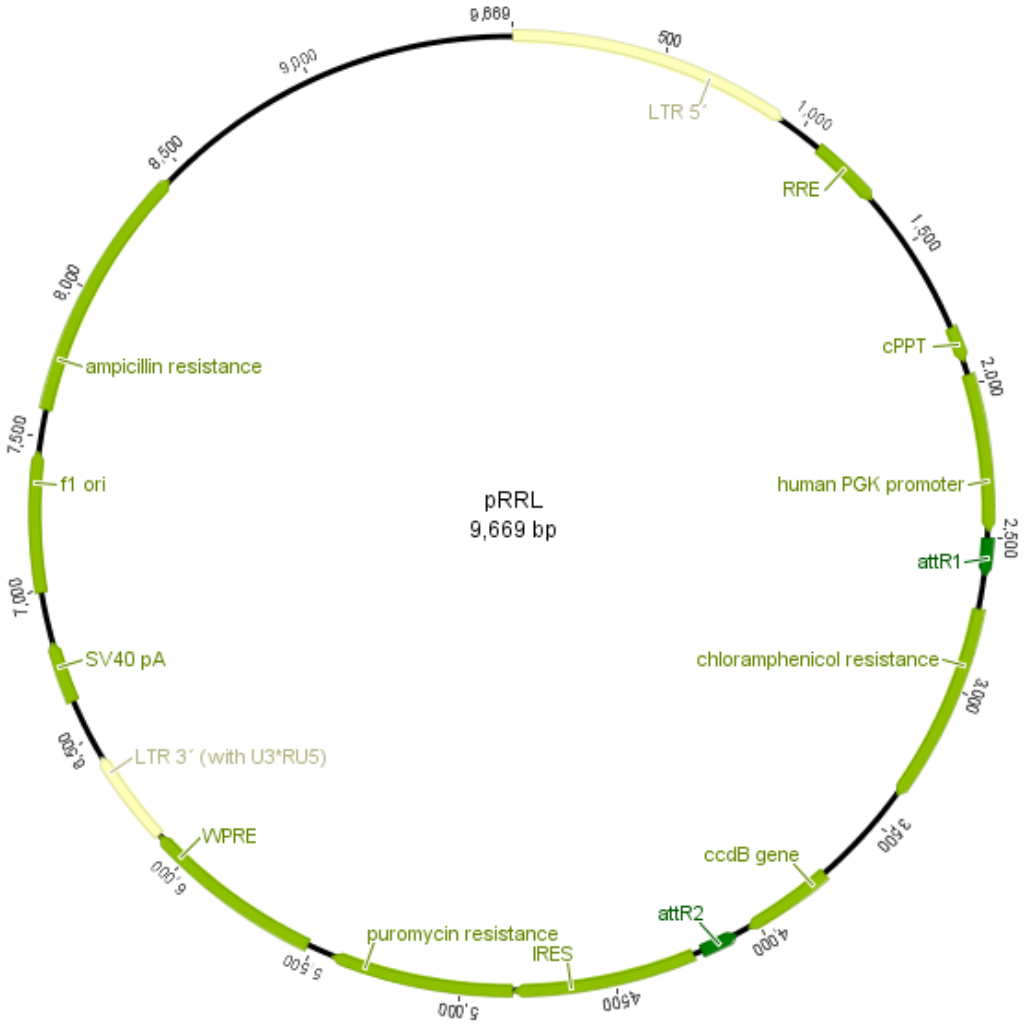

Figure 25: Map of the lentiviral vector pRRL.

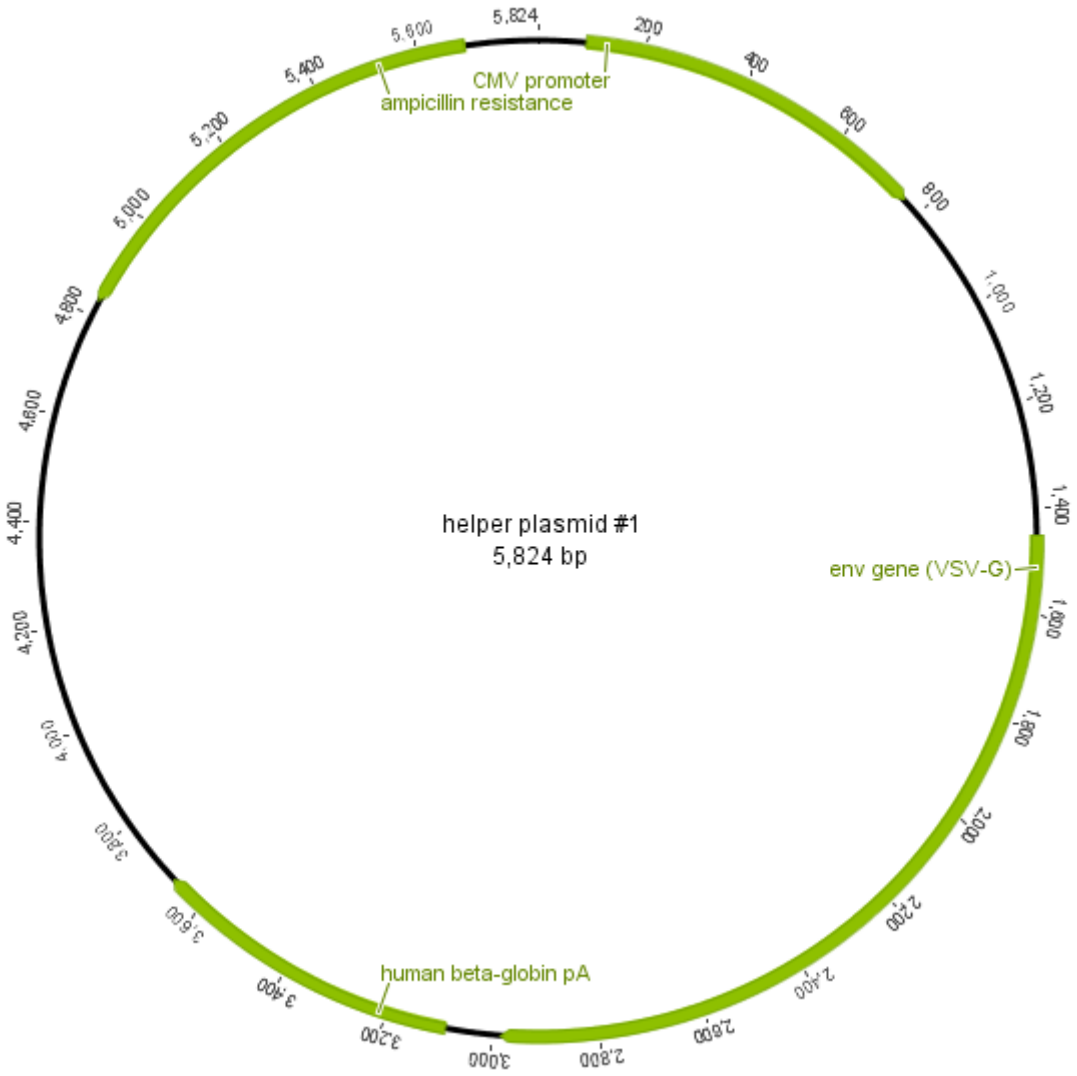

Figure 26: Map of the lentiviral helper plasmid #1.

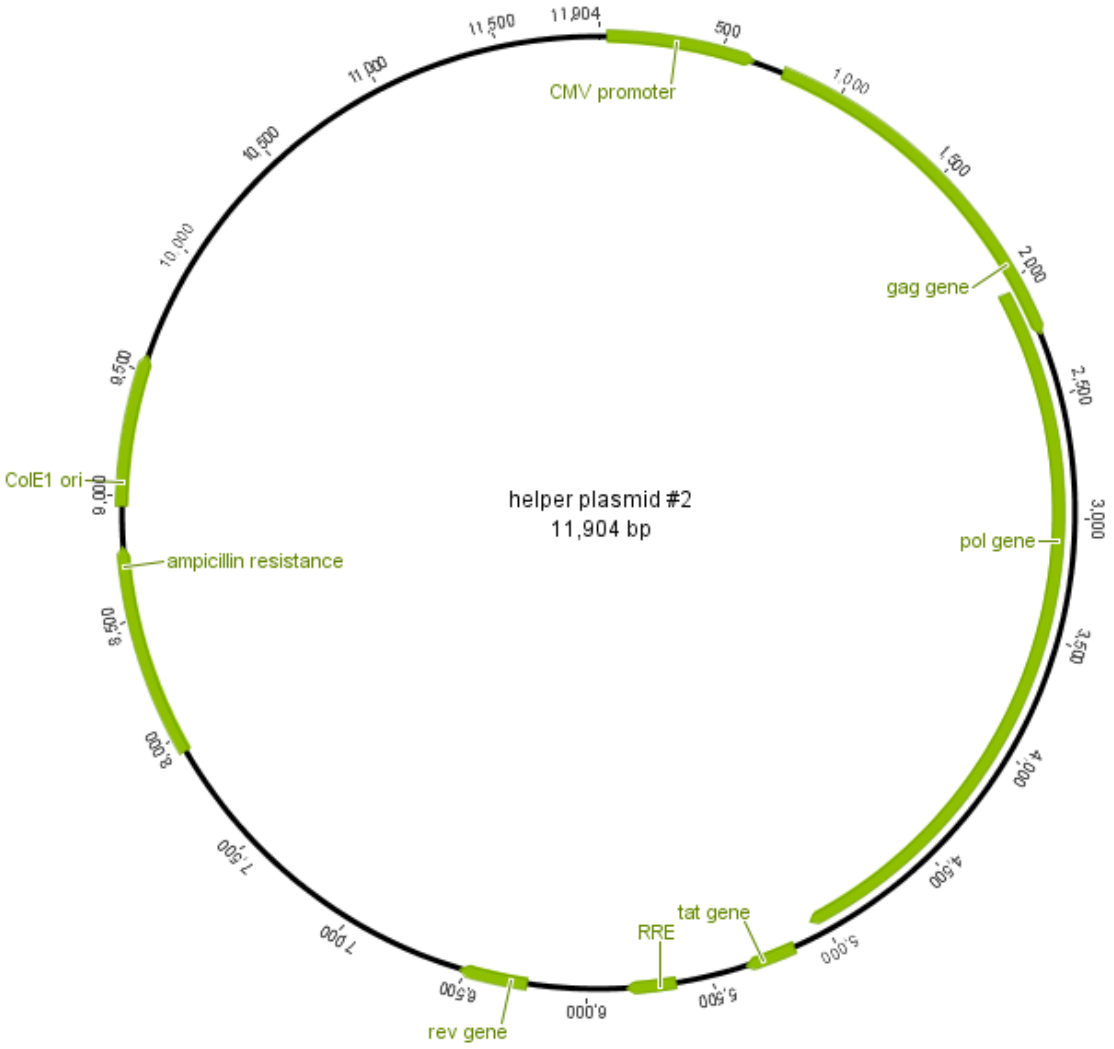

Figure 27: Map of the lentiviral helper plasmid #2.

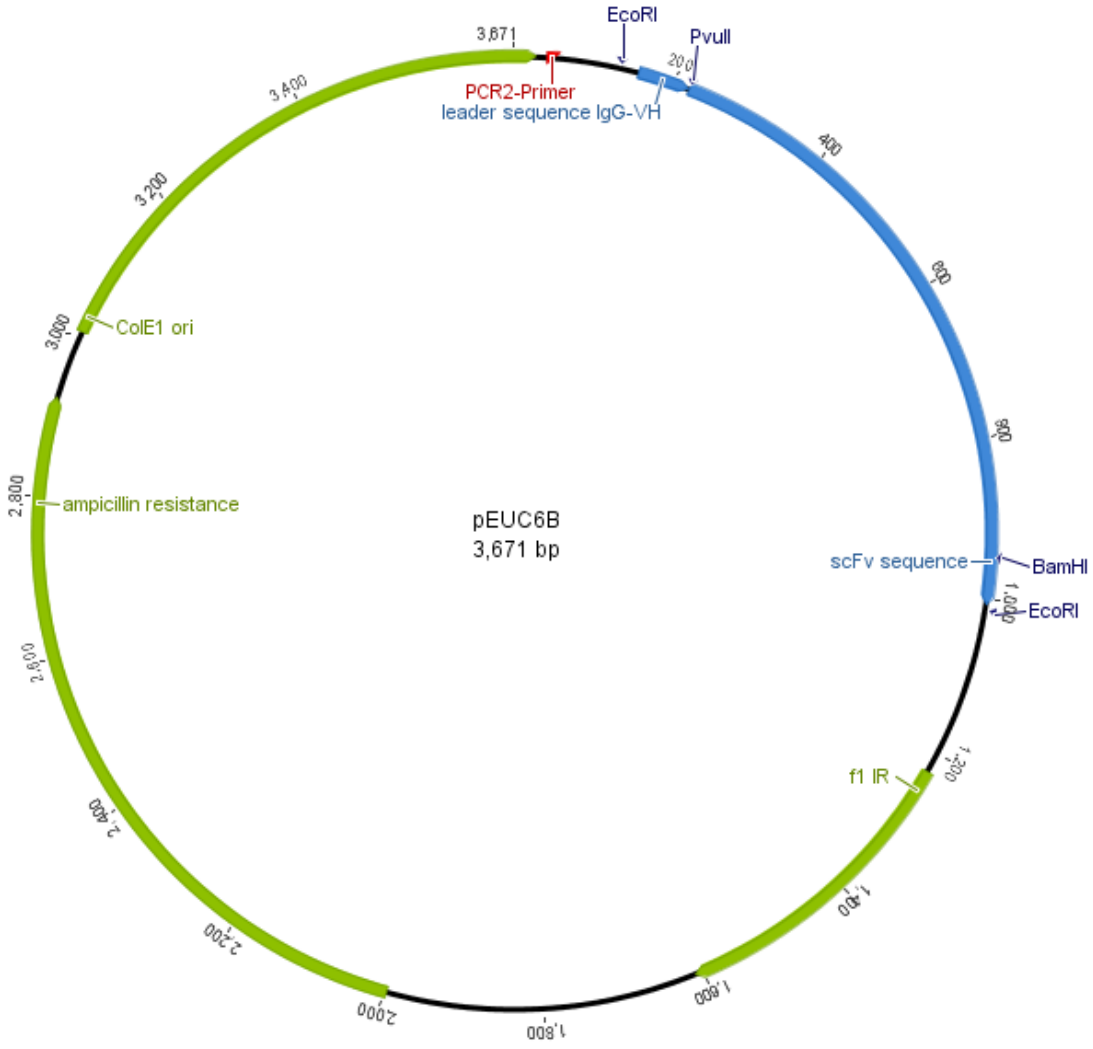

Figure 28: Map of the subcloning vector pEUC6B.

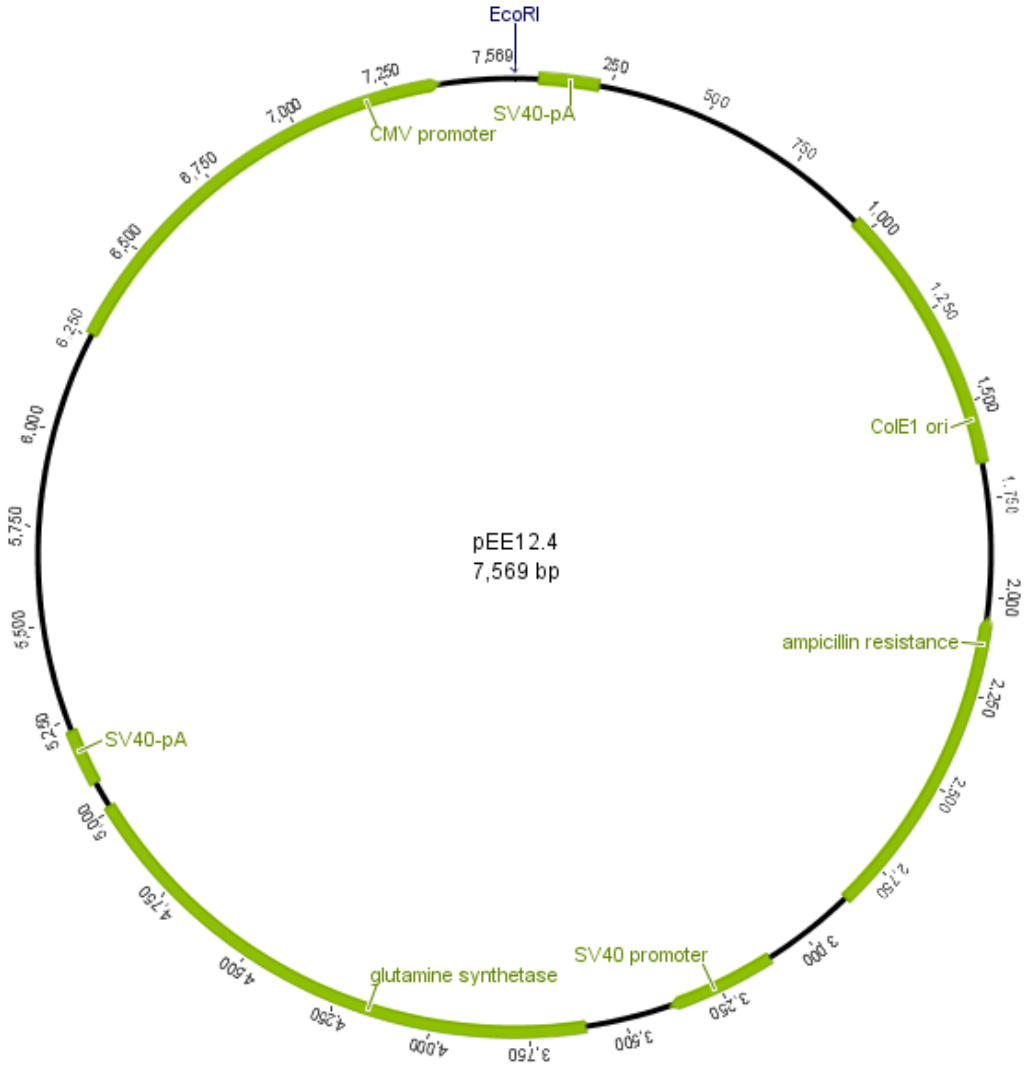

Figure 29: Map of the mammalian expression vector pEE12.4.

6.2 List of figures

6.3 List of tables

7 Acknowledgment

First, I would like to thank Prof. Dr. Dirk Jäger for giving me the opportunity to conduct my doctoral project in the Department of Medical Oncology at the National Center for Tumor Diseases in Heidelberg and for the support of this work.

Sincere thanks to Dr. Michaela Arndt and Prof. Dr. Jürgen Krauss for the opportunity to perform the laboratory work of my doctoral thesis in their group “Antibody-based Immunotherapeutics” at the NCT Heidelberg, for their scientific guidance, support and discussion.

Special thanks to Dr. Patrick Schmidt for his support and efforts in guiding me through this research project, for the discussions as well as for sharing a lot of CAR based knowledge.

I am grateful to our cooperation partners Prof. Dr. Hinrich Abken (Universität Köln) and Prof. Dr. Lars Nitschke (Universität Erlangen) for their scientific advices.

Many thanks go to my first referee Prof. Dr. Peter Angel for the support and evaluation of my doctoral thesis and the scientific guidance as member of my Thesis Advisory Committee.

I would also like to thank PD Dr. Alexandra Jensen for her scientific advices as member of my Thesis Advisory Committee.

Furthermore, I thank all the members of the “Tumor immunology” group for their support, discussion and for the enjoyable work atmosphere.

I express my gratitude to all former and current colleagues of the “Antibody-based Immunotherapeutics” group for the great teamwork, their support and the wonderful work atmosphere.

Last but not least, I thank Mathieu, my parents, my brothers David and Nicolas and my friends for their love, support, and encouragement. Without you, I would not be the person that I am today.